AD-A034 725

ANALYTICAL AND EXPERIMENTAL INVESTIGATION OF EJECTOR-POWERED ENGINE SIMULATORS FOR WIND TUNNEL MODELS

ARNOLD ENGINEERING DEVELOPMENT CENTER
ARNOLD AIR FORCE STATION, TENNESSEE

JANUARY 1977

026077

AEDC-TR-76-128

ANALYTICAL AND EXPERIMENTAL INVESTIGATION
OF EJECTOR-POWERED ENGINE SIMULATORS
FOR WIND TUNNEL MODELS

ENGINE TEST FACILITY
ARNOLD ENGINEERING DEVELOPMENT CENTER
AIR FORCE SYSTEMS COMMAND
ARNOLD AIR FORCE STATION, TENNESSEE 37389

January 1977

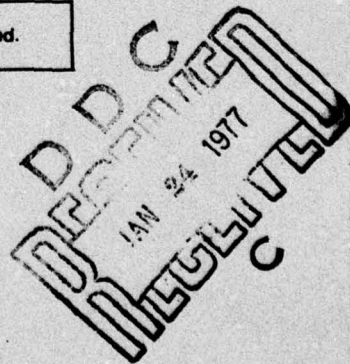Final Report for Period January 30 to June 30, 1976

Approved for public release; distribution unlimited.

Prepared for

DIRECTORATE OF TECHNOLOGY (DY)
ARNOLD ENGINEERING DEVELOPMENT CENTER
ARNOLD AIR FORCE STATION, TENNESSEE 37389

This report has been reviewed by the Information Office (OI) and is releasable to the National Technical Information Service (NTIS). At NTIS, it will be available to the general public, including foreign nations.

APPROVAL STATEMENT

This technical report has been reviewed and is approved for publication.

FOR THE COMMANDER

ELTON R. THOMPSON
Research & Development
   Division
Directorate of Technology

ROBERT O. DIETZ
Director of Technology

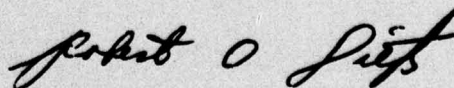| REPORT DOCUMENTATION PAGE		READ INSTRUCTIONS BEFORE COMPLETING FORM
1. REPORT NUMBER AEDC-TR-76-128	2. GOVT ACCESSION NO.	3. RECIPIENT'S CATALOG NUMBER
4. TITLE (and Subtitle) ANALYTICAL AND EXPERIMENTAL INVESTIGATION OF EJECTOR-POWERED ENGINE SIMULATORS FOR WIND TUNNEL MODELS		5. TYPE OF REPORT & PERIOD COVERED Final Report - January 30 to June 30, 1976
		6. PERFORMING ORG. REPORT NUMBER
7. AUTHOR(s) G. D. Smith, R. J. Matz, and R. C. Bauer - ARO, Inc.		8. CONTRACT OR GRANT NUMBER(s)
9. PERFORMING ORGANIZATION NAME AND ADDRESS Arnold Engineering Development Center (DY) Air Force Systems Command Arnold Air Force Station, Tennessee 37389		10. PROGRAM ELEMENT, PROJECT, TASK AREA & WORK UNIT NUMBERS Program Element 65807F
11. CONTROLLING OFFICE NAME AND ADDRESS Arnold Engineering Development Center (DYFS) Arnold Air Force Station Tennessee 37389		12. REPORT DATE January 1977
		13. NUMBER OF PAGES 87
14. MONITORING AGENCY NAME & ADDRESS(If different from Controlling Office)		15. SECURITY CLASS. (of this report) UNCLASSIFIED
		15a. DECLASSIFICATION/DOWNGRADING SCHEDULE N/A

16. DISTRIBUTION STATEMENT (of this Report)

Approved for public release; distribution unlimited.

17. DISTRIBUTION STATEMENT (of the abstract entered in Block 20, If different from Report)

18. SUPPLEMENTARY NOTES

Available in DDC

19. KEY WORDS (Continue on reverse side if necessary and identify by block number)

engine simulators	jet pumps
exhaust systems	transonic flow
ejectors	experimental data
diffusers	mathematical analysis

20. ABSTRACT (Continue on reverse side if necessary and identify by block number)

Ejector-powered engine simulators (EPES) that produce representative engine inlet and exhaust effects in wind tunnel models are currently under investigation at the Arnold Engineering Development Center (AEDC). Studies summarized in this report include theoretical and experimental investigations of single-stage, cold-flow EPES and theoretical investigations of two-stage, cold-flow EPES and of single-stage EPES driven with heated jets.

DD FORM 1 JAN 73 1473   EDITION OF 1 NOV 65 IS OBSOLETE

20. ABSTRACT (Continued)

Existing AEDC jet pump and ejector-diffuser analytical models were used to predict EPES exhaust-to-inlet total pressure ratio, inlet airflow, and velocity distributions during the jet mixing process. Pumping characteristics obtained both theoretically and experimentally with the single-stage, cold-flow EPES duplicated the afterburning cycle pumping characteristics of several representative turbojet and low-bypass turbofan engines. However, only conditions corresponding to unagumented operation at supersonic flight speeds can be duplicated without some EPES performance augmentation scheme such as inlet bleed. Computations for the two-stage, cold-flow EPES and the single-stage, hot-gas EPES indicate only marginal performance gains over the single-stage, cold-flow EPES. Both theoretical and experimental results indicate that multiple driving nozzles, operating in parallel in a single-stage EPES, will be required to achieve relatively uniform EPES exhaust conditions within the anticipated geometric and operational constraints imposed by wind tunnel models.

AFSC
Arnold AFS Tenn

PREFACE

The work reported herein was conducted by the Arnold Engineering Development Center (AEDC), Air Force Systems Command (AFSC), under Program Element 65807F. The Air Force Project Engineer was E. R. Thompson, Research and Development Division, Directorate of Technology. The results were obtained by ARO, Inc. (a subsidiary of The Sverdrup Corporation), contract operator of AEDC, AFSC, Arnold Air Force Station, Tennessee. The work was done under ARO Project Numbers RF432, R32P-53A, and R32P-92A. The authors of this report were G. D. Smith, R. J. Matz, and R. C. Bauer, ARO, Inc. The manuscript (ARO Control No. ARO-ETF-TR-76-81) was submitted for publication on July 26, 1976.

1

CONTENTS

ILLUSTRATIONS

Figure   **Page**

TABLES

APPENDIXES

1.0 INTRODUCTION

1.1 GENERAL

Multi-mission aircraft that spend a significant portion of their mission profile in the transonic flight regime must be carefully designed to minimize drag-related problems. A significant portion of the transonic drag arises from interactions between engine-induced flow fields and the airframe slipstream (Fig. 1). Inlet spillage and bleed, afterbody boundary layer development and separation, and mixing of the expanding engine exhaust gases with engine cooling air and the afterbody slipstream are the major complex and generally unpredictable engine-induced interactions affecting airframe drag. Since the interactions are too complex for complete theoretical evaluation, there is almost total dependence on wind tunnel programs to identify problem areas and to provide guidance for making corrective modifications.

Although a wide variety of wind tunnel techniques have been proposed to obtain coupled engine-airframe performance characteristics (Refs. 1 through 3), there is no universally acceptable test method – particulary in the transonic flight regime. One of the major reasons for the diversity of test methods is that a small, low cost device that can be installed in a wind tunnel model and will generate inlet and exhaust stream conditions which simulate conditions produced by turbine engines does not exist. Schemes (Fig. 2), such as (1) faired-over inlets and solid exhaust plume simulators, (2) simple flow-through nacelles, and (3) complex models with both air removal and air supply systems to simulate the engine intake and exhaust conditions, have been employed in combination with one another and in conjunction with complex drag force accounting systems in an attempt to assess engine-airframe interaction effects on total drag (Ref. 4).

Faired-inlet/solid-body plume simulators (Fig. 2a) are the simplest and least expensive devices which can be used to represent engine flow conditions that may affect airframe drag. These devices only approximate the engine inlet and exhaust stream tube shapes without any simulation of viscous effects along the boundaries. Simulators with pumped inlets and pressurized jets (Fig. 2c) have the potential for providing good simulation of engine inlet and exhaust conditions; however, large service lines are required to remove the air captured by the inlet and to supply the pressurized exhaust gases. This requires either a half-model mounted on the wind tunnel wall (Ref. 1) or a complete model mounted on an oversize strut which results in significant wind tunnel wall or strut interference. Various combinations of the solid body and the pumped simulators (Figs. 2a through c) have been employed in wind tunnel programs in an attempt to obtain the simplest and most realistic engine simulator for a given test program. The degree to which

the approximate test techniques have been successful in simulating flight conditions has been strongly dependent on the engine cycle and the afterbody and exhaust nozzle configuration involved. Airplane minimum drag coefficients obtained with faired-inlet wind tunnel models having either solid plume or pressure jet exhaust simulation were reported (Ref. 5) to be within ±5 percent of flight results for a single engine aircraft having a single, convergent-divergent, non-ejector exhaust nozzle and a carefully designed afterbody. However, multi-engine aircraft with complex engine afterbody closures and ejector or tertiary flow exhaust nozzles have exhibited significant performance discrepancies when compared with wind tunnel results obtained by the previously outlined techniques.

1.2 CURRENT STATUS OF ENGINE SIMULATOR DEVELOPMENT

In the past decade, increased emphasis has been placed on the development of wind tunnel model propulsion simulators which will simultaneously provide both inlet and exhaust conditions that are representative of aircraft gas turbines. In principle, it would appear that a small-scale turbine engine would be the most desirable simulator since it could have all of the characteristics of a full-scale engine. In practice, however, there are stringent limits in design and fabrication techniques which significantly reduce the component efficiencies achieved with very small-scale engines. The high probability of significant performance differences between small-scale and full-scale engines, together with the large development costs, operational reliability, and maintenance requirements, have substantially reduced the emphasis for small-scale turbine engine development for wind tunnel models, at least in the forseeable future. The ejector- and turbine-powered simulators evolved to date (Figs. 2d and e) do not have all of the performance characteristics of the full-scale engines but do provide a greater degree of simulation than the faired-inlets and solid-plume simulators.

1.2.1 Turbine-Powered Engine Simulators (TPES)

Turbine-powered engine simulators (Fig. 2d) – also referred to as "powered nacelles" or "powered simulators" – use high-pressure air or nitrogen to drive small fans or axial-flow compressors at rotational speeds up to 110,000 rpm. The TPES units with mass flow and overall pressure ratio characteristics representative of high-bypass turbofans (Ref. 6), turbojets (Ref. 7), and mixed-flow augmented turbofans (Ref. 8) have been developed which are compatible with wind tunnel models of fighter aircraft in the 5- to 10-percent scale range. Numerous applications of TPES units in wind tunnel programs have been reported (e.g., Refs. 1, 4, and 6) for high-bypass engine simulation but applications to turbojets and augmented turbofans have been very limited (Ref. 9). Comparisons of flight test and TPES wind tunnel data are also limited. The only

well-documented investigation (Ref. 9) is clouded by significant Reynolds number differences between wind tunnel and flight conditions.

1.2.2 Ejector-Powered Engine Simulators (EPES)

Jet- or ejector-powered engine simulators (Fig. 2e) also referred to as injector units or simulators use the ejector action of a high-pressure gas jet submerged in the model to pump the flow captured by the inlet to pressurized conditions representative of turbine engine exhaust. The EPES units are attractive for propulsion simulator applications because they are simple, relatively inexpensive devices with no moving parts. The EPES units were initially proposed for jet lift-engine simulation (Refs. 10, 11, and 12) with subsequent recommendation (Refs. 1 and 13) that they might also be applied to turbojet and mixed-flow, augmented turbofan applications. Actual use of EPES in reported wind tunnel programs (Ref. 14) has been even more limited than for TPES applications.

Probably the major reason why EPES units have not received more consideration in high-speed airframe/engine interaction studies is the lack of performance data on potential EPES systems. Wood's evaluation (Ref. 13) is the most significant contribution in this area but is limited to theoretical performance estimates based on a simple, one-dimensional analysis along with considerable speculation about system losses. Two practical examples were considered to illustrate use and limitations of the analysis. Comparable overall pressure ratios and inlet mass flow were computed for an EPES which would simulate the engine in a hypothetical fighter-strike aircraft flying at Mach 1.8 with afterburner operating. Evaluation of the requirements for simulating a 5:1 bypass-ratio engine, flying at Mach 0.8 at 30,000 ft revealed that an EPES would require 25- to 30-percent inlet mass flow removal in order to provide both inlet mass flow and overall pressure ratios representative of the engine. Wood concludes his evaluation with a plea for experimental investigations to establish the magnitude of the losses in practical EPES applicable to high performance aircraft propulsion simulation.

The only other quantification of EPES performance in the open literature* is included in Grunnet's discussion of wind tunnel propulsion simulation techniques (Ref. 1). Some general performance characteristics and limitations of EPES and other propulsion simulators considered by Grunnet are reproduced in Table 1, but the source or basis upon which the EPES performance estimates were made was not included in Ref. 1.

It may be concluded from the limited published information that many questions still exist concerning the application of EPES to high performance aircraft propulsion

---

*Performance characteristics of several existing EPES and TPES units are included in product bulletins prepared by Tech Development, Inc., Dayton, Ohio.

simulation. The portion of representative engine operating envelopes that EPES units can duplicate, the driving nozzle and mixing duct combinations required for optimum performance, and the internal losses and exit conditions associated with practical EPES units are items yet to be resolved.

This report presents results obtained to date from an EPES development investigation being conducted at the Arnold Engineering Development Center (AEDC). Existing theoretical models of similar systems were used to determine the effect of geometric and thermodynamic parameters on single-stage and two-stage EPES performance. The theoretical results were used to select several single-stage EPES for experimental evaluation. The experiments conducted were designed to verify the feasibility of the concept, provide experimental data to improve existing analytical models, and to establish the design criteria for an EPES which will be fabricated and tested in a wind tunnel model of a high-performance aircraft.

2.0 THEORY

2.1 SIMULATION REQUIREMENTS

Although the development of wind tunnel simulation criteria is beyond the scope of the present work, it is necessary to establish the most significant engine performance characteristics required to be produced by the engine simulator to allow an evaluation of the potential usefulness of EPES. Simulation of all engine characteristics which could potentially influence the flow field around the airframe (Ref. 15) would be a formidable task. However, if the determination of airframe drag is the objective of the wind tunnel program, it is generally conceded (Refs. 1, 16, 17, and 18) that the most important features of engine-airframe interactions will be reproduced if the proper amount of inlet flow is captured and the engine exhaust jet shape and entrainment characteristics are duplicated. Proper inlet capture characteristics can readily be achieved with a wind tunnel model having scaled inlet geometry if the engine simulator pumps the same inlet mass flux (W_{in}/A_{in}) as the engine being simulated. However, obtaining proper exhaust plume shape and entrainment characteristics with scaled exhaust nozzles requires nozzle exit velocities, pressures, temperatures, and kinematic viscosities corresponding to engine-produced conditions, which may be difficult to reproduce with any engine simulator.

If, for purposes of model simplicity, the engine exhaust jet is simulated in the wind tunnel model with unheated air, the requirements for producing proper plume shape and entrainment characteristics become even more difficult (Ref. 15). However, the general relationship between hot and cold jet pressure levels required to produce equal afterbody drag conditions can be deduced from the experiments conducted by Robinson and High

10

(Ref. 18). The afterbody drag measurements reported in Ref. 18 were made over a range of nozzle exit pressure ratios with combustion gases at various temperature levels and with unheated air. Ethylene/air burners were used to produce conditions in a convergent-divergent exhaust nozzle that were representative of (1) a mixed-flow turbofan with a 1:1 bypass ratio, and (2) a turbojet with an ejector-type exhaust nozzle. Drag coefficients obtained with the turbojet burner configuration operating at temperatures equivalent to normal power turbine exit conditions (1,800 to 2,200°F) were duplicated with unheated air jets at exhaust total pressures ranging from 2 to 12 percent greater than the burner exit total pressure levels. Drag coefficients obtained with the turbofan burner configuration operating at normal power temperatures were duplicated with an unheated air jet at essentially equal exhaust total pressure conditions. Drag coefficients obtained with maximum burner temperatures (3,000 to 3,300°R) were duplicated with unheated air jets operating at total pressures from 20 to 50 percent greater than burner exit total pressure conditions. Although the results were obtained with one particular nozzle/afterbody combination and, therefore, cannot be construed as being applicable to all models, they can be used as a guide in the establishment of cold-flow engine simulator performance requirements for wind tunnel models having exhaust nozzles which are geometrically similar to the one employed.

Thus, engine inlet mass flux and exhaust total pressure are accepted as the principal parameters characterizing the engine flow, and general EPES performance requirements can be determined from performance characteristics of several current technology turbine engines. To more directly relate the EPES requirements to the engine rather than the engine-inlet combination, and since the exhaust nozzle is always choked for the conditions being considered, it is convenient to define the required mass flux as W_{in}/A_{ex}^* . Of course, W_{in}/A_{ex}^* is directly related to W_{in}/A_{in} since A_{in}/A_{ex}^* for the model must equal A_{in}/A_{ex}^* for the full-scale vehicle. The mass flux parameter can be further generalized to be independent of flight Mach number and altitude by using the corrected inlet flow (W_{in_c}) in place of actual inlet flow rate (W_{in}). On this basis then, the inlet mass flow parameter (W_{EC}) to be used in all subsequent discussions is defined as

$$W_{EC} = W_{in_c}/A_{ex}^*$$

where

$$W_{in_c} = W_{in}\sqrt{\frac{T_{T_{in}}}{T_{T_{ref}}}}\frac{P_{T_{ref}}}{P_{T_{in}}}$$

with reference conditions

$$P_{T_{ref}} = 2116.22 \text{ psfa}$$

$$T_{T_{ref}} = 518.67 \text{ °R}$$

11

Exhaust pressures the simulator must provide, with geometrically similar exhaust nozzles, can be related (e.g., as in Ref. 18) to the engine exhaust-to-inlet total pressure ratio (EPR). Therefore, simulator performance requirements may be deduced from two engine performance parameters (W_{EC} and EPR).

Evaluation of two high-performance, single-spool afterburning turbojets and two low-bypass-ratio, mixed-flow, augmented turbofans yielded the performance bands shown in Fig. 3. It should be noted that the maximum W_{EC} and EPR conditions were associated with nonafterburning operation at subsonic and transonic flight conditions. The EPES performance capabilities will be judged on the basis of their ability to pump inlet corrected mass flux rates and overall total pressure ratios comparable to the values shown in Fig. 3, with the realization that simulator pressure ratios (SPR) up to 50 percent greater than EPR may be required for a cold-flow EPES, depending on the engine cycle involved and the engine operating condition to be simulated.

2.2 ANALYTICAL MODELS

Two general analytical models (Refs. 19 and 20) were applied to theoretically calculate EPES performance. The first model is a one-dimensional, perfect gas representation used to predict the overall pumping characteristics of single-stage and two-stage EPES (Fig. 4). The second model is a viscous, axisymmetric, two-stream, turbulent mixing analysis which was used to estimate pressure and velocity conditions in the EPES mixing duct.

2.2.1 Performance Analysis (Single-Stage EPES)

The control volume used for the basic single-stage EPES configuration analysis is presented in Fig. 4a. The one-dimensional, adiabatic analysis applied over the indicated control volume contains the following assumptions:

1. All gases involved are thermally and calorically perfect and conform to the Gibbs-Dalton Law.

2. Flow in the primary nozzle is one-dimensional and supersonic with exit Mach number (M_2) defined by A_2/A_2^* and the isentropic flow relationships.

3. Secondary flow approaching the mixing duct inlet is uniform and subsonic over surface ③ .

4. The mixing duct has a constant cross-sectional area.

5. The pressure on the base area $\textcircled{2b}$ of the primary nozzle is equal to the secondary flow inlet static pressure.

6. The mixing duct is of sufficient length to achieve complete mixing between the primary and secondary streams so that flow conditions at the mixing duct exit $\textcircled{B}$ are one-dimensional and subsonic.

7. Flow from the mixing duct exit $\textcircled{B}$ to the exhaust nozzle throat $\textcircled{ex*}$ is isentropic and one-dimensional.

8. Sonic conditions exist at the exhaust nozzle throat $\textcircled{ex*}$.

With these assumptions, the conservation equations are

Conservation of Mass:

$$W_2 + W_3 = W_B \tag{1}$$

Conservation of Momentum:

$$\frac{W_2}{g_c} U_2 + P_2 A_2 + \frac{W_3}{g_c} U_3 + P_3 A_3 + P_3 A_{2b} = F_s + \frac{W_B}{g_c} U_B + P_B A_B \tag{2}$$

Conservation of Energy:

$$W_{ex}^* C_{p_{ex}}^* T_{T_{ex}}^* = W_2 C_{p_2} T_{T_2} + W_3 C_{p_3} T_{T_3} \tag{3}$$

The mixing duct wall drag force (F_S) is determined from

$$F_s = C_{DS} A_s \bar{q}_s \tag{4}$$

where

$$\bar{q}_s = \frac{\gamma}{16} [P_3 + P_B][M_3 + M_B]^2 \tag{5}$$

and

$$A_s = \pi D_B L_B \tag{6}$$

for a mixing duct of circular cross section. The wall drag coefficient (C_{DS}) is the average skin friction coefficient between the mixing duct inlet and exit stations.

The conservation equations are solved for a specified EPES geometry (A_2^*, A_2, A_{2b}, A_B, A_{ex}^*, L_B, and L), gas properties (γ_2, C_{p_2}, $\bar{R}_2$, T_{T_2}, γ_3, P_{T_2}, C_{p_3}, $\bar{R}_3$, and T_{T_3}) and an appropriate wall drag coefficient (C_{DS}) at arbitrarily selected values of

13

secondary-to-primary mass flow ratio (k_E). For each selected value of k_E, iterations were made for the secondary-to-primary total pressure ratio that (1) satisfies the conservation equations with a subsonic mixing duct exit Mach number*, and (2) produces sonic conditions at the exhaust nozzle throat. For each solution, the basic EPES performance parameters (W_{SC} and SPR) are computed from

$$W_{SC} = \frac{k_E (\dot{m} P/P_T)_2^* \sqrt{T_{T_3}/T_{T_2}} (2116.22)}{(A_{ex}^*/A_2^*)(P_{T_3}/P_{T_2}) \sqrt{518.67}} \tag{7}$$

and

$$SPR = P_{T_B}/P_{T_3}$$

Comparison of the values of W_{SC} and SPR for the EPES with values of W_{EC} and EPR for the simulated full-scale engine indicates whether the EPES has the potential to pump the required inlet mass flow rate within the constraint of a fixed exhaust nozzle geometry and the one-dimensional flow assumptions.

2.2.2 Performance Analysis (Two-Stage EPES)

A modification was made to the basic performance analysis program so that an adiabatic two-stage EPES (Fig. 4b) could be investigated. The objective of this phase of the theoretical investigation was to determine if any significant gains in performance or operational flexibility could be achieved with multi-stage EPES configurations. The equations and assumptions pertaining to the single-stage EPES also apply to the first-stage of the two-stage EPES. The equations describing the overall performance of the second-stage addition are obtained by applying the conservation equations to the two additional control volumes shown in Fig. 4b. Additional assumptions applicable to the second-stage are:

1. Flow in the second-stage driving nozzle is one-dimensional and supersonic with the exit Mach number defined by A_4/A_4^* and the isentropic flow relations.

2. The second-stage mixing duct has a constant cross-sectional area equal to or greater than the cross-sectional area of the first-stage mixing duct.

3. The first-stage mixing duct base pressure (P_B) is equal to the first-stage exit static pressure.

---

*The conservation equations also have a supersonic branch solution which is not considered in EPES applications at the present time.

14

4. The pressure acting on the forebody and support strut of the second-stage driving nozzle is equal to the total pressure at the exit of the first-stage mixing duct (P_{T_B}).

5. The pressure on the base of the second-stage driving nozzle ④ is equal to P_5.

6. Both mixing ducts have sufficient length to achieve complete mixing so that exit conditions are one-dimensional and subsonic.

Within the constraints of the assumptions, the additional conservation equations for the second stage are

$$W_B = W_5 \tag{8}$$

and

$$\frac{W_B}{g_c} U_B + P_B A_B = F_{s_4} + \frac{W_5}{g_c} U_5 + P_5 A_5 \tag{9}$$

for control volume No. 2 (Fig. 4b) and

$$W_5 + W_4 = W_{B_1} \tag{10}$$

and

$$\frac{W_4}{g_c} U_4 + P_4 A_4 + \frac{W_5}{g_c} U_5 + P_5 (A_5 + A_{b_4}) = F_{s_1} + \frac{W_{B_1}}{g_c} U_{B_1} + P_{B_1} A_{B_1} \tag{11}$$

and

$$W_4 C_{p_4} T_{T_4} + W_5 C_{p_5} T_{T_5} = W_{B_1} C_{p_{B_1}} T_{T_{B_1}} \tag{12}$$

for control volume No. 3. The second-stage driving nozzle/support strut drag (F_{s_4}) and the mixing duct wall drag (F_{s_1}) are determined from

$$F_{s_4} = (A_4 + A_{4_b} + A_{strut}) P_{T_B} \tag{13}$$

and

$$F_{s_1} = C_{D_{s1}} A_{s_1} \bar{q}_{s_1} \tag{14}$$

where

$$\bar{q}_{s_1} = \frac{\gamma}{16} (P_5 + P_{B_1}) (M_5 + M_{B_1})^2 \tag{15}$$

and

$$A_{s_1} = \pi D_{B_1} L_{B_1} \tag{16}$$

for a mixing duct of circular cross section.

15

The solution technique for the two-stage EPES is similar to that employed for the single-stage EPES except that three control volumes (first stage, transition section, and second stage) are successively involved in the two-stage solution. Specified inputs are the two-stage EPES geometry details (A_2^*, A_2, A_{2b}, A_B, L_B, L, A_{strut}, A_4^*, A_4, A_{4b}, A_{B1}, A_{ex}^*, and L_{B1}), gas properties (γ_2, C_{p_2}, P_{T_2}, $\bar{R}_2$, T_{T_2}, γ_3, C_{p_3}, $\bar{R}_3$, γ_4, C_{p_4}, $\bar{R}_4$, and T_{T_4}), drag coefficients (C_{DS} and C_{DS1}), and arbitrarily selected values of first-stage secondary-to-primary mass flow ratios (k_E) and second-stage-to-first-stage driving nozzle total pressure ratios (P_{T_4}/P_{T_2}). At each selected value of k_E and P_{T_4}/P_{T_2}, iterations are made for the first-stage secondary-to-primary total pressure ratio (P_{T_3}/P_{T_2}) to find (1) the subsonic branch solution for the first-stage mixing duct exit Mach number (M_B), and (2) the total flow rate (i.e., sum of W_2, W_3, and W_4) that satisfies the conservation equations with a subsonic branch solution at the exit of the second-stage mixing duct and also produces sonic conditions at the exhaust nozzle throat. For each solution, the basic EPES performance parameters (W_{SC} and SPR) are computed from

$$W_{SC} = \frac{k_E (\dot{m}\, P/P_T)_2^* \sqrt{T_{T_3}/T_{T_2}}\,(2116.22)}{(A_{ex}^*/A_2^*)(P_{T_3}/P_{T_2})\sqrt{518.67}} \tag{17}$$

and

$$SPR = P_{T_{B1}}/P_{T_3} \tag{18}$$

2.2.3 Mixing Analysis

Estimates of single primary nozzle EPES mixing duct pressure and velocity distributions were determined with the ducted mixing analysis of Peters (Ref. 20). The analytical model uses an integral form of the steady-flow boundary-layer equations to describe the turbulent mixing of axisymmetric, coaxial gas streams. The form of the model applied to the current work was the "1-D Core Theory" in which the primary and secondary streams are assumed to be inviscid and one-dimensional and the turbulent shear along one control surface in the mixing layer is calculated by utilizing a semi-empirical model for the turbulent eddy viscosity. The general flow process considered in the Peters analysis is indicated in Fig. 5.

3.0 EXPERIMENTAL APPARATUS AND PROCEDURE

An experimental investigation of internal EPES performance was conducted with several single-stage cold-air-driven units to provide data for comparison with theoretical predictions and to develop operational techniques which could be utilized in wind tunnel applications. The experimental program was designed to

1. Determine the overall performance characteristics of single-stage EPES in terms of W_{SC} and SPR,

2. Determine the effects of varying system geometric and operating parameters (A_2/A_2^*, A_B/A_2, L/D_B, L_B/D_B, M_B, and k_E) on overall simulator performance, and

3. Determine the effect of mixing duct length on flow uniformity at the EPES exhaust nozzle exit station.

3.1 TEST APPARATUS

The experimental program was conducted in the AEDC Engine Test Facility (ETF) Propulsion Research Cell (R-1A-2). The test cell configuration is shown in Fig. 6. The EPES section consisted of an inlet plenum, a primary nozzle assembly, a variable length mixing duct section, and an exhaust nozzle. Air from a high-pressure supply system was used as the working fluid. A portion of the air was throttled to pressures from 50 to 500 psia to supply the ejector primary nozzle, and the remainder of the air was throttled to 5 to 40 psia to supply the engine simulator inlet mass flow. The simulator inlet mass flow rate was metered with a circular arc metering venturi located upstream of the plenum section. The primary nozzle mass flow rate was calculated from conditions at the throat of the primary nozzle.

Three convergent-divergent primary nozzle configurations were used in the investigations (Fig. 7). The first nozzle (Fig. 7a) has an elliptical contraction section, a contoured divergent section, and an area ratio of 4.44. The divergent section wall contour was derived from a method of characteristics solution (Ref. 21) to provide uniform, parallel, Mach number 3.05 flow at the nozzle exit. The second primary nozzle (Fig. 7b) has a circular arc contraction and a conical, area ratio 25, divergent section with a divergence half-angle of 15 deg. The third primary nozzle used (Fig. 7c) consists of a cluster of seven, area ratio 25, conical nozzles each having a divergence half-angle of 15 deg and a conical inlet section with a convergence half-angle of 30 deg. The inlet and divergence sections were blended at the nozzle throat to provide a smooth continuous contour through the throat section. The spacing pattern of the seven-nozzle cluster was selected to provide an approximately uniform distribution of primary mass flow over the inlet area of the mixing duct section. The design exit Mach number of all the area ratio 25 nozzles is 5.0.

Two convergent-divergent exhaust nozzles with inlet contraction ratios (A_B/A_{ex}^*) of 2.72 and 1.21 were used in the experiments. The high contraction configuration (Fig. 8a) has an inlet Mach number of 0.23 when choked. Operating choked, the low contraction

17

configuration (Fig. 8b) has an inlet Mach number of 0.58. Both exhaust nozzles were arbitrarily provided with exit-to-throat area ratios near unity (1.01 to 1.04) since only flow conditions up to the nozzle throat were of principal interest. Limited experiments were also conducted with no exhaust nozzle on the mixing duct to provide additional insight into the effect of mixing duct exit flow conditions on EPES performance.

The EPES mixing duct section consisted of up to five 4.5-in.-diam spool pieces (Fig. 6a). Each spool piece has a length-to-diameter ratio of two. Thus, various EPES configurations could be formed with mixing duct section length-to-diameter ratios between two and ten.

3.2 INSTRUMENTATION

Instrumentation stations for the experimental investigation are indicated in Fig. 6. Total temperatures were measured with single-shielded, self-aspirating, copper-constantan thermocouple probes using an ice bath reference junction. Pressures were measured with differential, strain-gage-type transducers which were referenced to atmospheric pressure. Traversing probe positions were determined with wire-wound potentiometers mechanically connected to the probes.

Total pressure probes with radial traversing capability were installed in each mixing duct section (Fig. 6b). Exhaust nozzle exit surveys were made with a combination total/static pressure probe (Fig. 6b, detail A). Static pressure orifices were installed in each mixing duct section at stations indicated in Fig. 6.

3.3 TEST PROCEDURES

Transducers and thermocouples were calibrated in-place before and after each test period. Pressures applied during calibration were measured with a multiple-turn, fused-quartz bourdon tube equipped with a servocontrolled optical transducer. The traversing probe position potentiometers were calibrated by measuring probe distance from the duct wall.

All data were obtained at steady-state conditions. Flow control parameters (secondary flow venturi inlet pressure and temperature, primary nozzle inlet pressure and temperature, and test cell exhaust pressure) were monitored continuously to verify that steady-state conditons did exist throughout the data acquisition process. Data acquisition was accomplished with an electronically controlled probe traversing unit and a Systems Engineering Laboratory (SEL) 600 digital data acquisition system. In the first step of the automatically controlled data acquisition sequence, mixing duct wall static pressures and flow control parameters were recorded with all probes retracted. Each probe survey was

then accomplished by setting the probe at eleven, approximately equally spaced positions across the mixing duct or exhaust plume and recording the probe pressures and flow control parameters at each location. Upon completion of the test sequence, the controller was reset, the next test condition was established, and the data acquisition process was repeated.

Pumping characteristics for a given EPES configuration were obtained at constant primary flow conditions with mixing duct inlet total pressures (P_{T_3}) varied between 0.2 and 2.0 atm to obtain a range of secondary-to-primary mass flow ratios. Primary nozzle total pressures ($P_{T_2} = P_{T_{21}}$) were in the following ranges:

Primary Nozzle Config. (A_2/A_2^*)	Range of P_{T_2}, psia
4.44	375 to 425
25.0 (Single Nozzle)	475 to 525
25.0 (7-Nozzle Cluster)	275 to 325

For experiments conducted with exhaust nozzles on the EPES, the test cell exhaust pressure was set at some convenient level to ensure a choked exhaust nozzle. For experiments with the exhaust nozzle removed, the test cell exhaust pressure was adjusted to provide measured mixing duct exit total-to-static pressure ratios corresponding to the desired mixing duct exit Mach numbers.

The matrix of test conditions conducted in the experimental program was selected to provide some insight into the effects of various geometric parameters and operating conditions on single-stage, cold-flow EPES performance. Geometric parameters and general performance characteristics of the EPES configurations investigated are sumarized in Table 2. Equations used for calculation of the principal experimental performance parameters are given in Appendix A.

3.4 PRECISION OF MEASUREMENTS

Uncertainties (bands which include 95 percent of the calibration data) of the basic experimental parameters were estimated from repeat calibrations of the instrumentation. Uncertainties of the instrumentation systems were estimated from repeat calibrations of the systems against secondary standards whose precisions were traceable to the National Bureau of Standard calibration equipment. The uncertainties were combined using the Taylor series method of error propagation (Ref. 22) to determine the precision of the experimental parameters presented in Table 3.

4.0 RESULTS AND DISCUSSION

4.1 EXPERIMENTAL RESULTS

Pumping characteristics of the six EPES configurations tested are presented in Fig. 9 as a function of secondary-to-primary mass flow ratio (k_E). With a given configuration, maximum values of SPR were obtained as k_E approached zero, whereas, in general, W_{SC} approached a maximum value asymptotically as k_E increased. In many of the configurations that had a single primary nozzle (Figs. 9a and b), mixing rates were insufficient to produce uniform subsonic flow conditions at the mixing duct exit, Station B (see Fig. 4a). As a result, simulator exit flows were characterized by significantly distorted velocity profiles containing large regions of supersonic flow, as shown in Fig. 10a, which would be undesirable for exhaust plume simulation. Supersonic mixing duct exit conditions* were also observed with the low contraction ratio ($A_B/A_{ex}^* = 1.21$) exhaust nozzle and the seven-conical-primary-nozzle configuration (Fig. 9c) with k_E less than 0.5. However, exit profiles obtained at all other test conditions with the seven-primary-nozzle configuration were found to be subsonic and uniform as shown by the nozzle exit surveys presented in Fig. 10b.

The data presented in Fig. 9 show that the exhaust nozzle contraction ratio has a significant effect on EPES performance. The maximum values of both W_{SC} and SPR were always obtained with the low contraction ratio ($A_B/A_{ex}^* = 1.21$) exhaust nozzle, and neither W_{SC} nor SPR was significantly different for the three primary nozzle configurations. With the high contraction ratio ($A_B/A_{ex}^* = 2.72$) nozzle, essentially identical performance was obtained with the single and multiple conical nozzles (Figs. 9b and c), while the single contoured primary nozzle configuration performed up to 15 percent better than the conical nozzle configurations.

Mixing duct length (L_B) and primary exit-to-mixing duct inlet spacing (dimension L, Fig. 4a) effects were difficult to assess from the single primary nozzle results (Figs. 9a and b) because of the incomplete mixing and corresponding supersonic mixing duct exit conditions that existed at most test conditions. Since the maximum mixing duct lengths evaluated exceeded length constraints in current wind tunnel models, single primary nozzle EPES are not practical if uniform, subsonic mixing duct exit conditions are required for proper exhaust simulation.

---

*Even in fully mixed systems, supersonic operation is theoretically possible (Section 2.2.1). The supersonic mode of operation can be achieved with (1) low contraction ratio exhaust nozzles, and (2) low exhaust pressures that will permit supersonic flow in the exhaust nozzle throat.

For EPES using the seven-primary-nozzle configuration, variations in L and L_B were generally found to have second-order effects on the pumping characteristics (Fig. 9c) and the primary-to-secondary total pressure ratio (P_{T_2}/P_{T_3}, Fig. 11).

The effect of exhaust nozzle contraction ratio on primary-to-secondary total pressure ratio (P_{T_2}/P_{T_3}) and mixing duct inlet Mach number (M_3) is also illustrated in Fig. 11. With the low contraction ratio exhaust nozzle ($A_B/A^*_{ex} = 1.21$), the mixing duct inlet Mach number is equal to or greater than 0.5 for all conditions evaluated with choking conditions in the region of the primary nozzle evident for k_E between 0.2 and 0.7. Configurations using the high contraction ratio exhaust nozzle ($A_B/A^*_{ex} = 2.72$) had inlet Mach numbers less than 0.2 for all conditions evaluated. Primary-to-secondary inlet total pressure ratios required with the low contraction exhaust nozzle were significantly greater than the high contraction nozzle values depending upon k_E.

A comparison of EPES experimental performance with engine simulation requirements is presented in Fig. 12. Intersections of EPES performance data and engine cycle conditions represent engine conditions that the EPES can duplicate (assuming SPR $\approx$ EPR provides valid exhaust plume simulation, as discussed in Section 2.1, with $W_{SC} = W_{EC}$). In fact, most of the EPES primary nozzle/mixing duct combinations shown in Fig. 12 have the capability for duplicating any of the engine cycle conditions to the left of the $A_B/A^*_{ex} = 1.21$ data with smaller exhaust nozzles (i.e., exhaust nozzle contraction ratios greater than 1.21). With different exhaust nozzles, all of the afterburning performance conditions could be obtained along with most of the supersonic portion of both nonafterburning cycles (EPR $\lesssim 1.7$).

The effect of mixing duct exit Mach number (M_B) on EPES performance was systematically investigated with the one configuration which had the exhaust nozzle removed. At each selected value of k_E, M_B was varied by varying exhaust pressure. The EPES performance with the exhaust nozzle removed was in substantial agreement with results obtained with the exhaust nozzles installed. Both SPR and W_{SC} increased monotonically with M_B up to about 0.6 with subsequent decreases at higher Mach numbers (Fig. 13). Therefore, a mixing duct exit Mach number of about 0.6 is the maximum value which should be considered from a practical standpoint.

4.2 COMPARISON OF THEORETICAL AND EXPERIMENTAL RESULTS

4.2.1 Pumping Characteristics

One of the assumptions in the theoretical EPES performance model (Section 2.2.1) is that mixing duct exit conditions are uniform and one-dimensional. Therefore,

21

comparison between theoretical and experimental EPES pumping characteristics will be limited to the seven-primary-nozzle configuration which has adequate mixing rates (Section 4.1) to produce uniform exit conditions.

Theoretical pumping characteristics from the basic performance analysis exhibited substantial differences from the experimental results obtained with both high (Fig. 14a) and low (Fig. 14b) contraction ratio exhaust nozzles. A major cause of the difference was found to be the assumption in the theoretical performance model that primary nozzle exit conditions (Station 2, Fig. 4) can be determined from the nozzle area ratio (A_2/A_2^*) and isentropic flow relationships. This implies that flow in the primary nozzle remains attached from the throat to the exit plane regardless of secondary stream conditions. However, experimental investigations of supersonic nozzles exhausting into a quiescent environment (e.g., Ref. 23) indicate that flow in a nozzle will separate if the back pressure is greater than the fully expanded nozzle exit static pressure. Both theoretical and experimental data shown in Fig. 15 indicate that the EPES mixing duct inlet static pressures (P_3) generally exceed a simple flow separation criterion (Ref. 19) over most of the conditions of interest so that M_2 is not defined by (A_2/A_2^*). The basic performance analysis was modified (Appendix B) to compensate for primary nozzle separation. Results from the modified analysis (dashed lines in Fig. 14) are in substantial agreement with the experimental results obtained at conditions where the secondary inlet is unchoked, i.e. SPR less than 2.5. At SPR above about 2.5, the exhaust flow is distorted and perhaps partially supersonic which is not a practical EPES operating condition.

4.2.2 Mixing-Duct Flow Fields

Typical streamwise wall pressure distributions found in the EPES mixing ducts are presented in Fig. 16 along with the theoretical results from the axisymmetric flow mixing analysis (Section 2.2.3). Both trends and levels obtained from the theoretical analysis are in good agreement with experimental results in the initial $(X/D_B \lesssim 3)$ portion of the mixing duct. Beyond X/D_B of about 3, the experimental data indicate a more rapid mixing than predicted by theory which is probably the result of the complex shock system in the mixing duct that is not considered in the theoretical model. For EPES that differed only in mixing duct length, configurations with longer mixing ducts typically had similar but slightly lower level wall pressure distributions than the shorter ducts as indicated in Fig. 16 for $k_E = 1.5$.

A representative comparison of theoretical and experimental Mach number profiles across the mixing duct is presented in Fig. 17. Experimental Mach numbers were determined from total pressure measurements, mixing duct wall pressures, and the assumption that static pressure was constant across the duct. At the upstream survey

station (Fig. 17a, X/D_B = 4), the experimental results indicate more rapid dissipation of the primary nozzle core flow than the theoretical prediction. Farther downstream (Fig. 17b, X/D_B = 8), experimental Mach number distributions are similar in shape but somewhat greater in magnitude than the theoretical predictions, which is attributed to the difference between measured and predicted wall pressures shown in Fig. 16.

4.3 THEORETICAL PARAMETRIC STUDY

4.3.1 Single-Stage Cold-Flow EPES

Typical single-stage EPES operating characteristics obtained with the unmodified performance analysis (see Section 2.2.1) are presented in Fig. 18. Results of computations for two EPES configurations that are identical in all respects except for the exhaust nozzle contraction ratio are presented along with engine cycle characteristics from Fig. 3. Comparison of Fig. 18b with Figs. 9c and 11 indicates quantitative differences but similar trends in the theoretical and experimental results for secondary-to-primary mass flow ratios where the secondary inlet Mach number (M_3) is subsonic. Therefore, it should be possible to obtain correct trends and determine effects of various parameters using the unmodified theoretical model with the realization that the theoretical predictions will probably be quantitatively incorrect.

Results of some of the theoretical investigations of various design parameters on EPES performance are summarized in Figs. 19 through 22. The theoretical effect of primary nozzle Mach number on EPES performance is illustrated in Fig. 19 for three exhaust nozzle contraction ratios (i.e. mixing duct exit Mach numbers). Limitations of the indicated EPES configurations with respect to engine cycle conditions required to be simulated is readily apparent. Although the afterburning performance line is within the range of some of the selected EPES operating conditions, only nonafterburning engine conditions with W_{EC} less than about 55 lbm/sec-ft^2 can be duplicated with any of these EPES configurations. The profound effect of exhaust nozzle contraction ratio on EPES performance is once again evident, but a comparison of Figs. 19a, b, and c reveals that the performance changes actually result from a coupled effect between primary nozzle Mach number and exhaust nozzle contraction ratio. For example, with M_B equal to 0.4 all of the EPES configurations evaluated (Fig. 19a) are characterized by a performance characteristic which has decreasing SPR with increasing W_{SC} with SPR approaching unity as W_{SC} approaches 50 lbm/sec-ft^2. However, with M_B equal to 0.6 (Fig. 19c), only EPES configurations with M_2 less than about 1.5 have the decreasing SPR with increasing W_{SC} operating characteristic. With M_2 greater than about 1.5, all of the EPES shown in Fig. 19c exhibit "high performance" characteristics with maximum values of SPR between 1.8 and 6.9 with W_{SC} in the 55 to 57 lbm/sec-ft^2 range. In the "high performance" cases, all of the EPES operating lines are characterized by choked secondary inlet conditions (M_3 = 1) at the maximum SPR point. Since SPR greater than unity is required with W_{SC}

23

greater than 30 lbm/sec-ft^2 for most engine conditions to be simulated, a criterion which distinguishes between "high" and "low" performance EPES would be useful in the EPES design process. Investigations of the momentum and continuity equations for the single-stage EPES (Section 2.2.1) established a relationship between the stream thrust (ϕ) at the primary nozzle and mixing duct exit that determines whether or not the high performance mode of operation will be achieved with a particular primary nozzle and exhaust nozzle contraction ratio. It was found (see Appendix C) that exhaust nozzle contraction ratios less than about 1.6 are required with Mach number 5 primary nozzles to achieve the high performance mode of operation. Furthermore, as the primary nozzle Mach number decreases, lower contraction ratio exhaust nozzles must be employed to achieve high performance operation.

One of the more significant EPES design requirements that has been largely ignored in previous investigations is the mixing duct length which affects both SPR and the exhaust nozzle velocity distribution. A series of calculations was made with an axisymmetric ducted turbulent mixing analysis (Ref. 20) to determine the degree of distortion in the mixing duct velocity field for representative single primary nozzle EPES geometries and operating conditions. Typical variations of the velocity differences between the centerline and the wall with mixing duct length are presented in Fig. 20. Duplication of exhaust velocity distributions (Ref. 24) with an EPES would require mixing duct length-to-diameter ratios in the range of 6 to 15 with a single primary nozzle for a low-bypass mixed-flow turbofan. The more uniform exit velocity conditions in turbojet tailpipes (Ref. 24) will require single primary EPES with mixing ducts from 8 to 20 diameters in length. Since potential EPES applications will be limited in some wind tunnel model applications to mixing duct lengths in the 4 to 6 diameter range, the theoretical results confirm that single primary nozzle EPES are not of practical interest.

Theoretical effect of the primary-to-secondary total temperature ratio (T_{T_2}/T_{T_3}) on EPES performance is presented in Fig. 21 for two representative high-performance single-stage EPES configurations. In both cases, increasing the temperature of the driving fluid decreases W_{SC} at a fixed value of SPR, which is opposite to the change required to simulate more of the engine operating conditions. Therefore, low primary-to-secondary total temperature ratio EPES are necessary if the maximum coverage of the engine simulation requirements is to be achieved.

4.3.2 Two-Stage EPES

A number of exploratory calculations were made to determine if significant EPES performance benefits could be achieved with two-stage ejector systems. Investigations were limited to two-stage units because of the excessive overall length that would be

24

associated with a larger number of stages. No simple geometry optimizing relationship was devised for the two stage system; however, the low performance/high performance modes of operation, which were observed in the single-stage EPES results, were also noted in the two-stage systems.

Pumping characteristics of the two-stage EPES configuration with the highest performance capability of those evaluated is shown in Fig. 22. While the two-stage EPES typically produced higher overall pressure ratio (SPR), maximum secondary flows (W_{SC}) were only 70 to 90 percent of the maximum flows obtained with a high performance single-stage EPES (e.g., Fig. 12). The most obvious advantage of the staged system is the additional flexibility in operating performance range for a given system which can be achieved by varying the total pressure in the driving nozzles. Through a judicious choice of geometry for the two stages, it may be possible to operate the simulator over the range of conditions indicated by the shaded performance band in Fig. 22.

Since only a limited number of two-stage EPES configurations were considered, it is possible that some other combination of geometric variables might produce performance gains over those presented in Fig. 22. However, because of the additional length requirements and the probability that maximum secondary flows will still be less than high-performance single-stage systems, it is felt that staged EPES do not warrant further consideration.

4.4 IMPACT OF RESULTS ON EPES APPLICATIONS

Results from both the theoretical and experimental studies reported herein indicate that practical EPES units can be designed that will provide flow conditions representative of afterburning aircraft turbine engines and nonafterburning turbojet engines operating at supersonic flight conditions where W_{EC} is less than about 45 to 50 lbm/sec-ft^2 (Fig. 23). Simulation of subsonic/transonic nonafterburning engine operation, for which W_{EC} is greater than 50 lbm/sec-ft^2, will require the use of some augmentation scheme in conjuction with the basic EPES unit. For example, to simulate the extreme, rated power turbine engine conditions considered with the experimentally evaluated seven-conical-nozzle cluster EPES installed in a wind tunnel model, it would be necessary to remove from 40 to 50 percent of the flow captured by the inlet through the model support strut. However, the seven-nozzle EPES configuration is somewhat less than optimum in terms of primary nozzle configuration. An increase in the mixing duct-to-primary nozzle area ratio (A_B/A_2) could potentially increase inlet pumping capability by perhaps as much as 10 percent with a corresponding decrease in the auxiliary pumping requirements. Nevertheless, EPES performance potentials from the present studies are found to be in substantial agreement with previous investigations (Refs. 1 and 13 and Table 1).

The present studies also indicate that only single-stage EPES equipped with a multinozzle injector are consistent with length-to-diameter ratios comparable to high-performance turbine engines (L/D between 3 and 6) if uniform exhaust flow conditions must be produced with the simulator. However, the operating characteristics of an EPES with a fixed geometry will generally be compatible with only a limited range of engine operating characteristics, thus requiring a variable-area ratio configuration with inlet bleed capacity to cover a large range of flight conditions.

5.0 CONCLUSIONS

Theoretical and experimental investigations of ejector-powered engine simulators (EPES) applicable to wind tunnel models of turbine engine aircraft are being conducted at the Arnold Engineering Development Center. Conclusions from the initial investigations described in this report are:

1. Exhaust nozzle contraction ratio (or mixing duct exit Mach number) has the most significant effect on EPES performance. Maximum performance is obtained with mixing duct exit Mach numbers between 0.5 and 0.7.

2. Primary nozzle area ratio (or primary nozzle design Mach number) has only a second-order effect on EPES performance over the range of area ratios investigated.

3. Only single-stage EPES equipped with multinozzle injectors appear to have the capability of producing uniform exhaust flow conditions with overall length-to-diameter ratios (3 to 6) comparable to high-performance turbine engines.

4. The EPES configurations evaluated do not have the potential for simulating all conditions of interest without some augmentation. While conditions representative of current technology turbine engine afterburning operation are within EPES performance capabilities, only nonafterburning, rated power engine conditions corresponding to supersonic flight can be produced without an auxiliary system to remove a portion of the inlet flow.

5. Primary nozzle-to-mixing duct inlet spacing (L/D_B, Fig. 4) had an insignificant effect on EPES performance.

6. The current analytical model modified to consider primary nozzle separation agrees well with experiment for configurations in which the mixing duct was of sufficient length for complete mixing to occur.

6.0 RECOMMENDATIONS FOR ADDITIONAL WORK

Initial investigations of ejector-powered engine simulators (EPES) described in this report have suggested the need for further work in the following areas:

1. Additional experimental investigations are required to

   a. Optimize the configuration of primary driving nozzles,

   b. Determine the effect of flow distortions representative of aircraft inlet ducts on EPES performance, and

   c. Evaluate the effect of auxiliary bleed ports on EPES performance.

2. The existing theoretical EPES performance analysis should be modified to include considerations of primary nozzle separation and secondary inlet flow distortion at choking conditions. A parametric study should then be accomplished with the modified analysis to confirm the conclusions of this report with respect to optimum performance EPES geometries.

3. A wind tunnel program should be conducted with an EPES-equipped high-performance aircraft model to demonstrate proof-of-concept and to determine if simulation of representative engine-airframe interactions can be improved with an EPES driven with unheated air.

4. Further investigations are required to define parameters which must be simulated to obtain precise values of afterbody drag with wind tunnel models. One of the major areas of uncertainty at the present time which can have a profound effect on EPES design procedures is the degree to which engine exhaust velocity and temperature and their distributions must be duplicated with engine simulators.

REFERENCES

1. Grunnet, James L. "Designing Jet Aircraft Wind-Tunnel Test Programs with Propulsion System Simulation." Journal of Aircraft, Vol. 8, No. 6, June 1971.

2. Goldsmith, E. L. and Carter, E. C. "A Review of Methods Used for the Representation of Engine Flows in High Speed Wind Tunnel Testing." Royal Aircraft Establishment TR72012 (AD903522), April 1972.

3. Melzer, E. and Wulf, R. "Use of Model Engines (V/S/CTOL)." Paper No. 6, AGARD-R-601, April 1973.

4. "AGARD Conference Proceedings No. 150 on Airframe/Propulsion Interference." AGARD-CP-150, March 1975.

5. Bittrick, W. C. "Installation Benefits of the Single-Engine Exhaust Nozzle of the YF-16." Paper No. 74-1101 presented at the AIAA/SAE 10th Propulsion Conference, October 1974.

6. Keating, J. "Airframe/Propulsion System Integration Analysis Using the Propulsion Simulation Techniques." Paper No. 16, AGARD CP71, January 1971.

7. Steffen, F. W., et al. "A Turbojet Simulator for Mach Numbers up to 2.0." ASME Paper 72GT89, ASME/Gas Turbine and Fluids Engineering Conference, March 1972.

8. Delaney, B. R. and West, H. "Multimission Aircraft Propulsion Simulator Initial Aero/Mechanical Test Results and Evaluation." AFAPL-TR-73-77, December 1973.

9. Wilcox, F. A. and Chamberlin, R. "Reynolds Number Effects on Boattail Drag of Exhaust Nozzles from Wind Tunnel and Flight Tests." Paper No. 21, AGARD-CP-150, March 1975.

10. Wood, M. N. and Howard, J. B. W. "The Development of Injector Units for Jet-Lift Engine Simulation on Low-Speed-Tunnel Models." Aeronautical Research Council R&M No. 3464, February 1965.

11. Sacerdote, U. "Techniques for the Simulation of Jet-Lift Engines in Wind-Tunnel Models of V/STOL Aircraft." Paper No. 22 AGARDograph 103, October 1965.

12. Margason, R. J. and Gentry, Garl L. "Static Calibration of an Ejector Unit for Simulation of Jet Engines in Small-Scale Wind-Tunnel Models." NASA TND-3867, March 1967.

13. Wood, M. N. "The Use of Injector Units for Engine Simulation on Wind Tunnel Models at High Speeds." Royal Aircraft Establishment TR71215, November 1971.

14. Lockwood, V. E. and Matarazzo, A. "Subsonic Wind-Tunnel Investigation of a Twin-Engine Attack Airplane Model Having Nonmetric Powered Nacelles." NASA TN-D-7752, November 1974.

15. Roffe, G. and Miller, G. "Similarity Parameters and Their Sensitivity for Transonic Airframe Exhaust Nozzle Interactions." AFFDL-TR-73-9, January 1973.

16. Compton, W. B., III. "An Experimental Study of Jet Exhaust Simulation Parameters." NASA TMX-69961, August 1973.

17. Bergman, D. "Effects of Engine Exhaust Flow on Boattail Drag." Journal of Aircraft, Vol. 8, No. 6, June 1971, pp. 434-439.

18. Robinson, C. E. and High, M. D. "Exhaust Plume Temperature Effects on Nozzle Afterbody Performance over the Transonic Mach Number Range." AEDC-TR-74-9 (AD781377), July 1974.

19. Bauer, R. C., Matkins, E. H., and Barebo, R. L. "A Theoretical and Experimental Study of a Jet Stretcher Diffuser System." AEDC-TR-72-26 (AD738646), March 1972.

20. Peters, C. E. "Turbulent Mixing and Burning of Coaxial Streams inside a Duct of Arbitrary Shape." AEDC-TR-68-270 (AD680397), January 1969.

21. Clippinger, R. F. "Supersonic Axially Symmetric Nozzles." Ballistic Research Laboratories Report 794, December 1951.

22. Abernethy, R. B., et al., Pratt and Whitney Aircraft, and Thompson, J. W. Jr., ARO, Inc. "Handbook, Uncertainty in Gas Turbine Measurements." AEDC-TR-73-5 (AD770069), November 1973.

23. Farley, J. M. and Campbell, C. E. "Performance of Several Method-of-Characteristics Exhaust Nozzles." NASA TN D-293, October 1960.

24. Wehofer, S. and Matz, R. J. "Turbine Engine Exhaust Nozzle Performance with Nonuniform Inlet Flow." AEDC-TR-75-82 (ADA014261), August 1975.

25. Smith, R. E. Jr. and Matz, R. J. "A Theoretical Method of Determining Discharge Coefficients for Venturis Operating at Critical Flow Conditions." American Society of Mechanical Engineers, Journal of Basic Engineering, Vol. 84, Series D., No. 4, December 1962, pp. 434.

26. Johnson, R. C. "Real-Gas Effects in Critical Flow through Nozzles and Tabulated Thermodynamic Properties." NASA TN D-2565, January 1965.

27. Hess, J. L. and Smith, A. M. O. "Calculation of Potential Flow about Arbitrary Bodies." Progress in Aeronautical Sciences, Edited by D. Kuchemann, Vol. 8, Pergamon Press, New York, 1967.

28. Moretti, G., et al. "Supersonic Flow about General Three-Dimensional Bodies." General Applied Science Laboratory Report ASD-TR-67-727, 1961.
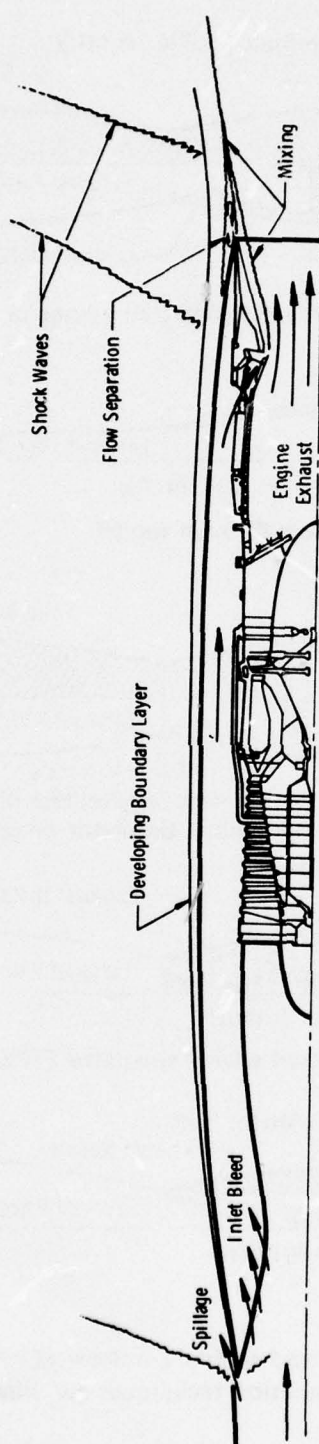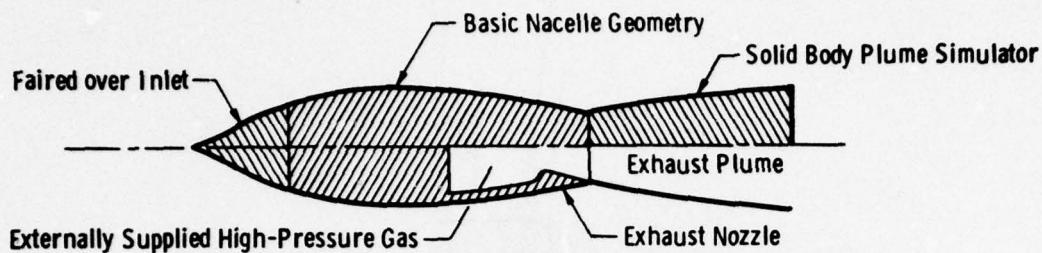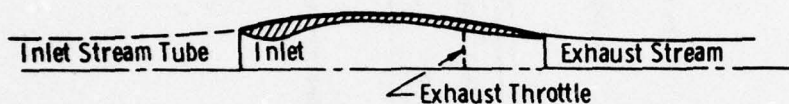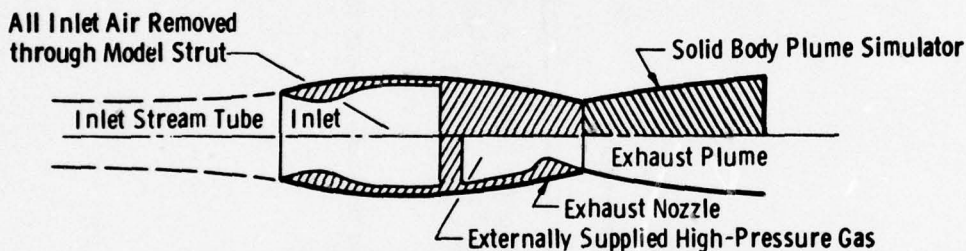
Figure 1. Major engine/airframe interaction areas for supersonic operation.
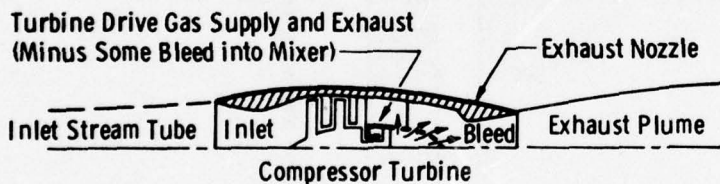
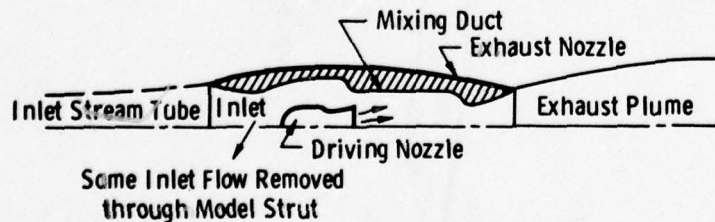a. Faired inlet model with solid plume simulator or pressure jet

b. Flow-through model

c. Pumped inlet with solid-plume simulator or pressure jet

d. Turbine-powered engine simulator (TPES)

e. Ejector-powered engine simulator (EPES)

Figure 2. Current engine simulation techniques for wind tunnel testing.

Simulation Requirements

▬ ▬ ▬ ▬ Nonafterburning Turbojet
▬ ▬ ▬ ▬ Nonafterburning Turbofan
▬▬▬▬▬▬ Afterburning (Both Cycles)
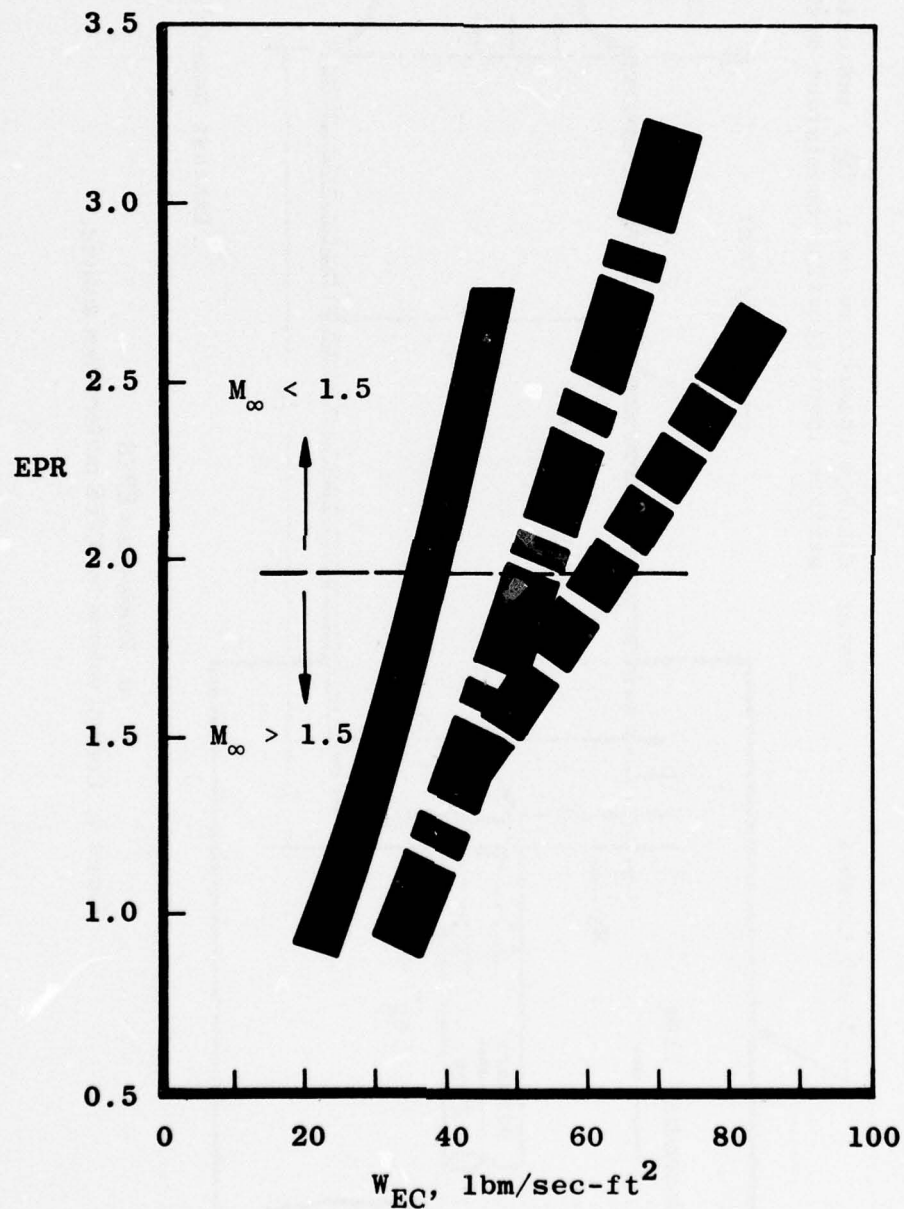
Figure 3. Pumping characteristics of current engine cycles at rated power conditions.

Note: Circled characters, e.g. ②, indicate control surface identification consistent with analysis.
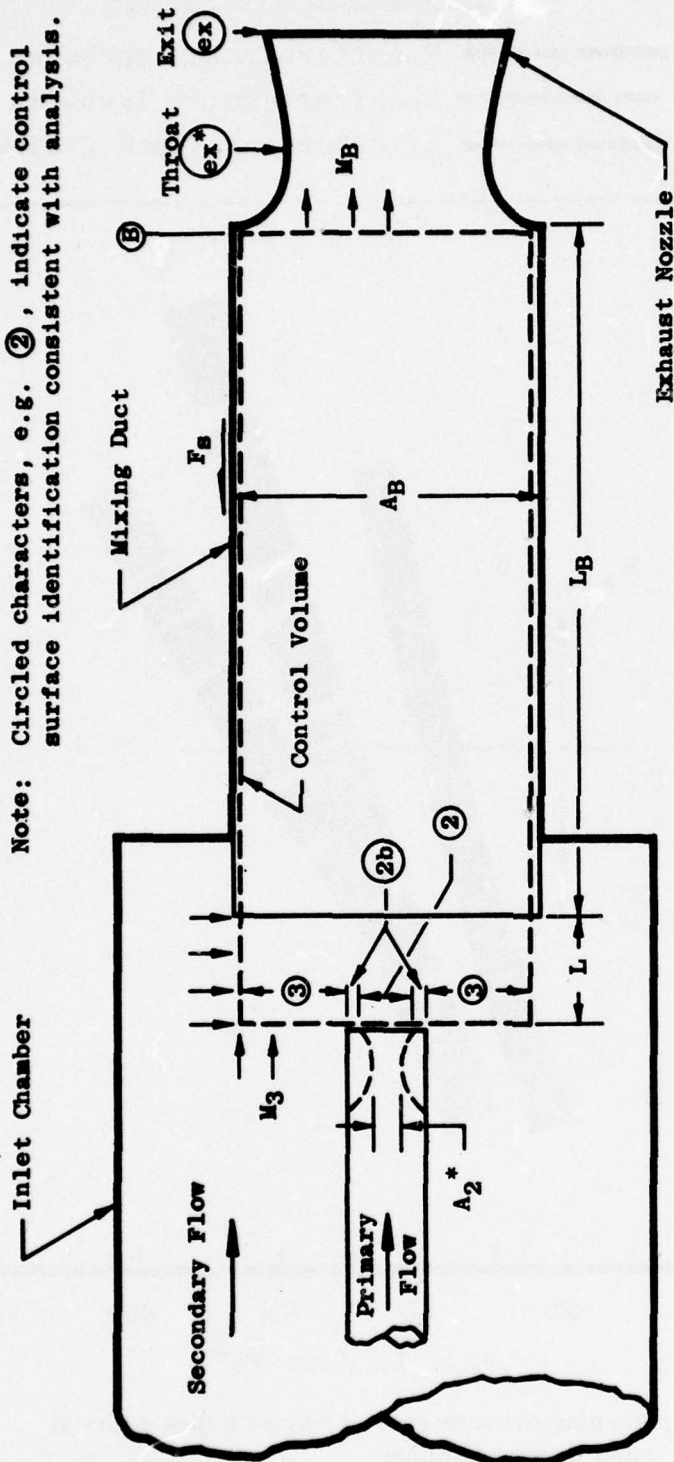
a. Single-stage EPES

Figure 4. Control volume for EPES performance analysis.
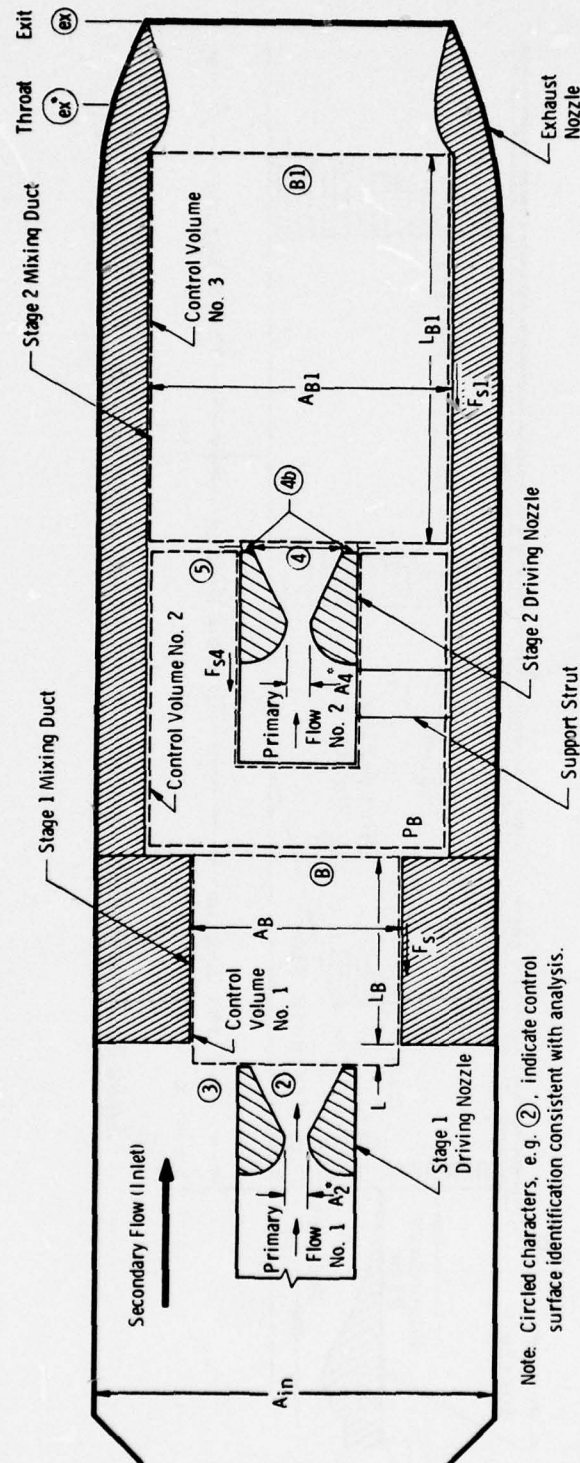
34

b. Two-stage EPES
Figure 4. Concluded.

Note: Circled characters, e.g. ②, indicate control surface identification consistent with analysis.

35

Figure 5. Flow process considered in the ducted mixing analysis.

Secondary Inlet Plenum (18.8 ID)

Flow Distributor (Perforated Plate, 80-percent Solidity)

Flow Smoothing Screens (3) (3-1/2 Mesh, 0.063 Wire Diam)
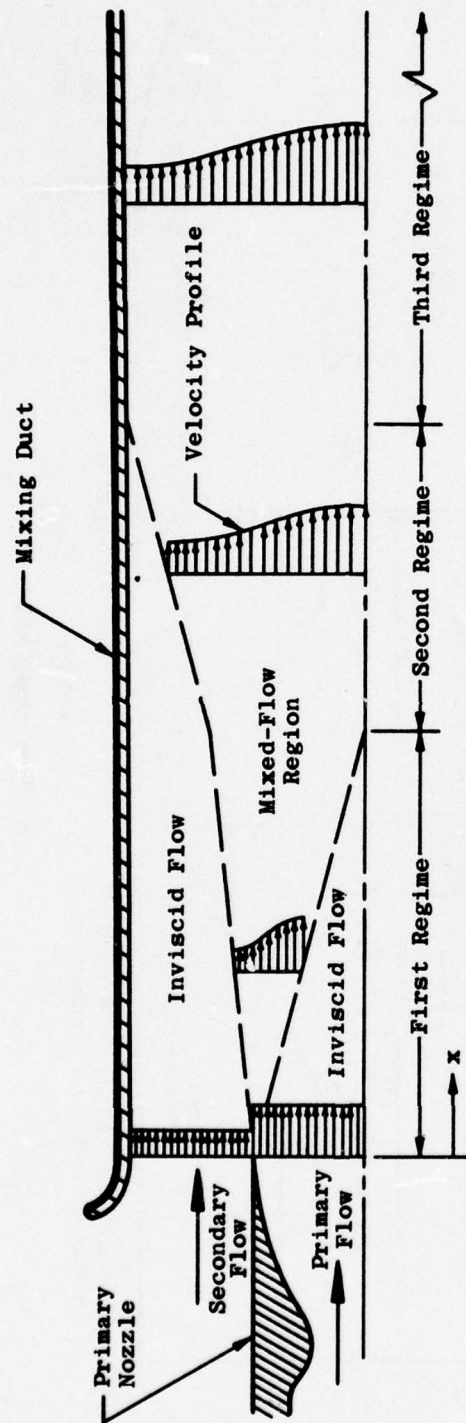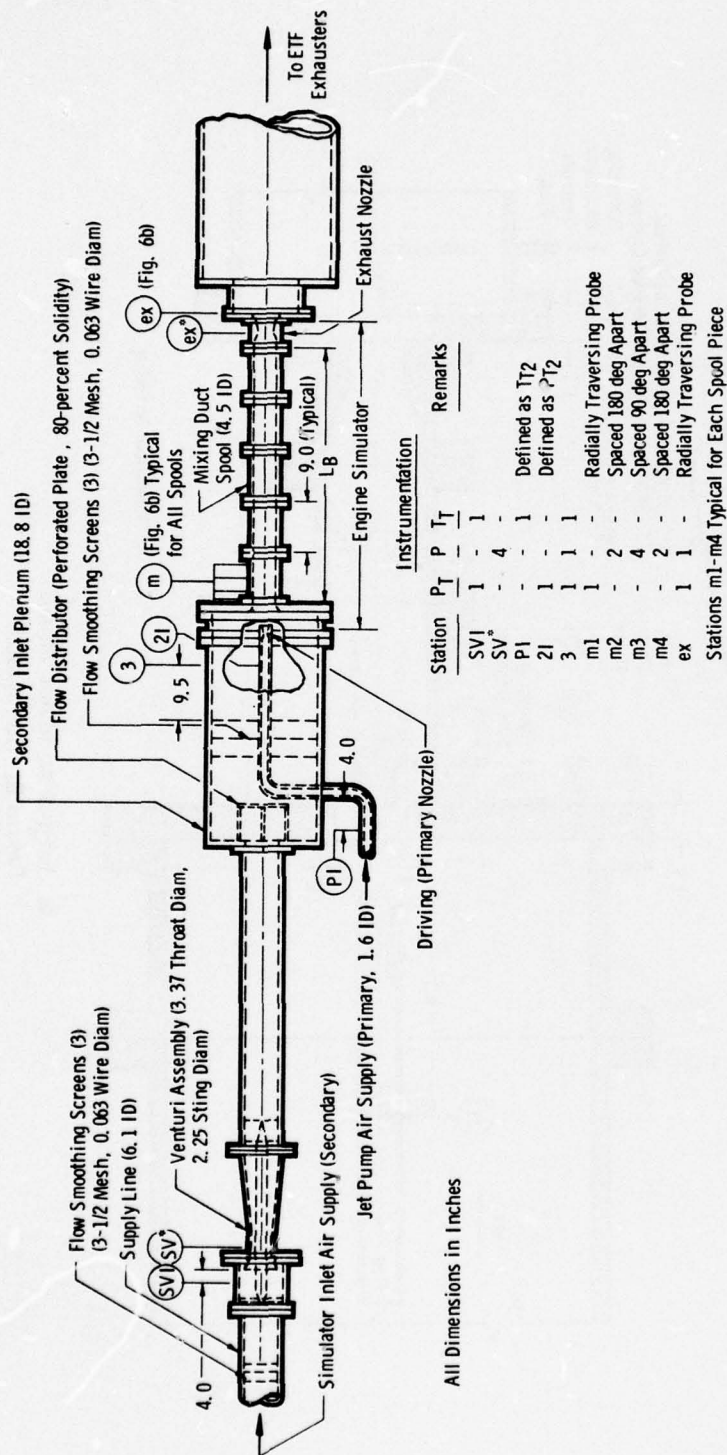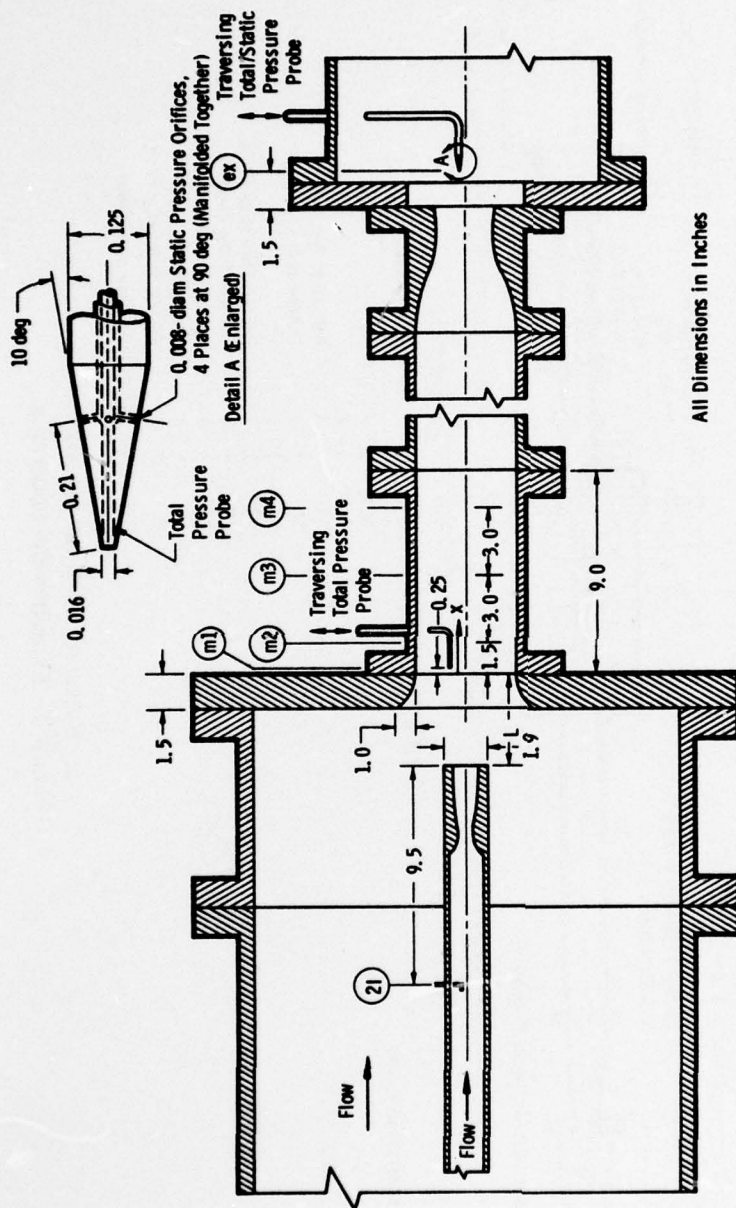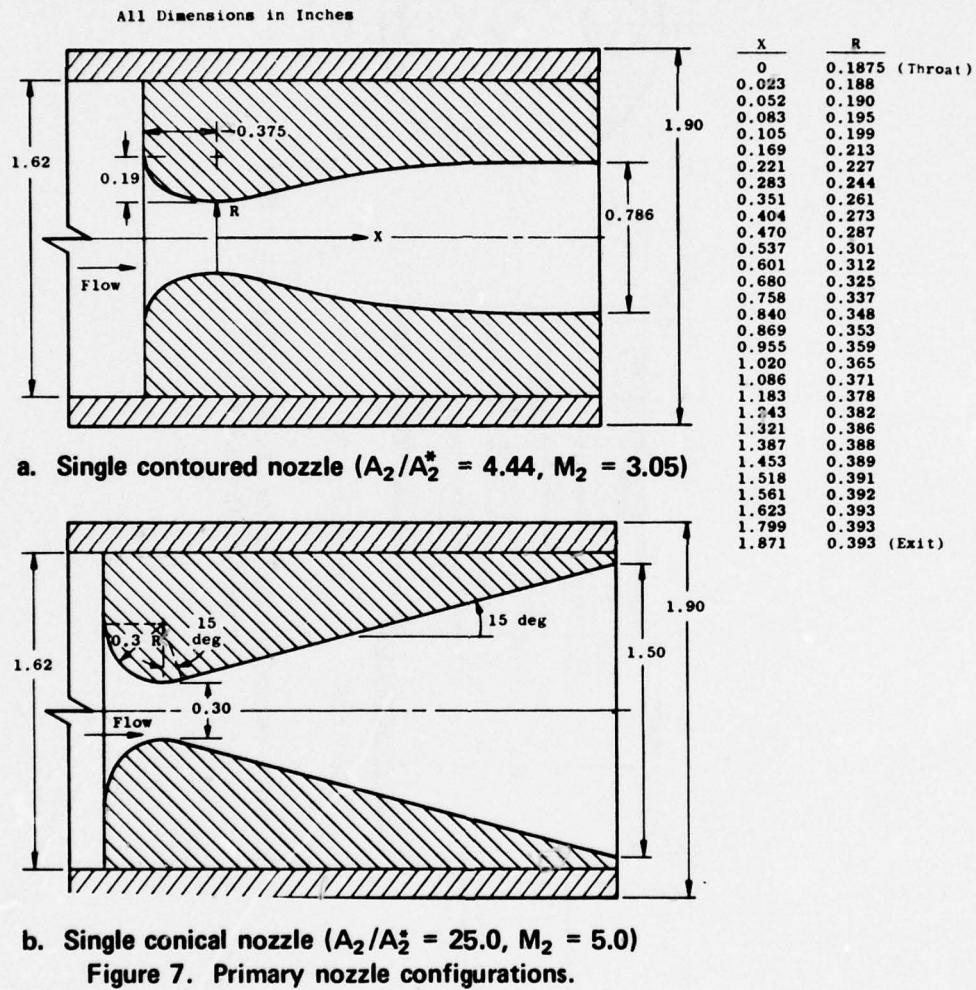
ex (Fig. 6b)

ex°

Exhaust Nozzle

m (Fig. 6b) Typical for All Spools

Mixing Duct Spool (4.5 ID)

9.0 (Typical)

L_B

Engine Simulator

21

3

9.5

4.0

Driving (Primary Nozzle)

P1

To ETF Exhausters

Instrumentation

Station	P_T	P	T_T		Remarks
SV1	1	-	-	1	
SV°	-	4	-	1	
P1	-	1	-	1	Defined as T_{T2}
21	1	1	1	1	Defined as P_{T2}
3	1	1	1	1	
m1	1	-	2	-	Radially Traversing Probe
m2	-	2	4	-	Spaced 180 deg Apart
m3	-	4	2	-	Spaced 90 deg Apart
m4	-	2	1	-	Spaced 180 deg Apart
ex	1	1	1	-	Radially Traversing Probe

Stations m1-m4 Typical for Each Spool Piece

Flow Smoothing Screens (3)
(3-1/2 Mesh, 0.063 Wire Diam)

Supply Line (6.1 ID)

SV1 SV°

Venturi Assembly (3.37 Throat Diam, 2.25 Sting Diam)

Jet Pump Air Supply (Primary, 1.6 ID)

Simulator Inlet Air Supply (Secondary)

4.0

4.0

All Dimensions in Inches

a. Research cell arrangement
Figure 6. Experimental apparatus.

37

b. Engine simulator details
Figure 6. Concluded.

38

All Dimensions in Inches

X	R	
0	0.1875	(Throat)
0.023	0.188	
0.052	0.190	
0.083	0.195	
0.105	0.199	
0.169	0.213	
0.221	0.227	
0.283	0.244	
0.351	0.261	
0.404	0.273	
0.470	0.287	
0.537	0.301	
0.601	0.312	
0.680	0.325	
0.758	0.337	
0.840	0.348	
0.869	0.353	
0.955	0.359	
1.020	0.365	
1.086	0.371	
1.183	0.378	
1.243	0.382	
1.321	0.386	
1.387	0.388	
1.453	0.389	
1.518	0.391	
1.561	0.392	
1.623	0.393	
1.799	0.393	
1.871	0.393	(Exit)

a. Single contoured nozzle ($A_2/A_2^* = 4.44$, $M_2 = 3.05$)

b. Single conical nozzle ($A_2/A_2^* = 25.0$, $M_2 = 5.0$)
Figure 7. Primary nozzle configurations.

39

c. Seven conical nozzle cluster ($A_2/A_2^* = 25.0$, $M_2 = 5.0$)
Figure 7. Concluded.

Section AA

All Dimensions in Inches

40

X	R
0	2.250 (Inlet)
0.20	2.250
0.40	2.237
0.60	2.220
0.80	2.196
1.00	2.172
1.20	2.142
1.40	2.108
1.60	2.069
1.80	2.024
2.00	1.976
2.20	1.920
2.40	1.854
2.60	1.773
2.80	1.697
3.00	1.605
3.20	1.525
3.40	1.463
3.60	1.415
3.80	1.377
3.95	1.365 (Throat)
4.20	1.369
4.40	1.372
4.60	1.376
4.80	1.379
5.00	1.382
5.20	1.385
5.40	1.389
5.70	1.393 (Exit)

All Dimensions in Inches
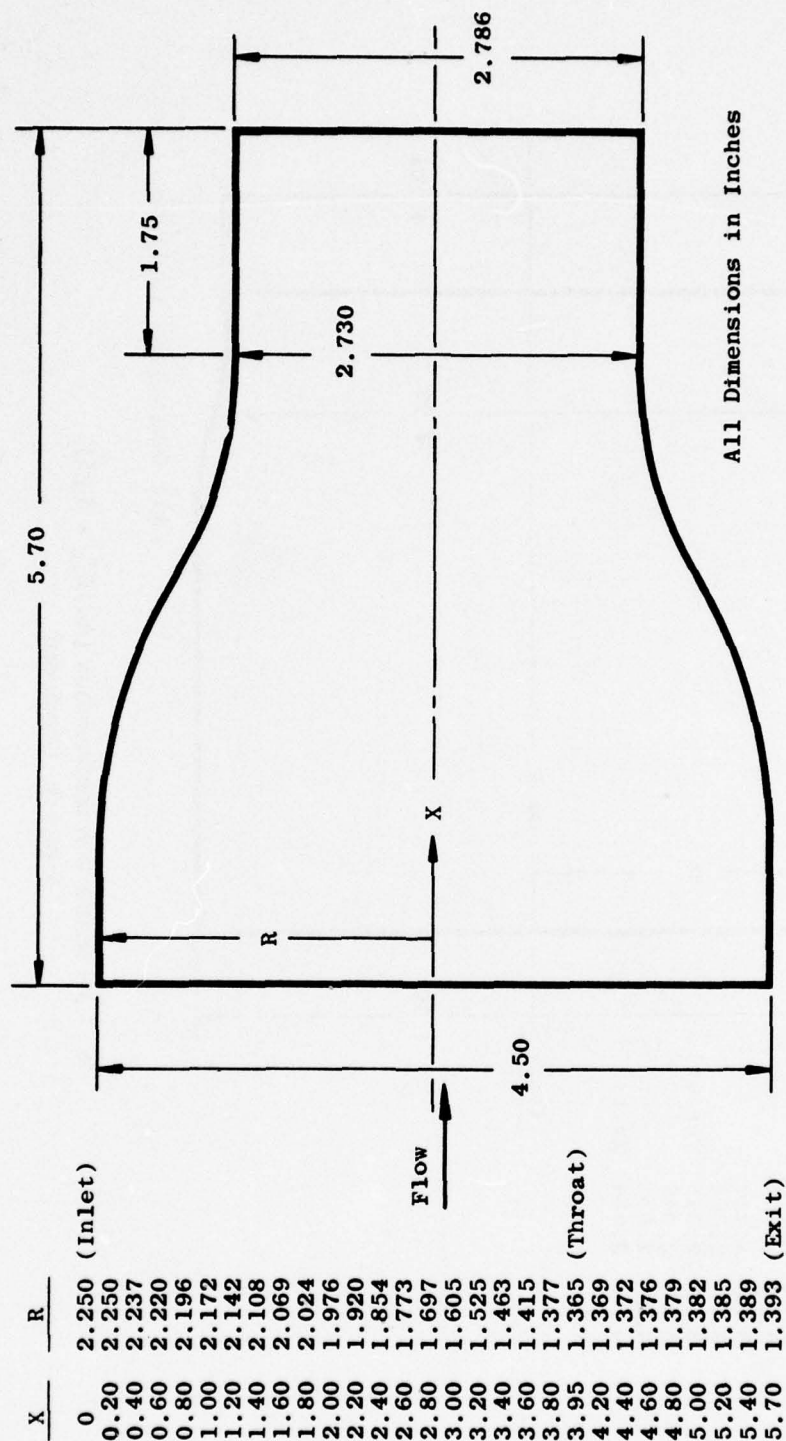
a. High contraction configuration ($A_B/A_{ex}^* = 2.72$)

Figure 8. EPES exhaust nozzles investigated.

41

| X	R	
0	2.250	(Inlet)
2.90	2.250	
3.00	2.242	
3.25	2.188	
3.50	2.117	
3.75	2.064	
3.95	2.045	(Throat)
4.10	2.048	
4.20	2.051	
4.30	2.054	(Exit)

All Dimensions in Inches
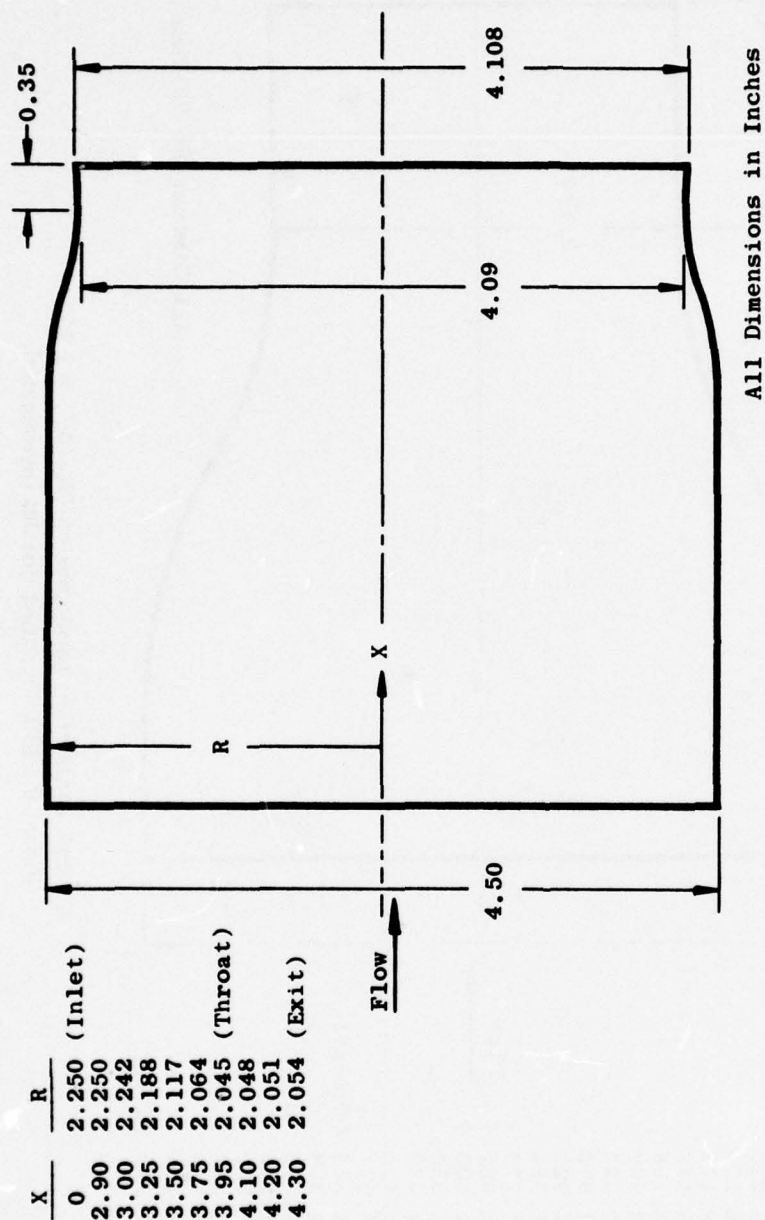
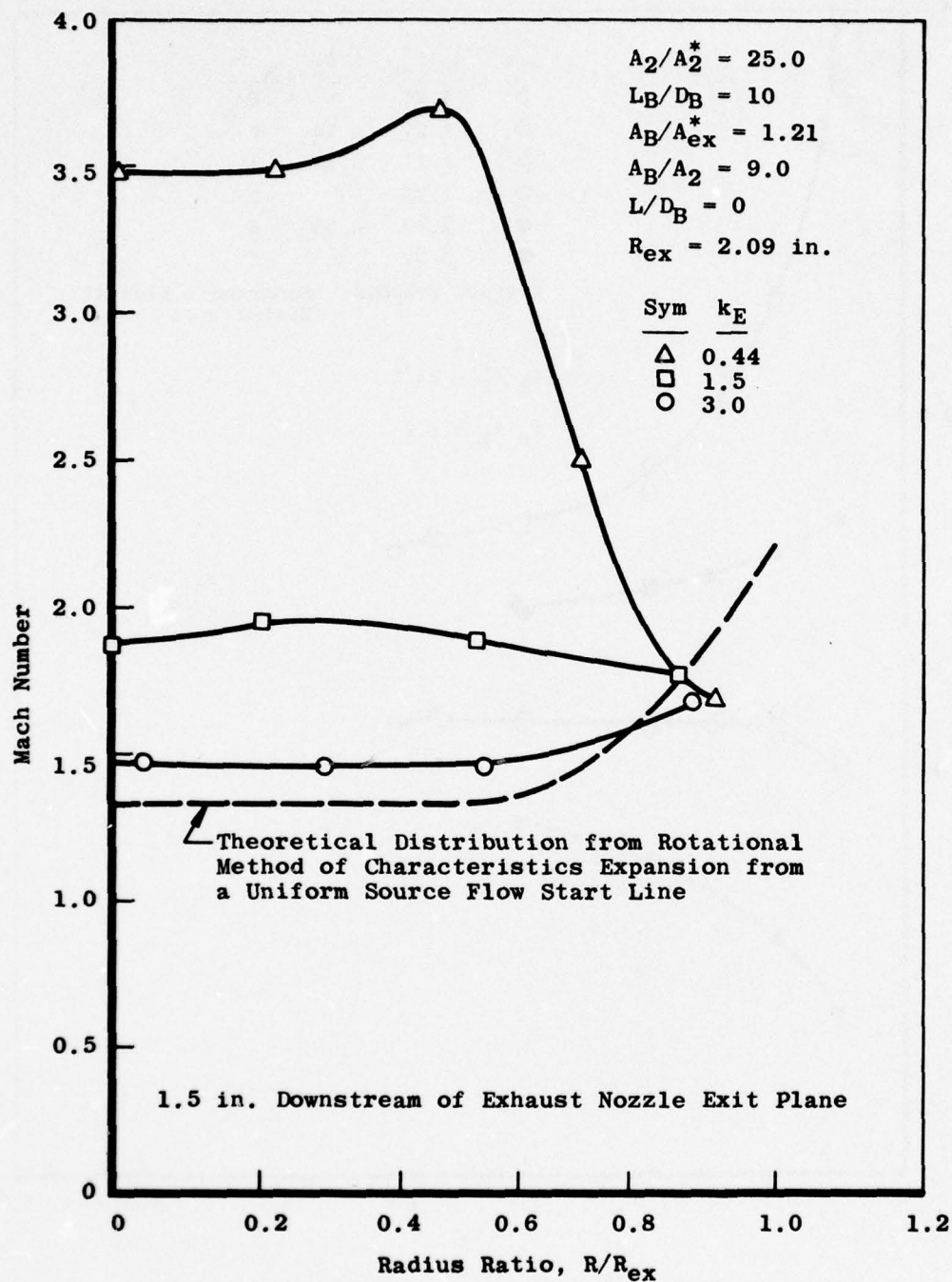b. Low contraction configuration ($A_B/A_{ex}^* = 1.21$)

Figure 8. Concluded.

42
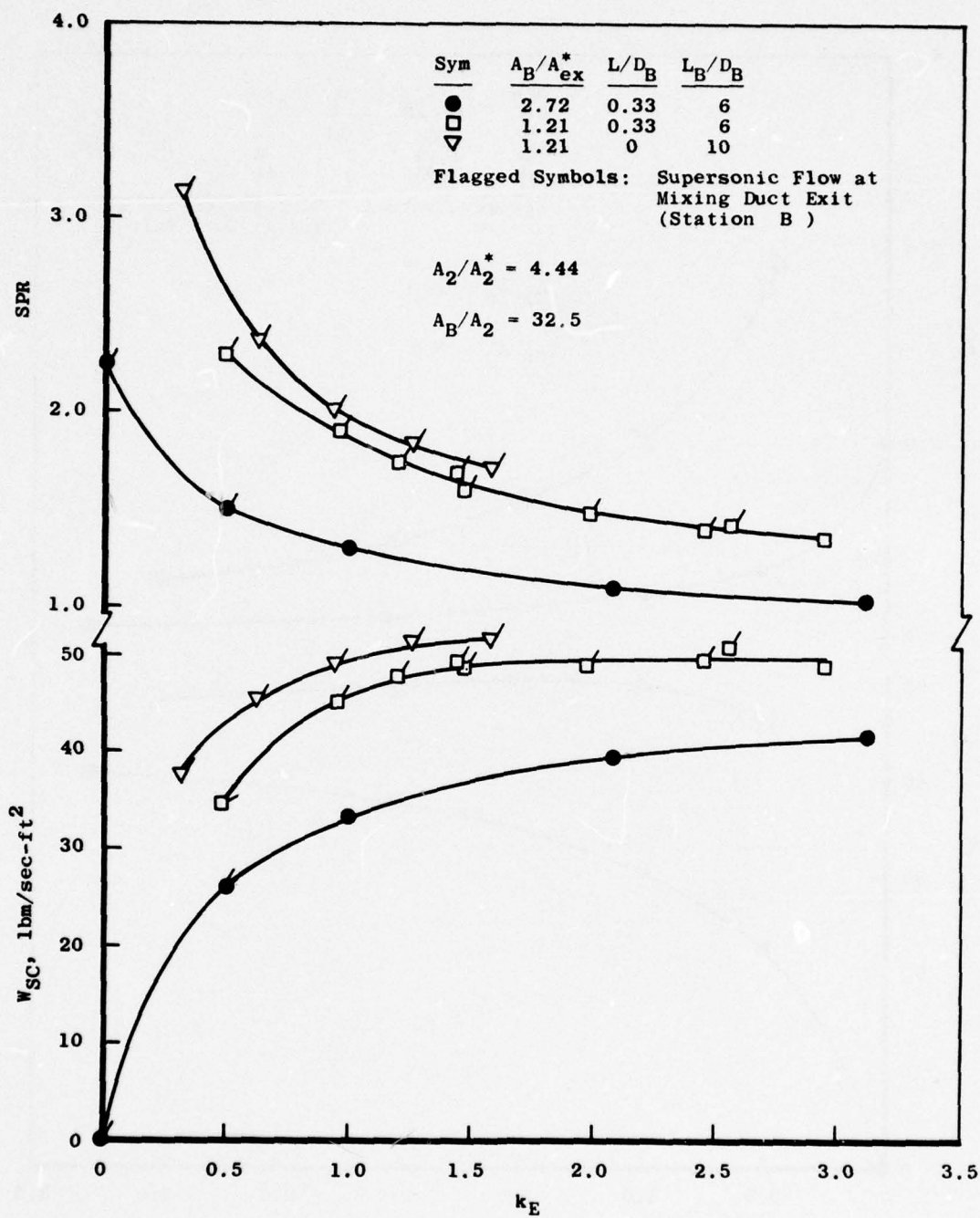
a. Single contoured primary nozzle configurations
Figure 9. Experimental EPES pumping characteristics.
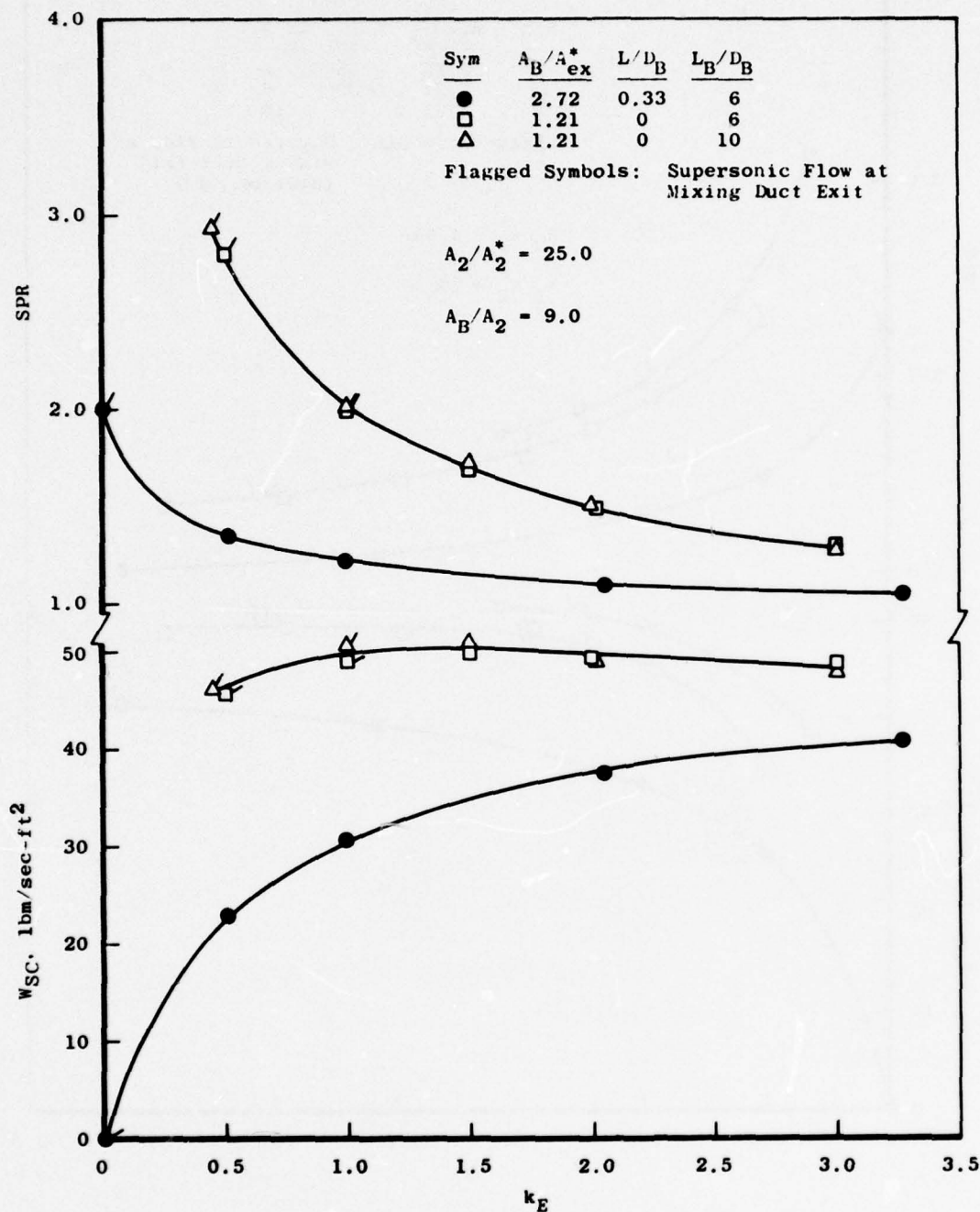
b. Single conical primary nozzle configurations
Figure 9. Continued.

44
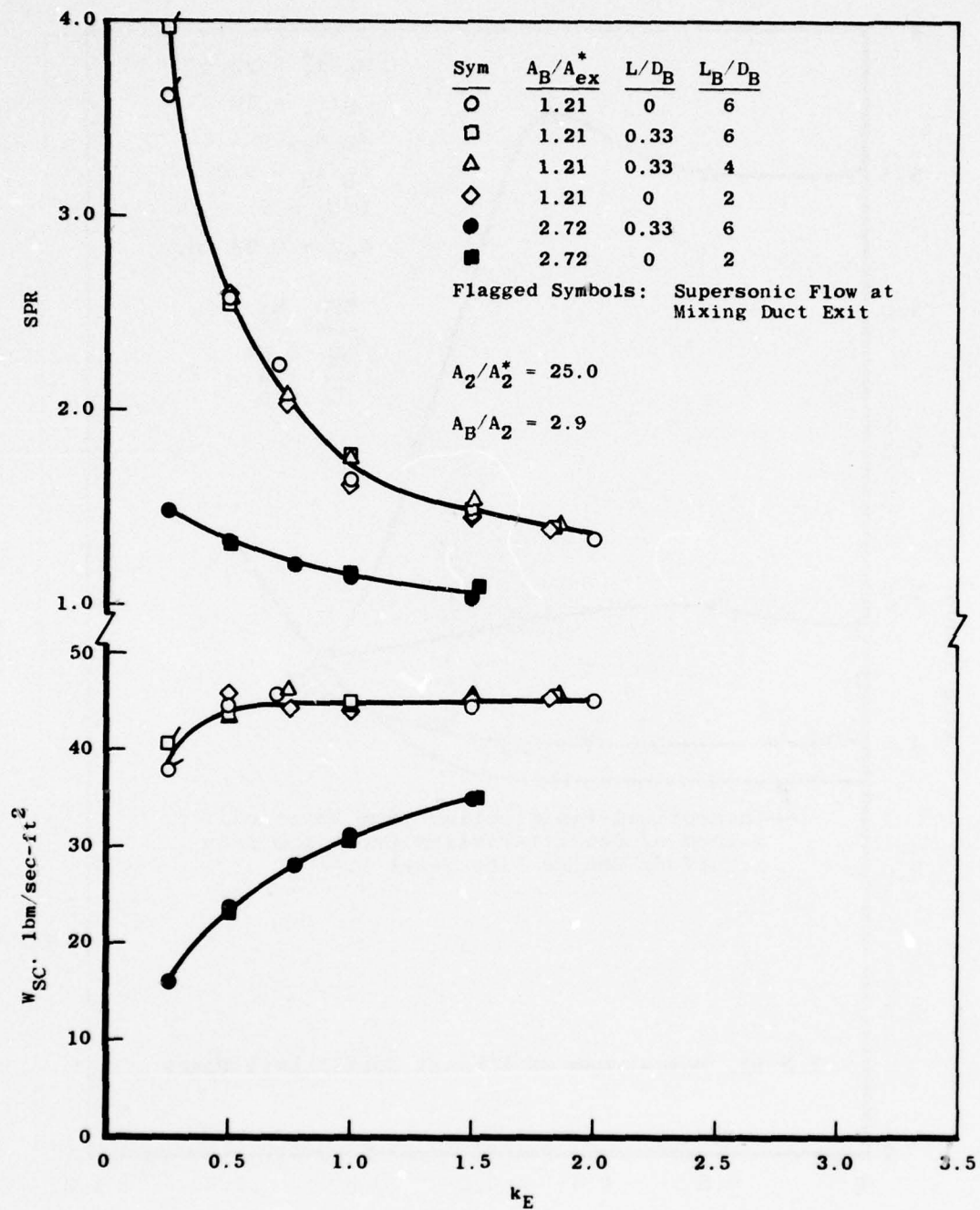
c. Seven conical primary nozzle configurations
Figure 9. Concluded.

45

a. Single conical primary nozzle configuration

Figure 10. Typical Mach number distributions in the low contraction exhaust nozzle plume.
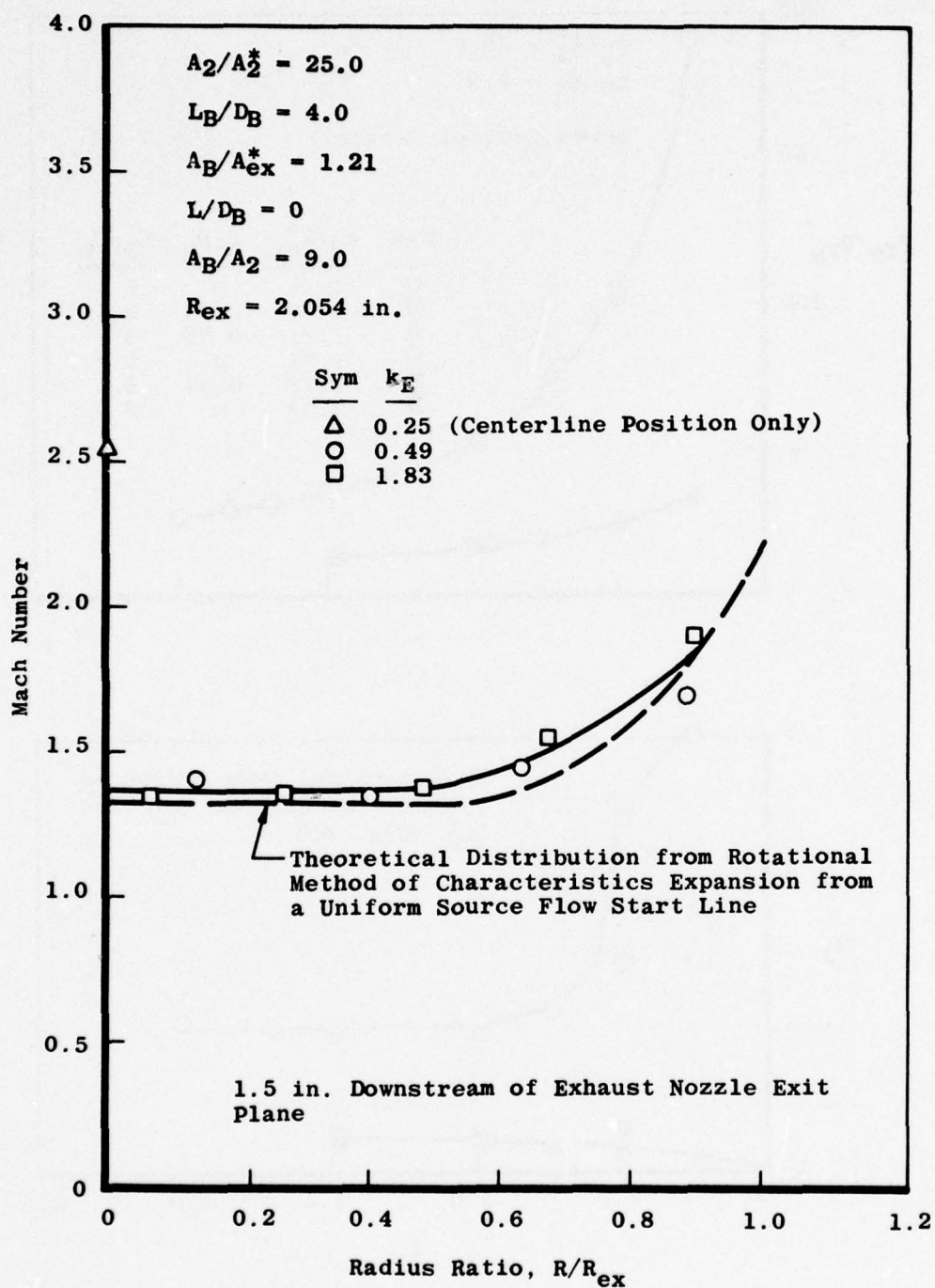
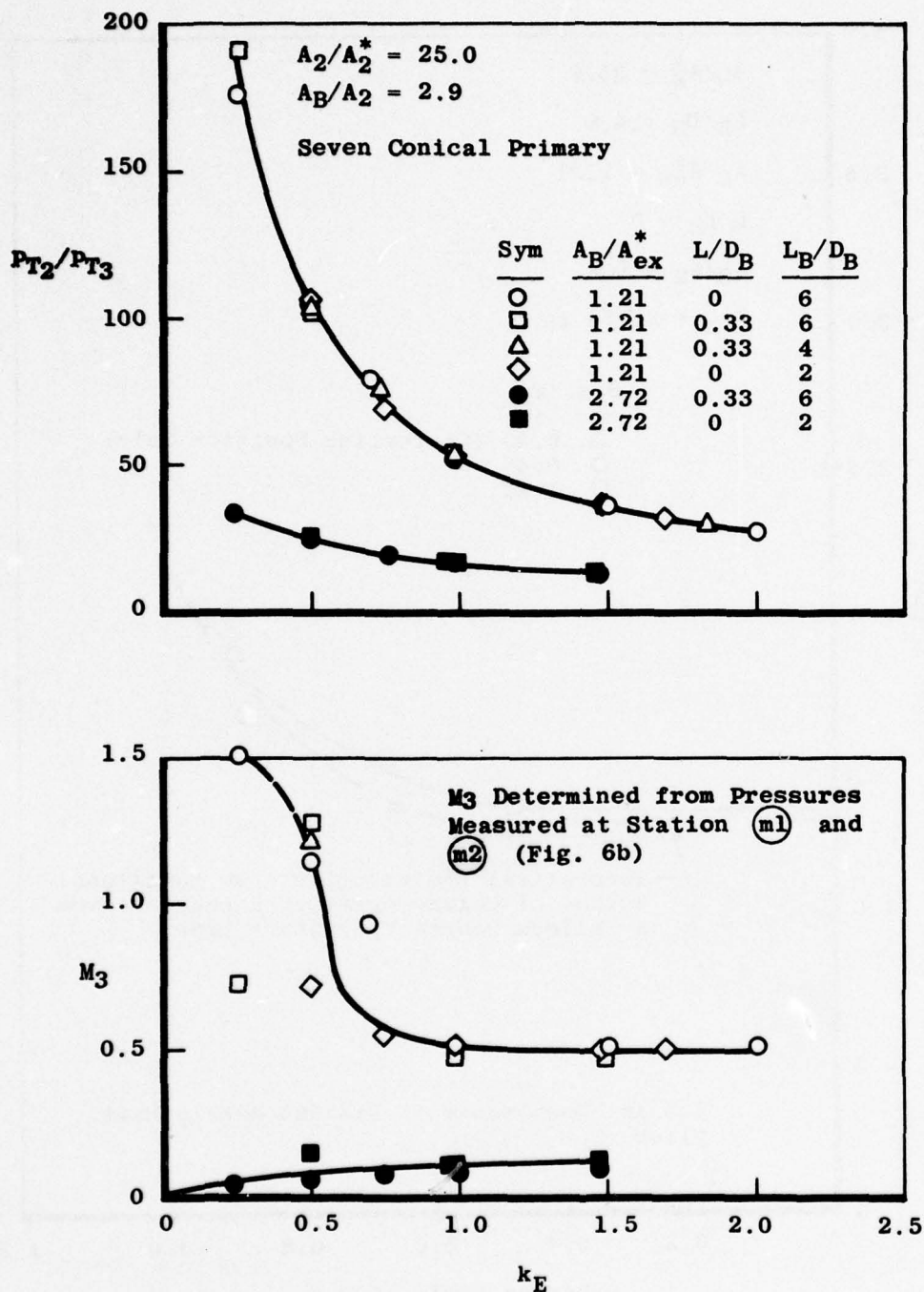b. Multiple conical primary nozzle configuration
Figure 10. Concluded.

Figure 11. Variation of P_{T_2}/P_{T_3} and M_3 with k_e for seven nozzle primary.

EPES Configurations

Sym	A_2/A_2^*	Primary Nozzles	A_B/A_2	A_B/A_{ex}^*
○	25.0	7	2.9	1.21
●	25.0	7	2.9	2.72
□	25.0	1	9.0	1.21
■	25.0	1	9.0	2.72
△	4.44	1	32.5	1.21
▲	4.44	1	32.5	2.72

Simulation Requirements (Fig. 3)

— — — — Nonafterburning Turbojet
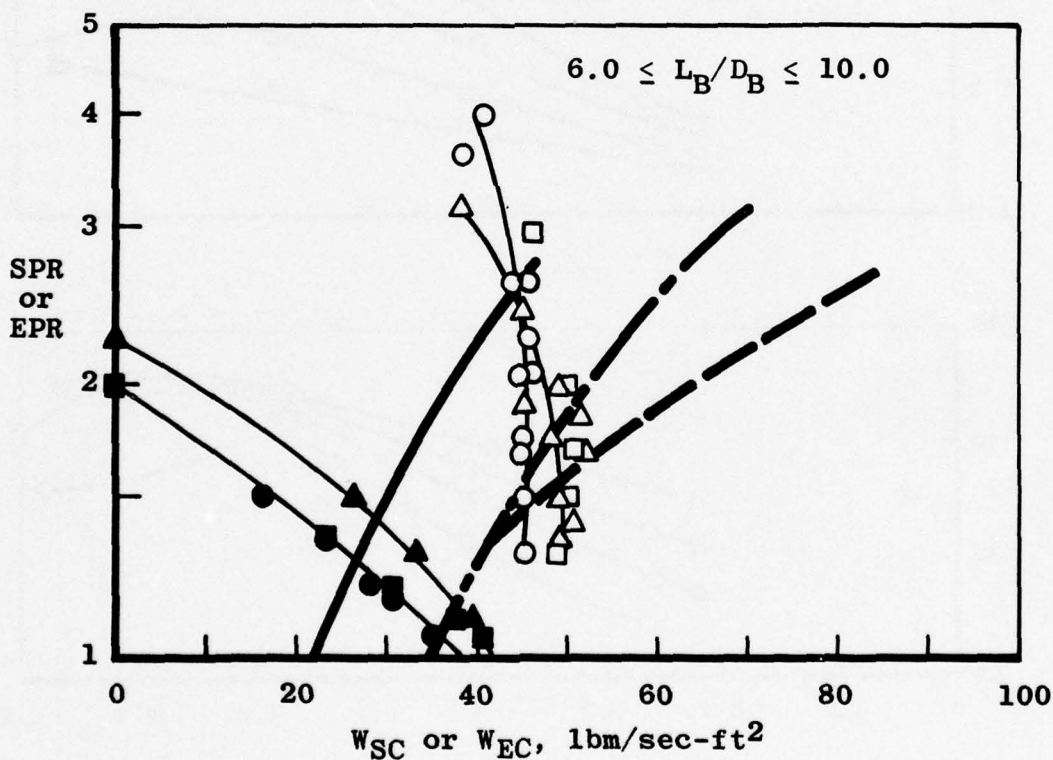— — — Nonafterburning Turbofan
———— Afterburning (Both Cycles)

Figure 12. Comparison of EPES experimental performance and engine simulation requirements.
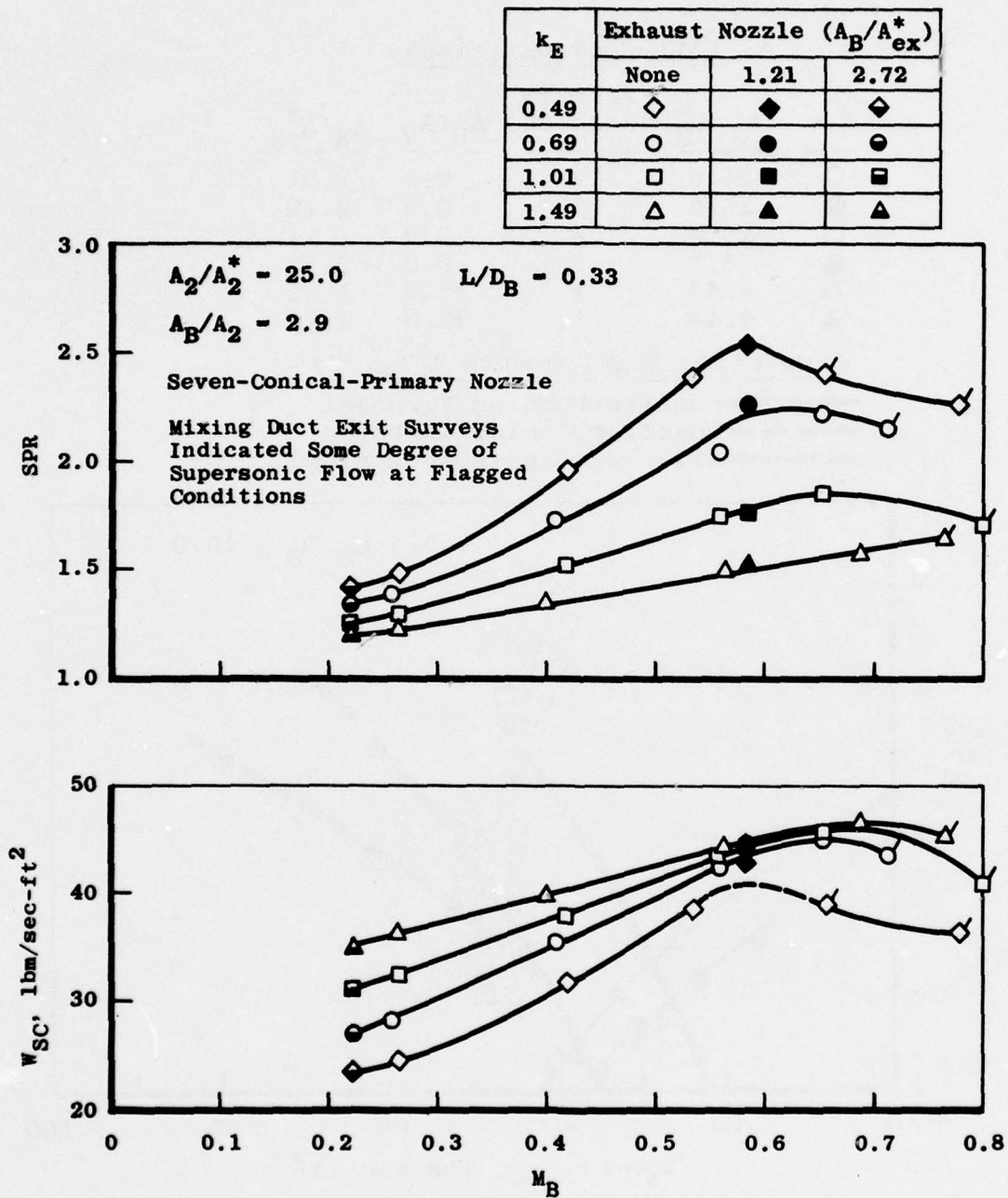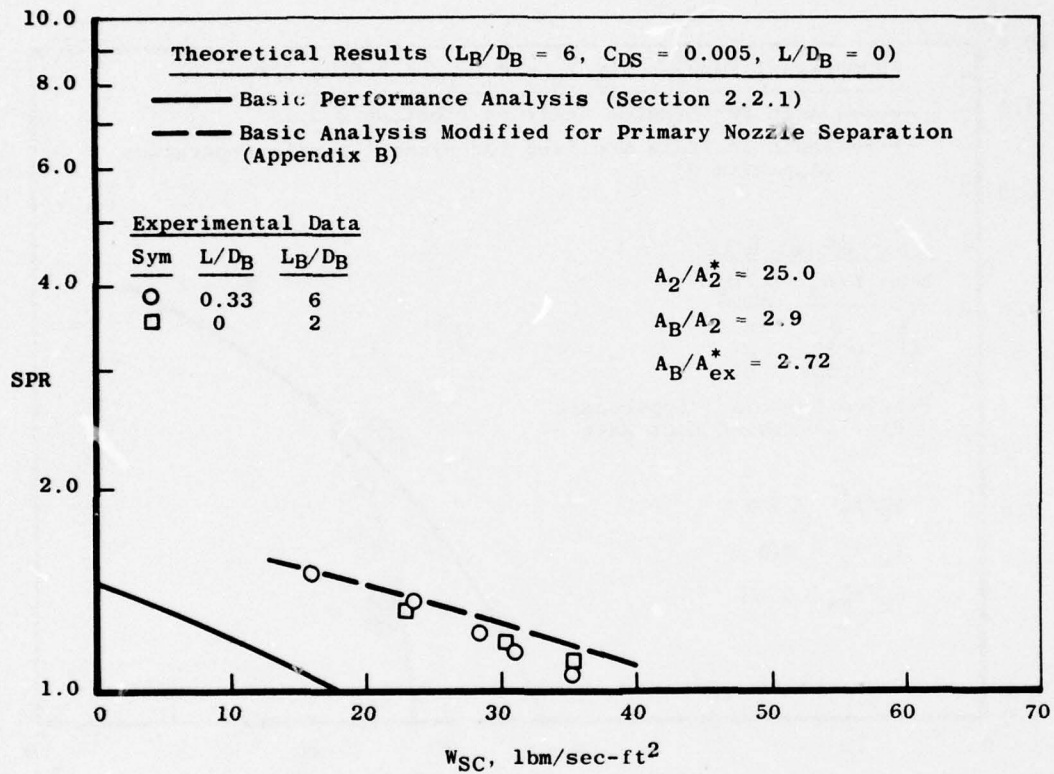
49

k_E	Exhaust Nozzle (A_B/A^*_{ex})		
	None	1.21	2.72
0.49	◇	◆	◈
0.69	○	●	◐
1.01	□	■	◲
1.49	△	▲	◮

$A_2/A^*_2 = 25.0$ $L/D_B = 0.33$

$A_B/A_2 = 2.9$

Seven-Conical-Primary Nozzle

Mixing Duct Exit Surveys
Indicated Some Degree of
Supersonic Flow at Flagged
Conditions

Figure 13. Variation of SPR and W_{SC} with mixing duct exit
Mach number.

50

a. With high contraction ($A_B/A_{ex}^* = 2.72$) exhaust nozzle installed
Figure 14. Comparison of theoretical and experimental pumping characteristics from the multiple conical primary nozzle EPES.
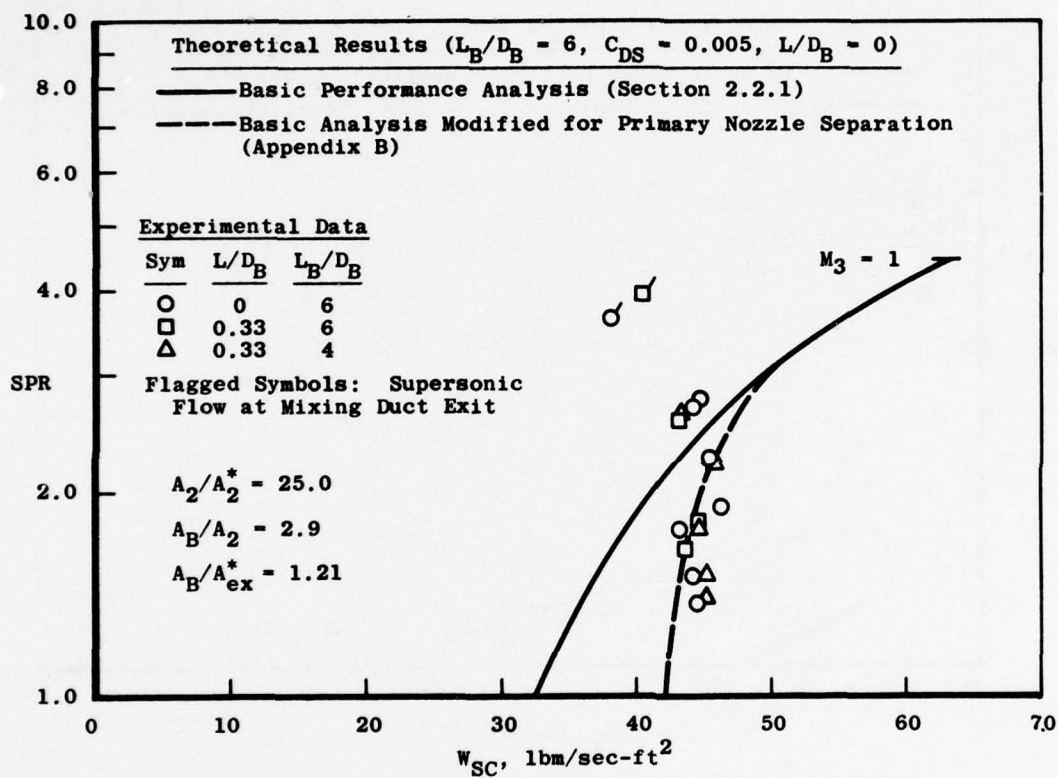
b. With low contraction ($A_8/A_{ex}^* = 1.21$) exhaust nozzle installed
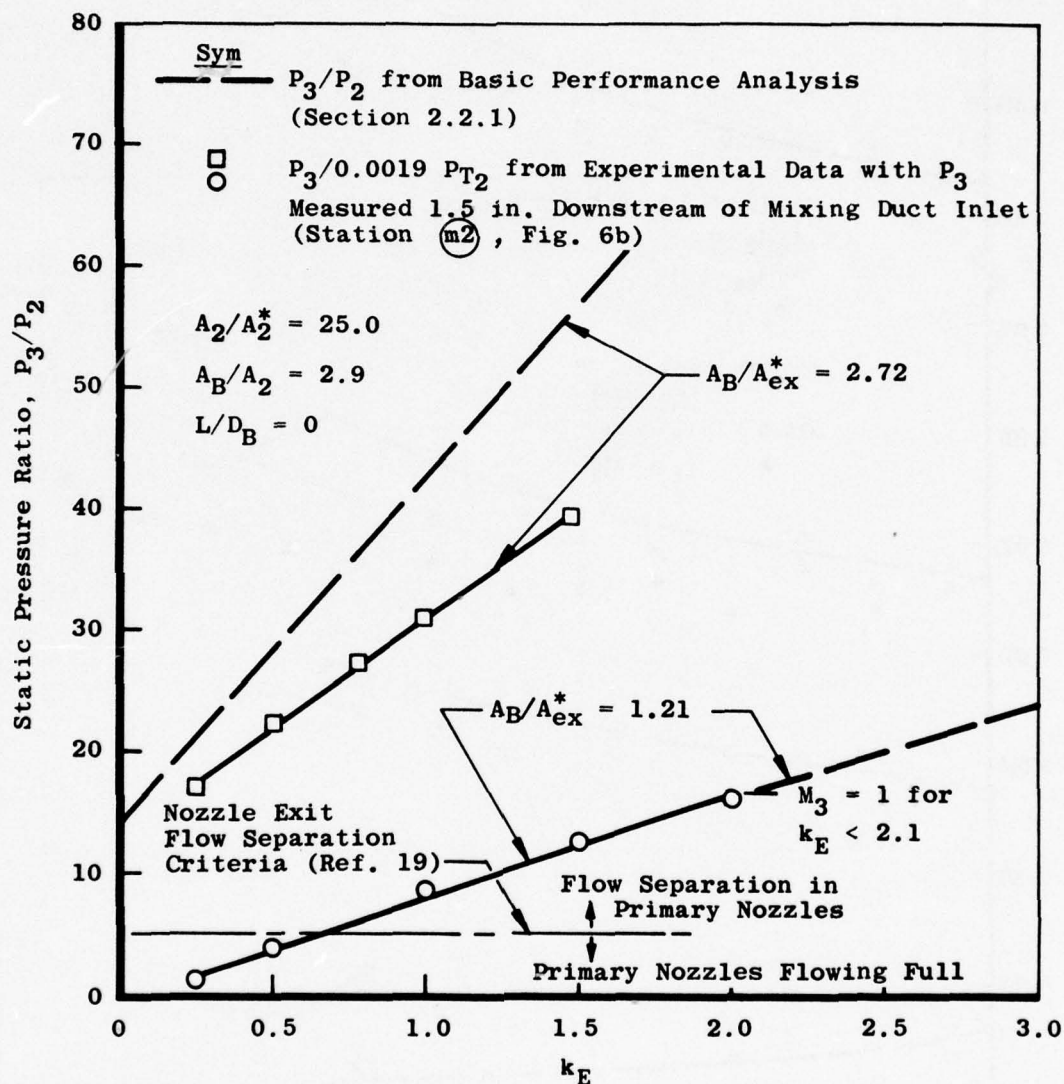
Figure 14. Concluded.

Figure 15. Variation of theoretical and experimental mixing duct
inlet-to-primary nozzle exit static pressure ratio with k_E
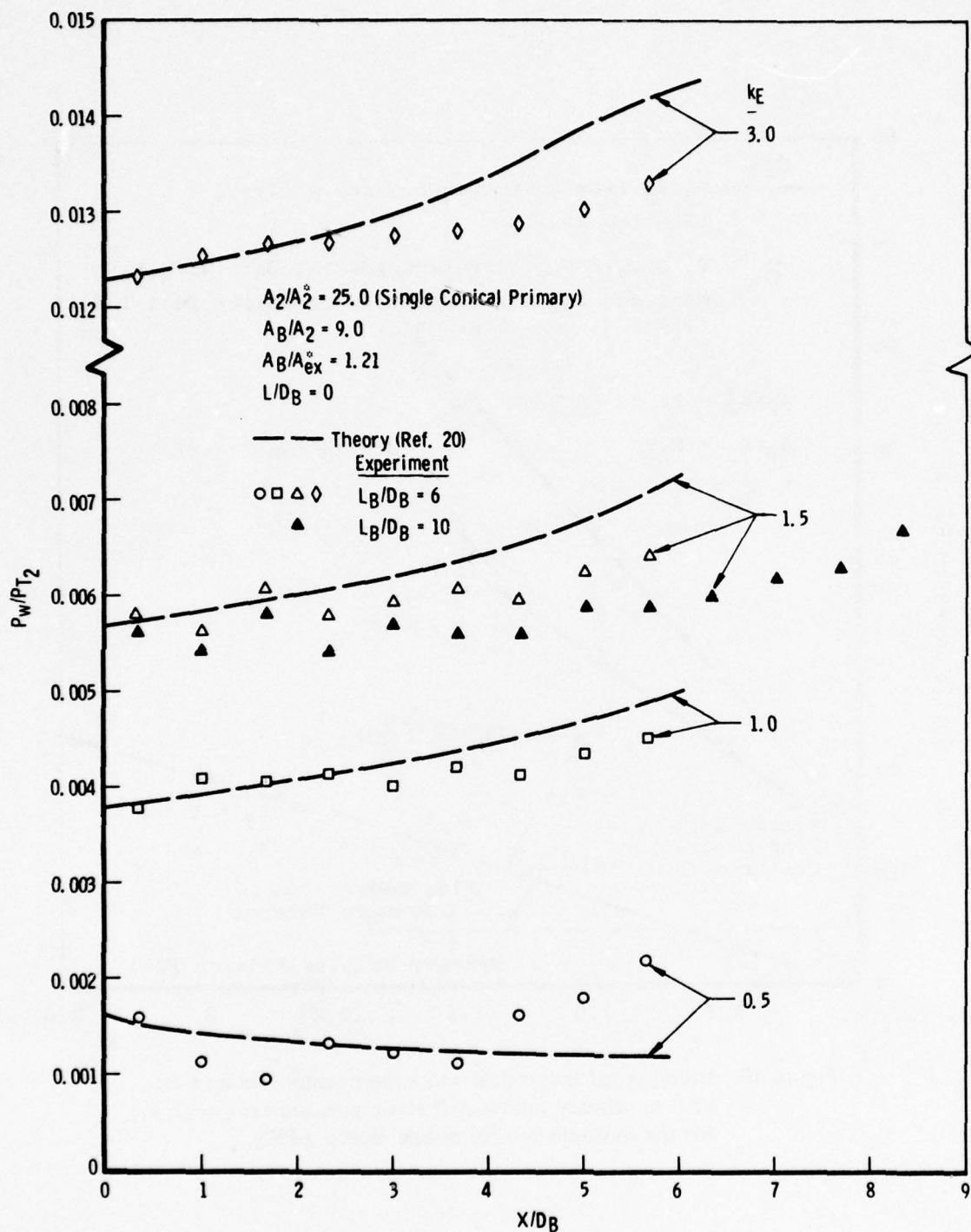for the multiple conical nozzle cluster EPES.

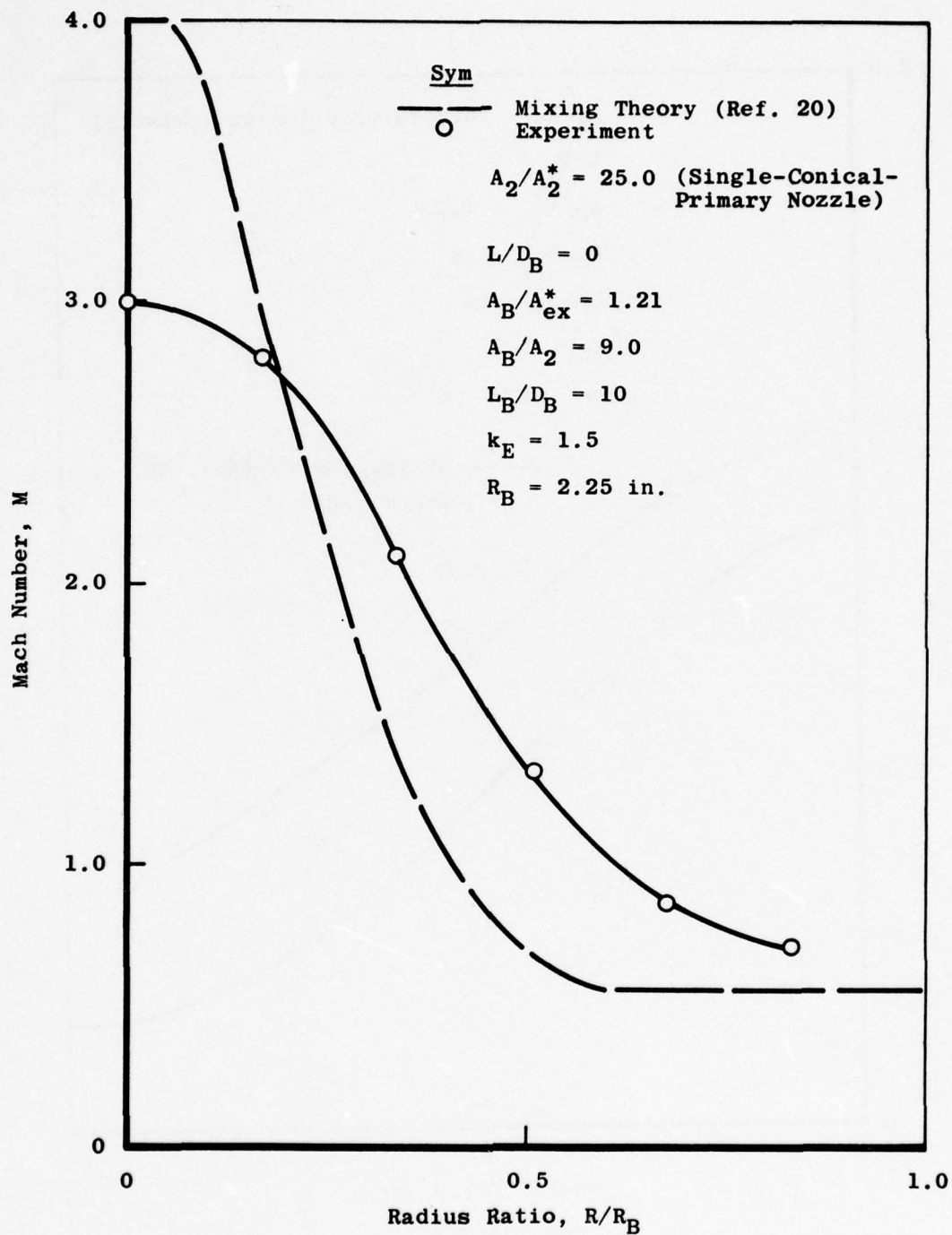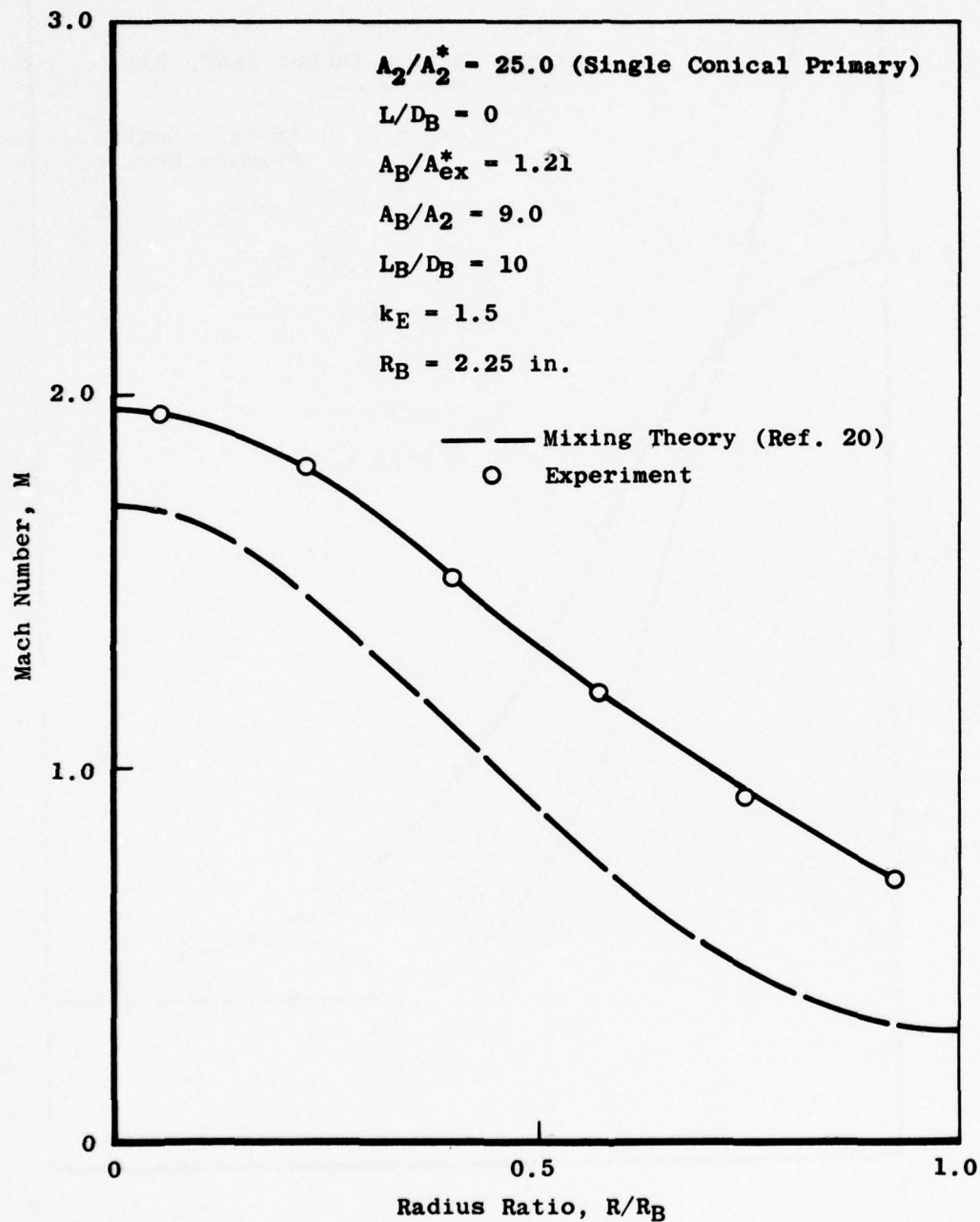Figure 16. Typical streamwise mixing duct wall pressure distributions.

a. $X/D_B = 4$

Figure 17. Typical mixing duct Mach number profiles.

b. $X/D_B = 8$
Figure 17. Concluded.

Basic Geometry for Theoretical EPES Configurations

$A_2/A_2^* = 4.23 \ (M_2 = 3.0)$ $C_{DS} = 0.005$
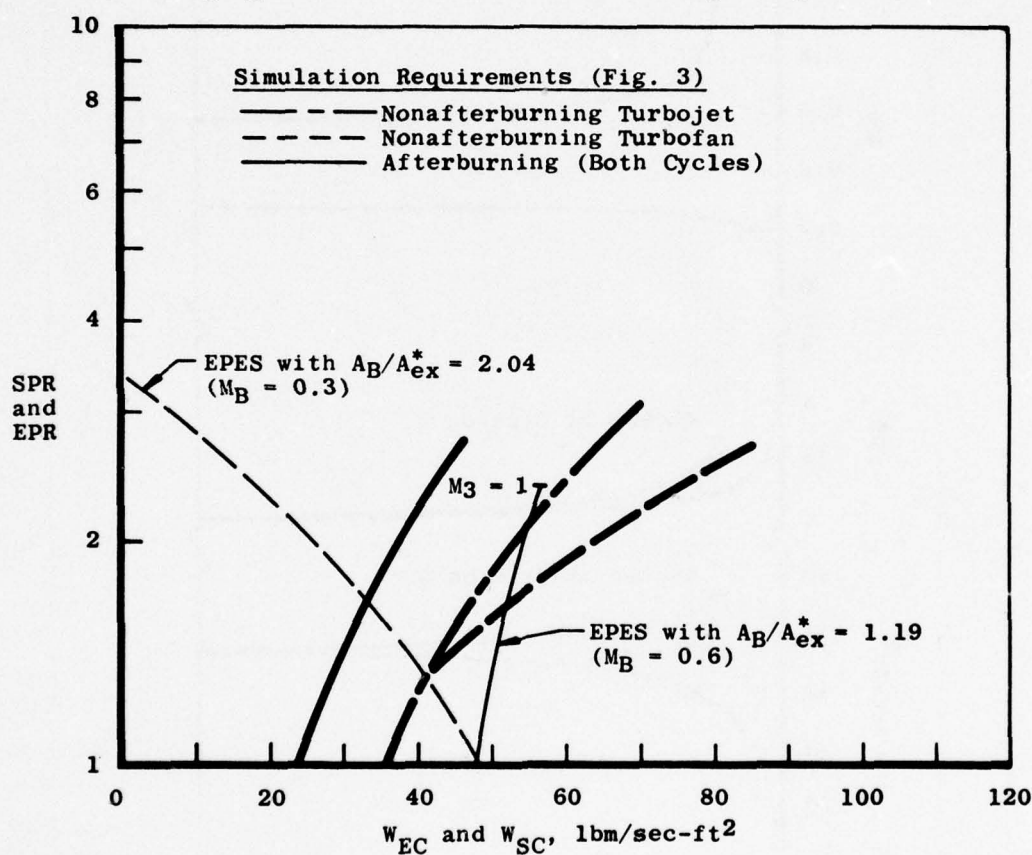
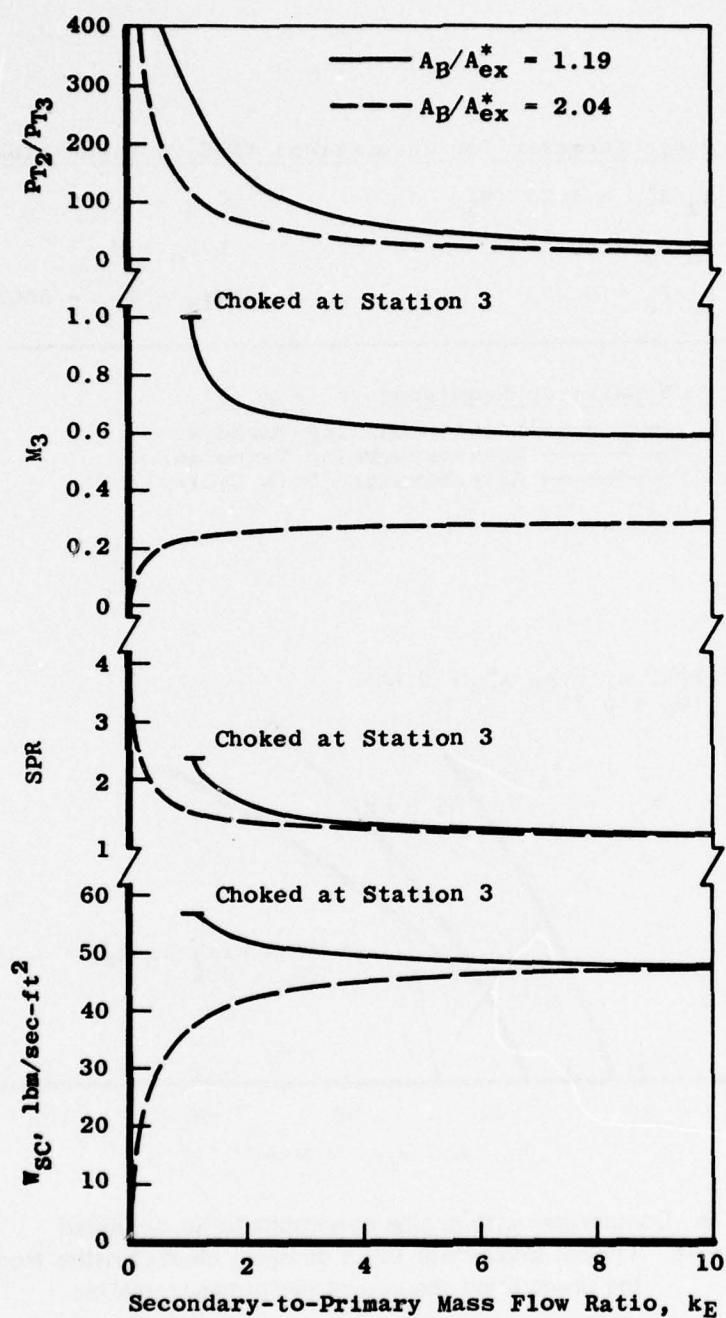$A_B/A_2 = 40$ $L/D_B = 0$

$L_B/D_B = 4$ $T_{T2} = T_{T3} = 500^\circ R$

a. Comparison with engine conditions to be simulated
Figure 18. Typical single-stage EPES pumping characteristics from
the unmodified theoretical performance analysis.

57

b. Variation of P_{T_2}/P_{T_3}, M_3, SPR, and W_{SC} with secondary-to-primary mass flow ratio.

Figure 18. Concluded.
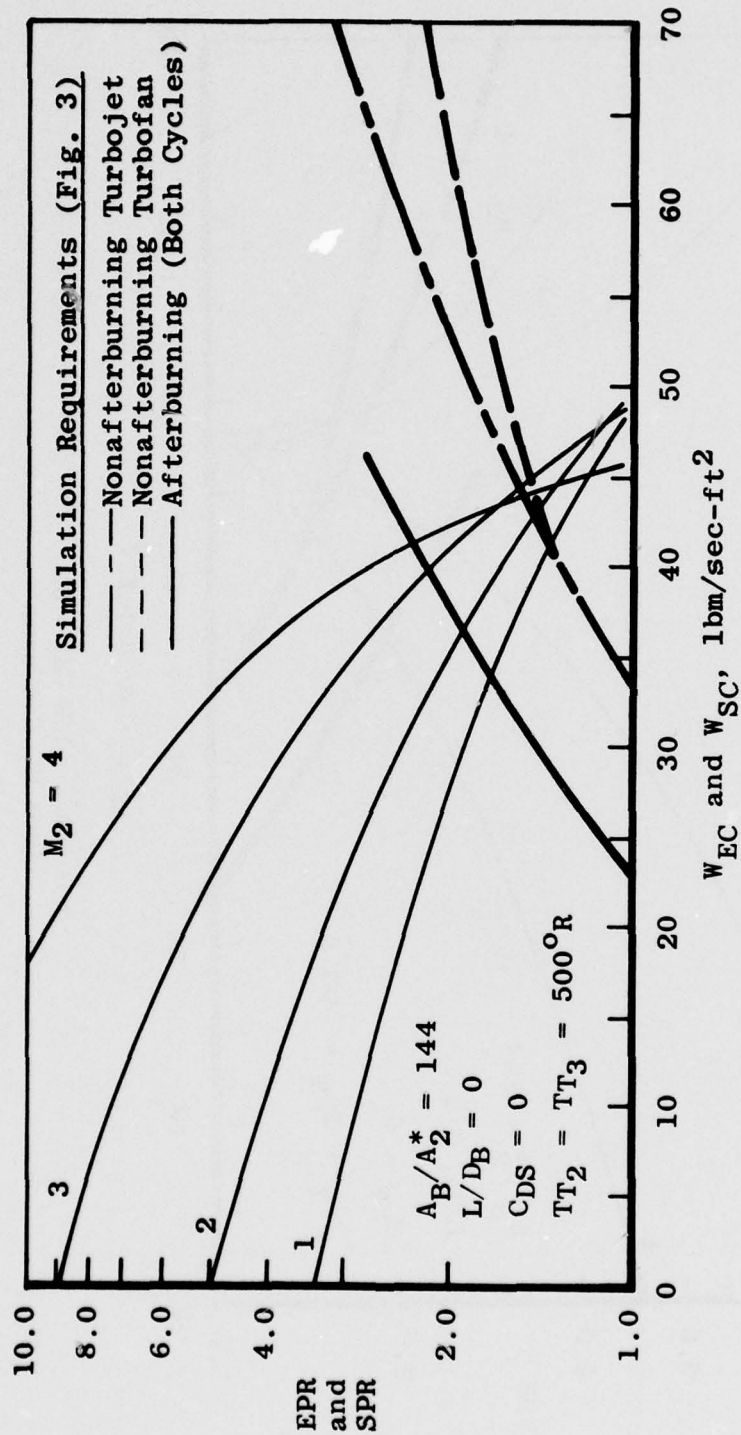
a. $A_B/A_{sx}^* = 1.59$ ($M_B = 0.4$)

Figure 19. Theoretical variation of EPES performance with primary nozzle Mach number and exhaust nozzle contraction ratio.
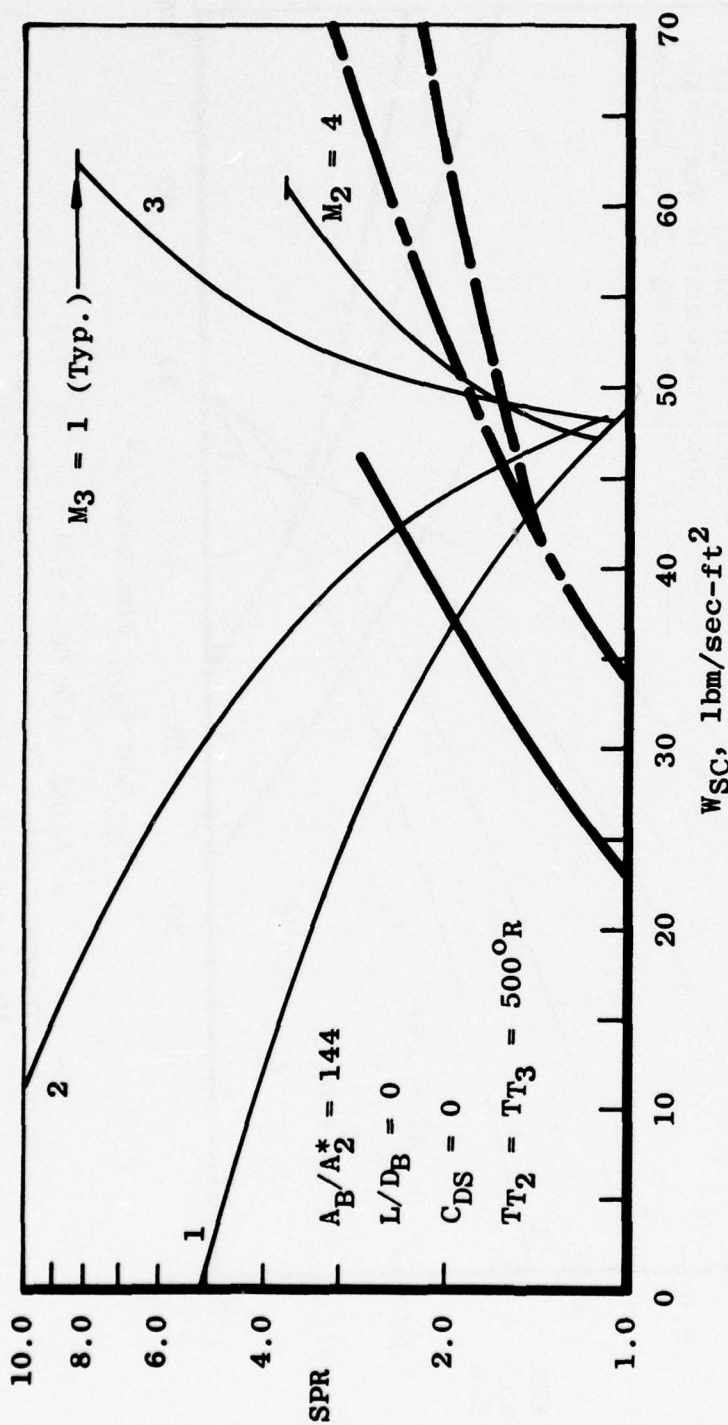
b. $A_B/A_x^* = 1.34$ ($M_B = 0.5$)
Figure 19. Continued.
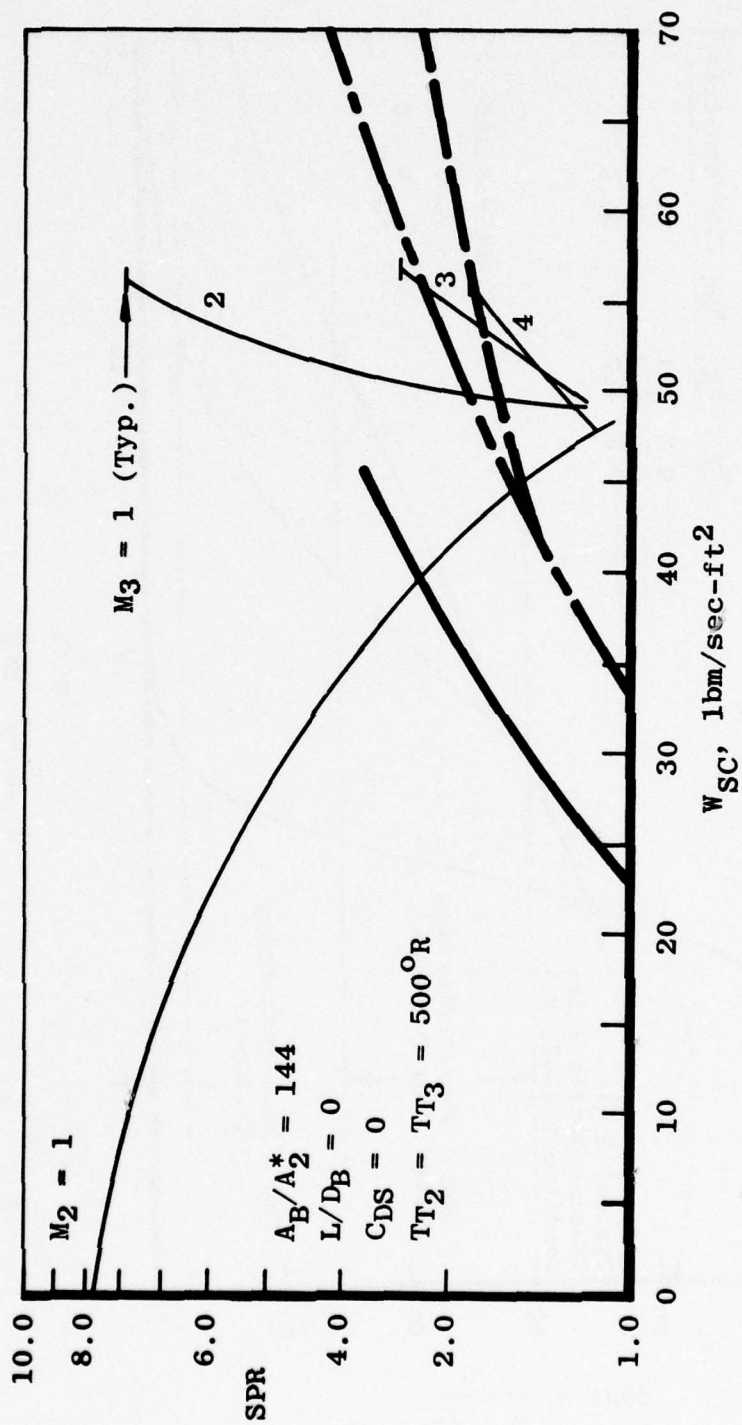
c. $A_B/A_{sx}^* = 1.19$ ($M_B = 0.6$)
Figure 19. Concluded.
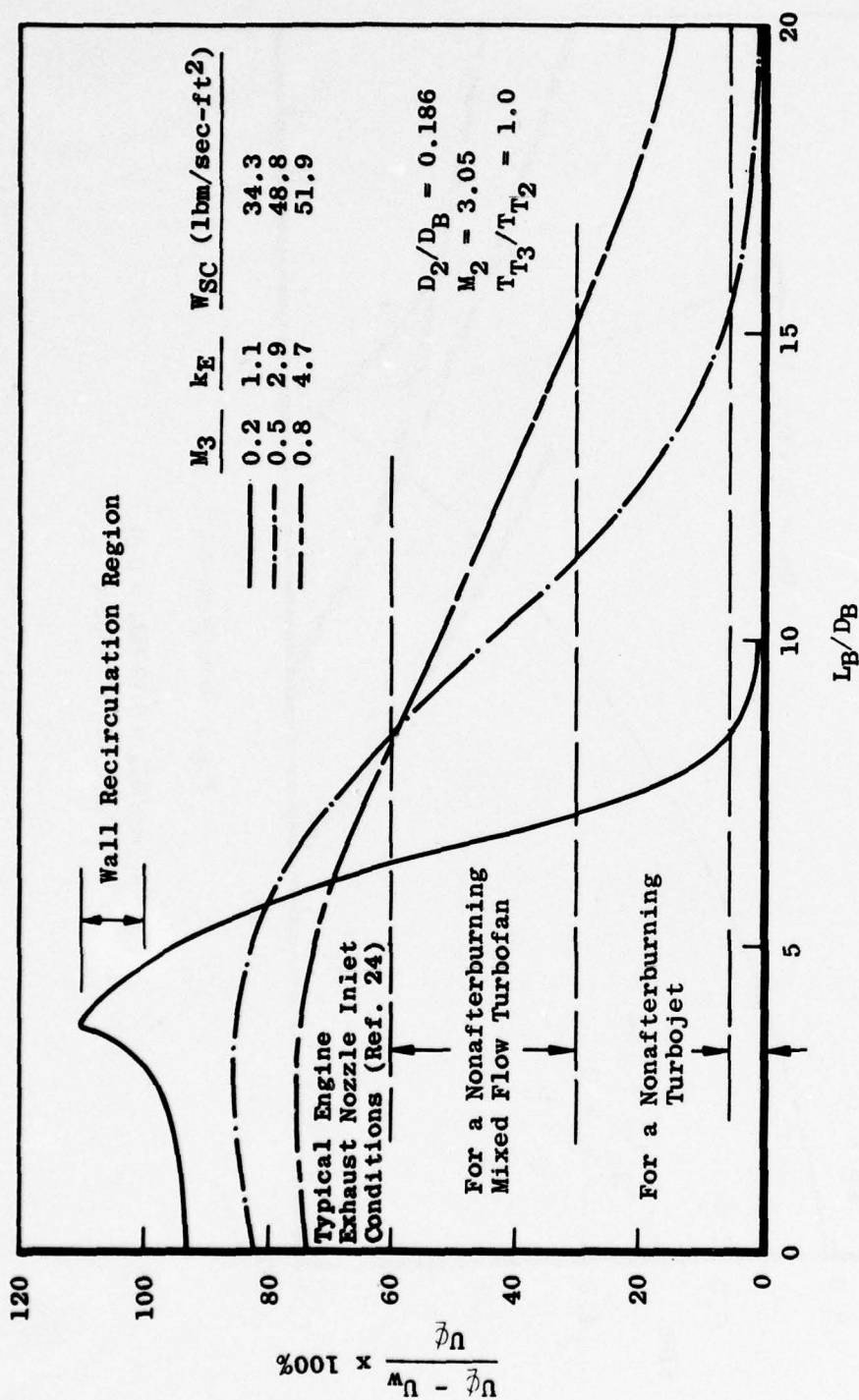
a. $A_B/A_2 = 28.9$

Figure 20. Theoretical variation of centerline-to-wall velocity differences with L_B/D_B and A_2/A_B for representative cold-flow single-stage EPES.
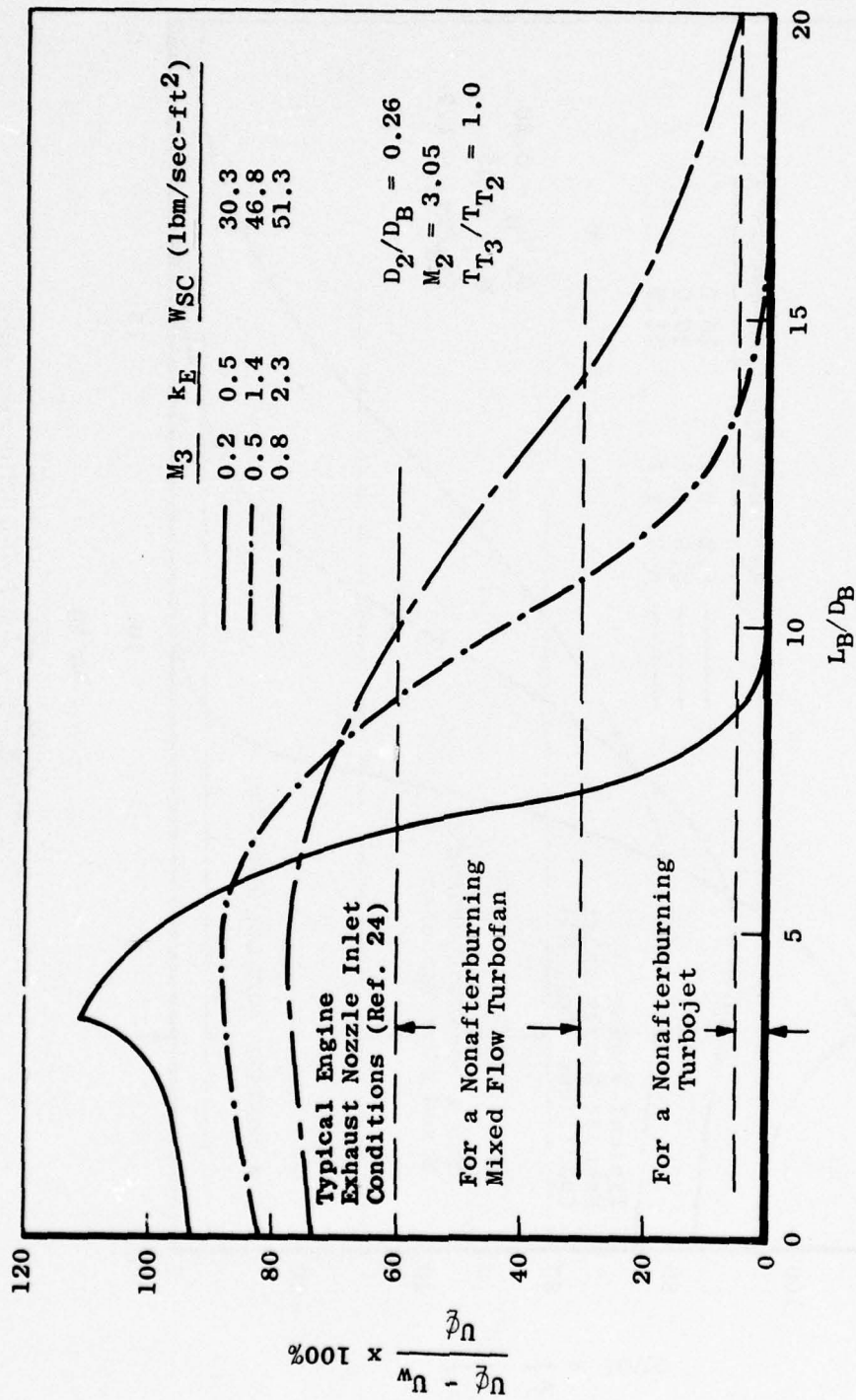
b. $A_B/A_2 = 14.8$
Figure 20. Continued.
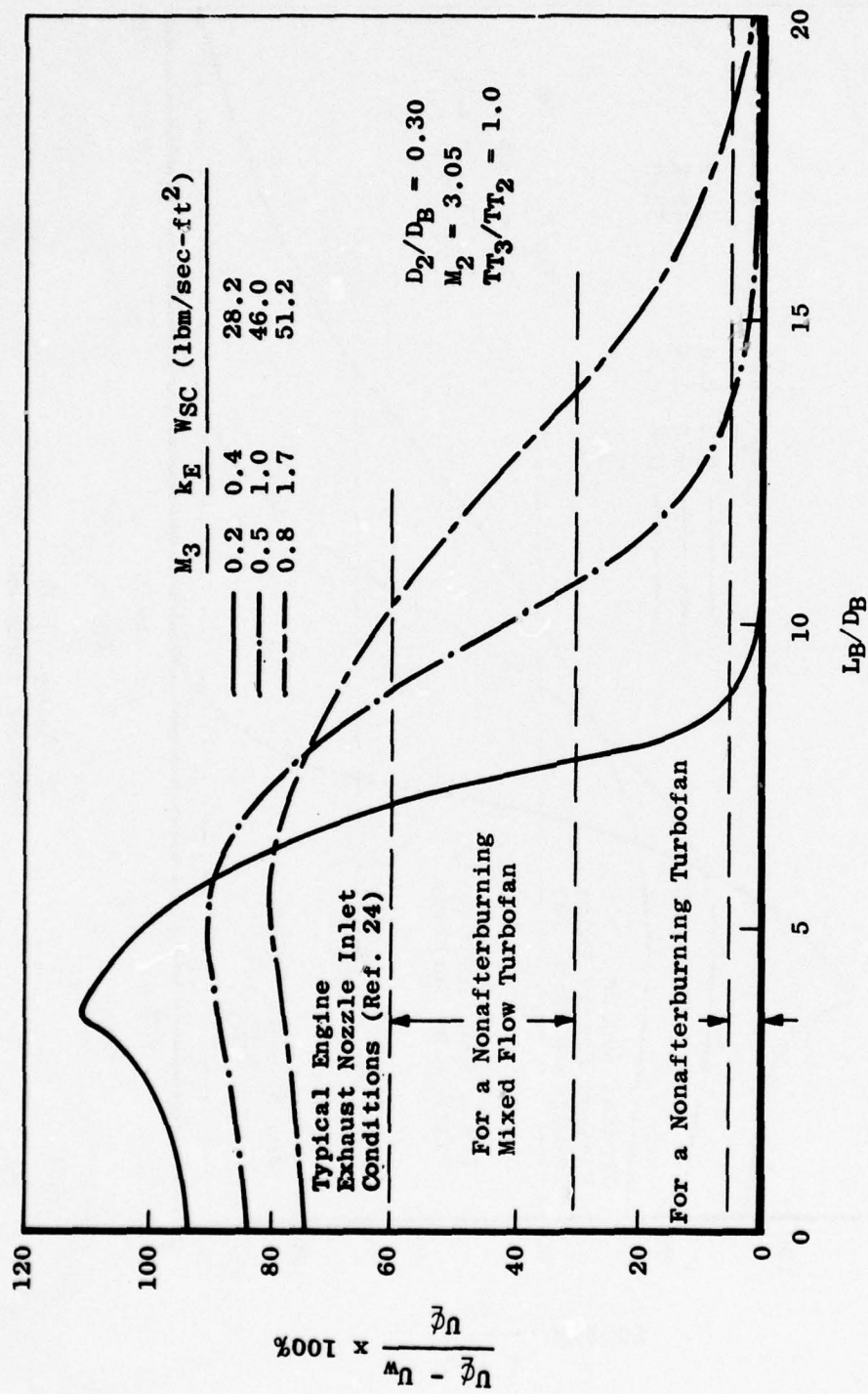
c. $A_B/A_2 = 11.1$
Figure 20. Concluded.
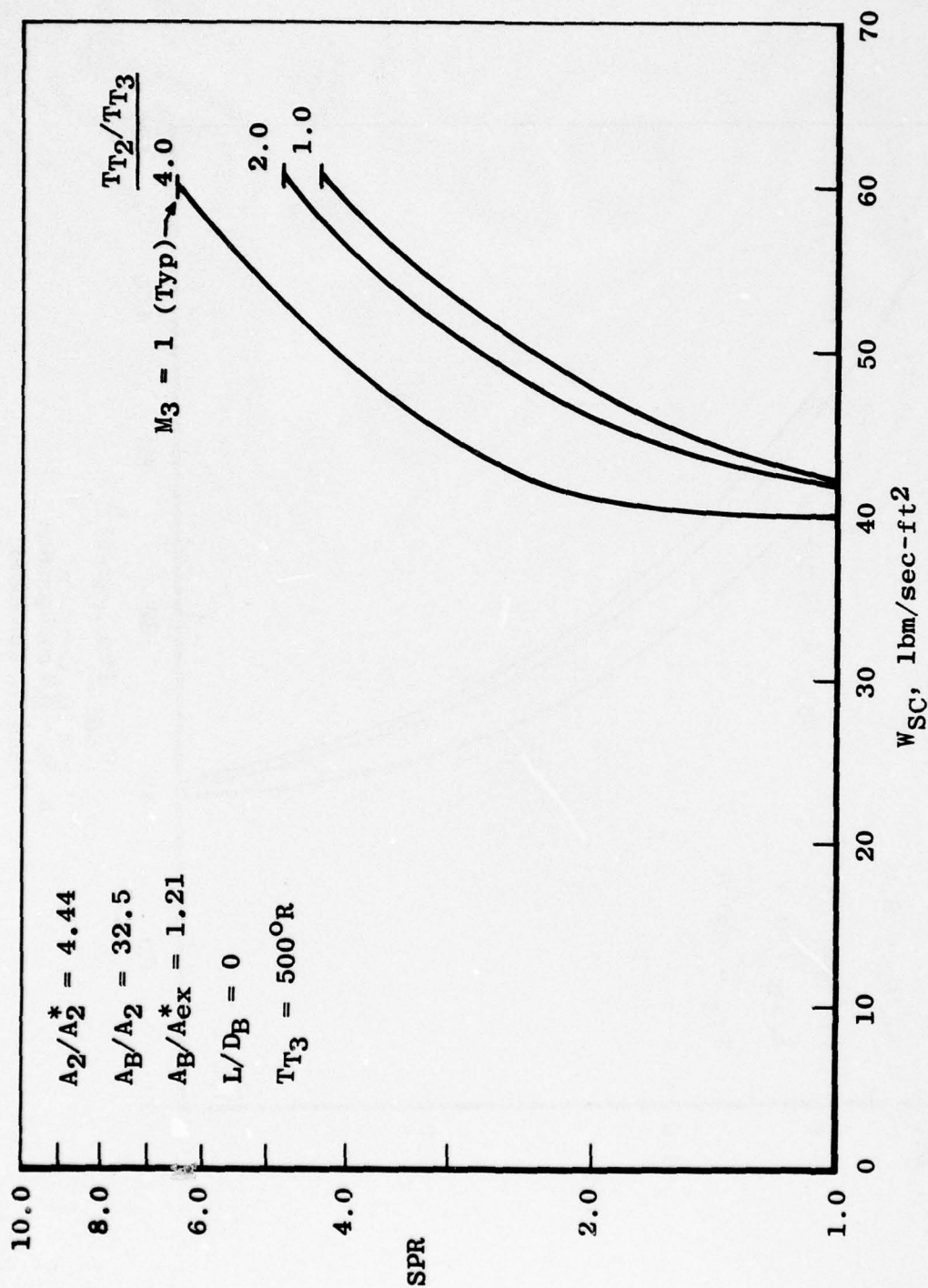
a. $M_2 = 3.05$ configuration

Figure 21. Theoretical effect of primary-to-secondary total temperature ratio on EPES performance.

$A_2/A_2^* = 4.44$

$A_B/A_2 = 32.5$

$A_B/A_{ex}^* = 1.21$

$L/D_B = 0$

$T_{T3} = 500^\circ R$

65
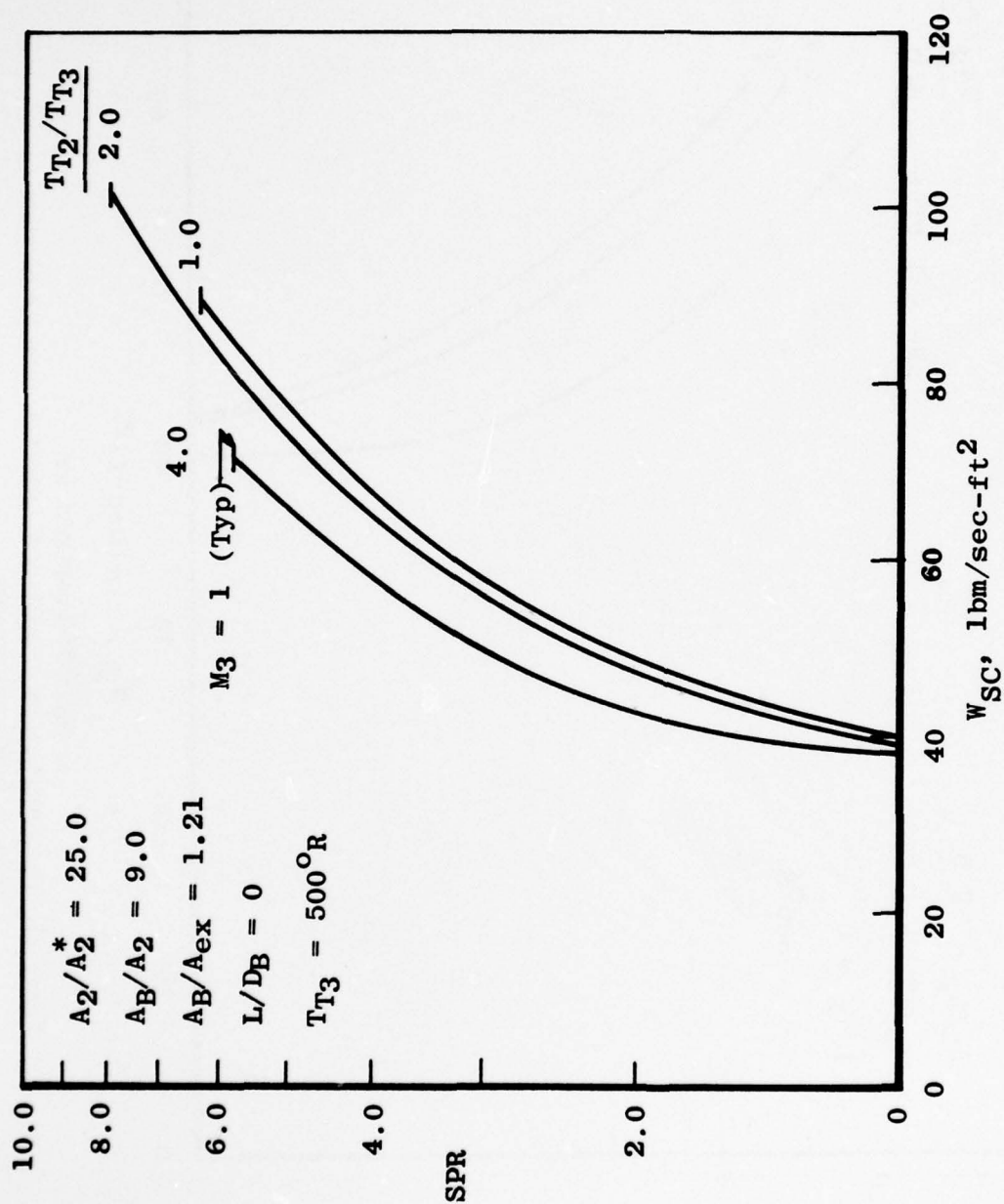
b. $M_2 = 5.0$ configuration
Figure 21. Concluded.
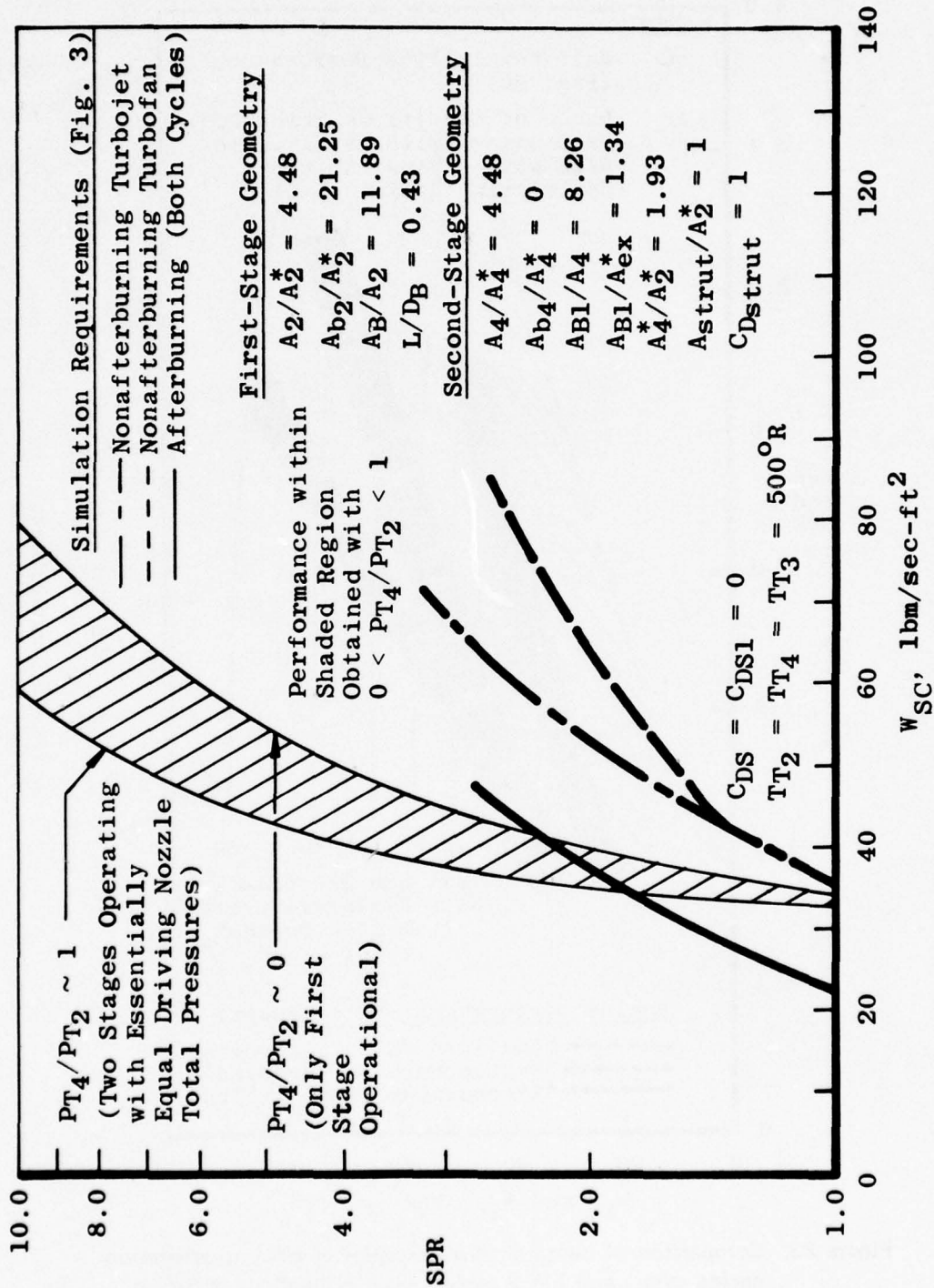
Figure 22. Theoretical performance obtained with a two-stage EPES.

67
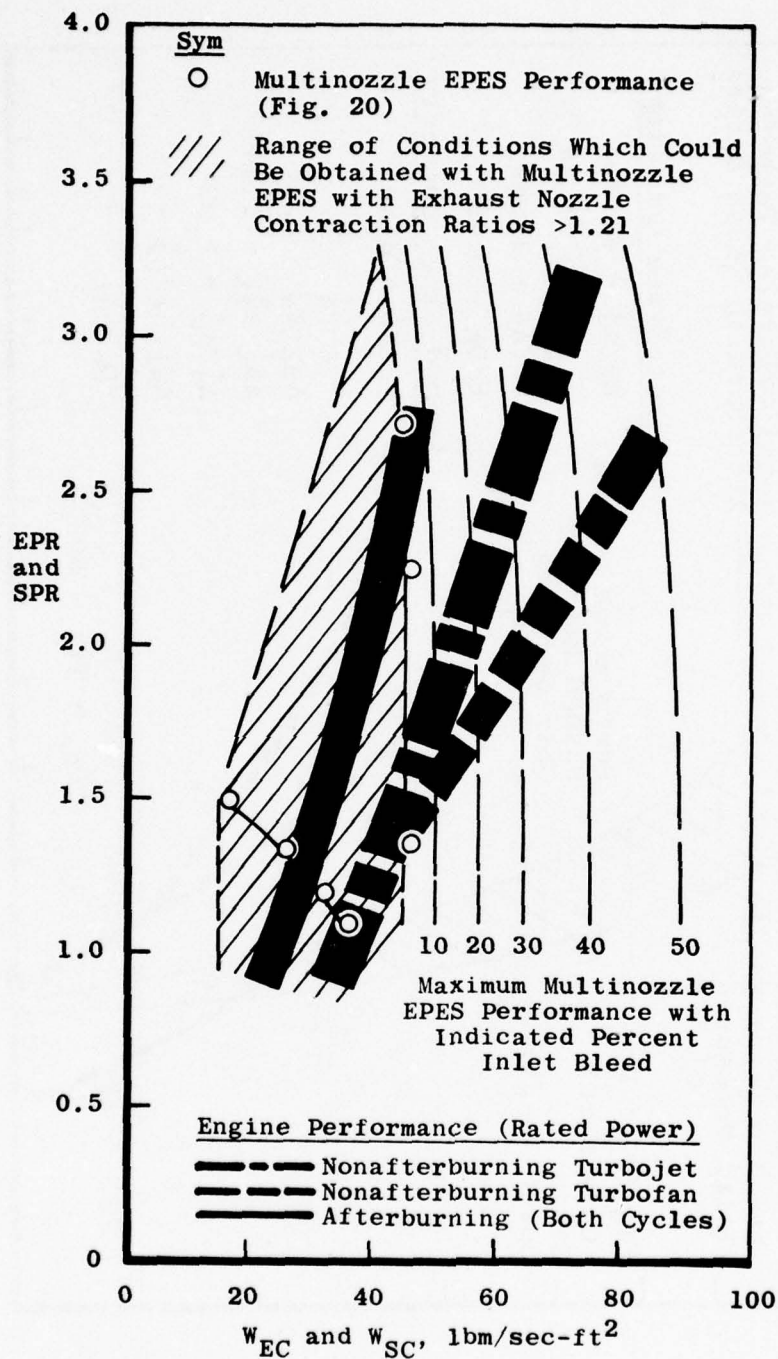
Figure 23. Comparison of pumping characteristics of current generation engine cycles and EPES performance projections based on present multinozzle EPES results.

Table 1. Engine Simulation Techniques and Their Characteristics (from Ref. 1)

Simulation technique	Peculiarities	Inlet Flow Removal and Exhaust Flow Supply Requirements for Proper Propulsive Stream Tube Simulation						Relative Cost
		Turbofan		Turbojet		Afterburning turbojet		
		% Inlet flow that must be removed	% Exhaust flow that must be supplied	% Inlet flow that must be removed	% Exhaust flow that must be supplied	% Inlet flow that must be removed	% Exhaust flow that must be supplied	
Small-scale engine	Near 100% simulation	0	Negligible	0	Negligible	0	Negligible	Maximum
Turbine-powered engine simulator	Texh not simulated	20 to 25	20	30 to 40	30	0 to 20	20	Increasing
Ejector-powered engine simulator	Texh not simulated	35 to 40	Over 50	50	Over 50	0	Over 50	
Supplied-air jet-pumped inlet	Texh not simulated	100	100	100	100	100	100	
Flow-thru nacelle	Texh not simulated PTexh not simulated	0 to 75	0	0 to 75	0	0 to 75	0	
Solid nacelle	No simulation of propulsive stream tube	—	—	—	—	—	—	Minimum

Table 2. Experimental Test Matrix

Primary Nozzles		Mixing Duct Details			Exhaust Nozzle	Range of Experimentally Obtained Results			
A_2/A_2^*	No.	A_B/A_2	L/D_B	L_B/D_B	A_B/A_{ex}^*	M_3	k_E	W_{SC} (lbm/sec-ft^2)	SPR
4.44	1	32.5	0	10	1.21	0.66 to 0.95	0.3 to 1.6	37.4 to 51.6	1.7 to 3.1
4.44	1	32.5	0.33	6	2.72	0 to 0.16	0.5 to 3.1	0 to 41.1	1.1 to 2.2
4.44	1	32.5	0.33	6	1.21	0.32 to 0.65	0.5 to 2.5	34.5 to 50.8	1.4 to 2.3
25.0	1	9.0	0	6	1.21	0.49 to 0.97	0.5 to 2.9	41.8 to 50.0	1.3 to 2.8
25.0	1	9.0	0	6	NEN[a] (0.29 to 0.52)	0.17 to 0.46	1.0 and 2.0	33.7 to 43.2	1.3 to 1.6
25.0	1	9.0	0	10	1.21	0.38 to ~1.0	0.5 to 2.9	33.7 to 51.2	1.3 to 2.1
25.0	1	9.0	0.33	6	2.72	0 to 0.16	0 to 3.2	0 to 40.7	1.1 to 2.0
25.0	7	2.9	0	6	1.21	0.50 to ~1.0	0.3 to 2.0	37.6 to 45.5	1.4 to 3.7
25.0	7	2.9	0	2	2.72	0.13 to 0.17	0.5 to 1.5	23.1 to 34.6	1.2 to 1.4
25.0	7	2.9	0	2	1.21	0.51 to 0.72	0.5 to 1.7	43.3 to 47.3	1.6 to 2.7
25.0	7	2.9	0.33	6	2.72	0.08 to 0.29	0.2 to 1.5	15.8 to 34.8	1.2 to 1.5
25.0	7	2.9	0.33	6	1.21	0.46 to ~1.0	0.3 to 1.8	40.6 to 44.9	1.4 to 4.1
25.0	7	2.9	0.33	4	1.21	0.46 to ~1.0	0.5 to 1.8	42.8 to 45.8	1.4 to 2.6
25.0	7	2.9	0.33	4	NEN[a] (0.26 to 0.80)	0.07 to ~1.0	0.5 to 1.5	24.9 to 46.7	1.3 to 2.4

[a]No exhaust nozzle installed; range of M_B indicated instead.

70

Table 3. Measurement Uncertainty

Experimental Parameter	Uncertainty, * Percent of Value	Range
Overall Pressure Ratio, SPR	± 2.1	0 to 5
Mass Flow Parameter, Wsc	± 1.1	0 to 60 lbm/sec–ft^2
Mass Flow Ratio, k_E	± 2.7	0 to 5
Mach Number, M	± 2.0	0 to 4.0
Pressure, Ratio, P_w/P_{T2}	± 1.4	0 to 0.02

*Uncertainty determined from technique presented in Ref. 22.

APPENDIX A
METHODS OF CALCULATION FOR EXPERIMENTAL DATA

The general method and equations used to compute the experimental parameters presented are given below. Where applicable, arithmetic averages of measured pressure were used.

SECONDARY (EPES INLET) AIRFLOW

Secondary airflow was determined with a circular arc, critical-flow venturi using the following relationship:

$$W_3 = \frac{0.5318 \, C_{ds} \, A_{SV}^* \, P_{T_{SVI}}}{\sqrt{T_{T_{SVI}}}} \tag{A-1}$$

where C_{d_s} is an empirically determined flow coefficient based on venturi geometry and inlet stagnation conditions (Ref. 25).

PRIMARY (DRIVING) AIRFLOW

Primary airflow was determined at the throat of the driving nozzles using the following relationship:

$$W_2 = \frac{0.5318 \, C_{d_2} \, C_R A_2^* \, P_{T_{2_{IN}}}}{\sqrt{T_{T_{PI}}}} \tag{A-2}$$

where C_{d_2} is 0.993 in all cases, C_R is a correction factor to compensate for real gas effects (Ref. 26), and A^*_2, the primary nozzle throat area, is the summation of the seven nozzle throat areas for the seven-conical-nozzle-cluster configuration (Fig. 5c).

SECONDARY-TO-PRIMARY MASS FLOW RATIO

$$k_E = W_3/W_2 \tag{A-3}$$

EPES EXHAUST TOTAL PRESSURE

A representative value of nozzle exit total pressure ($P_{T_{ex}}$) was required at each test condition to establish SPR. Operation of some EPES configurations with short mixing ducts and $k_E \lesssim 1$ resulted in incomplete mixing of the primary and secondary flows. As a result, significant exhaust nozzle flow nonuniformities were produced which precluded summation of the total pressure surveys to obtain a representative value of $P_{T_{ex}}$. To ensure consistent results, $P_{T_{ex}}$ was determined as follows:

Preceding page blank

With an exhaust nozzle installed (and choked)

$$P_{T_{ex}} = \frac{(W_2 + W_3)\sqrt{T_{T_B}}}{0.5318 \, A^*_{ex}} \qquad (A-4)$$

where

$$T_{T_B} = \frac{W_2 T_{T_2} + W_3 T_{T_3}}{W_2 + W_3}$$

For experiments conducted without an exhaust nozzle, the mixing duct exit mass flow function ($\dot{m}_B$) was determined from

$$\dot{m}_B = \frac{(W_2 + W_3)\sqrt{T_{T_B}}}{P_{ex} A_B} \qquad (A-5)$$

The subsonic mixing duct exit Mach number (M_B) was then determined implicity from the definition of $\dot{m}_B$, i.e.,

$$\dot{m}_B = \sqrt{1.4 \, g_c / \overline{R}} \; M_B \, [1 + 0.2 \, M_B^2]^{1/2} \qquad (A-6)$$

with

$$\overline{R} = 53.35 \; \text{ft-lbf/lbm-}°R$$
$$g_c = 32.174 \; \text{ft-lbm/lbf-sec}^2$$

Finally, $P_{T_{ex}}$ was determined from

$$P_{T_{ex}} = P_{ex} \, [1 + 0.2 \, M_B^2]^{3.5} \qquad (A-7)$$

SIMULATOR PRESSURE RATIO

$$SPR = \frac{P_{T_{ex}}}{P_{T_3}}$$

SIMULATOR MASS FLUX PARAMETER

The simulator mass flux parameter is defined by the EPES inlet corrected airflow and the exhaust nozzle throat area.

For experiments conducted with an exhaust nozzle on the EPES mixing duct,

$$W_{SC} = \frac{W_3 \sqrt{T_{T_3}/T_{T_{ref}}}}{P_{T_3}/P_{T_{ref}} \, A^*_{ex}} \qquad (A-8)$$

with A^*_{ex} in ft^2, and

$$P_{T_{ref}} = 2116.22 \text{ psfa}$$

$$T_{T_{ref}} = 518.67°R$$

For experiments conducted without an exhaust nozzle, an effective exhaust nozzle throat area ($A^*_{ex_{eff}}$) for use in Eq. (A-8) was determined from

$$A^*_{ex_{eff}} = \frac{216 \, A_B M_B}{125(1 + 0.2 M_B^2)^3} \tag{A-9}$$

EXHAUST NOZZLE EXIT MACH NUMBER

Mach number profiles in the EPES exhaust were determined from total and static pressures measured with a cone probe (Fig. 4b). The relationship between free-stream Mach number and measured pressures was determined with the theoretical models outlined in Refs. 27 and 28.

APPENDIX B
MODIFIED EPES PERFORMANCE ANALYSIS

Correlations of experimental data and results from the basic EPES performance analysis (eg., solid lines in Fig. 14) indicate significant differences at conditions where flow separation could have occurred in the primary nozzles of the experimental configurations. These differences are largely attributed to the assumption in the basic performance analysis (see Section 2.2.1) that the primary nozzle exit Mach number (and associated conditions) can be determined from the primary nozzle area ratio (A_2/A_2^*) and the isentropic relationship

$$\frac{A}{A^*} = \frac{1}{M} \left[\frac{2 + (\gamma - 1)M^2}{\gamma + 1} \right]^{\frac{\gamma+1}{2(\gamma-1)}} \tag{B-1}$$

With relatively low values of secondary inlet static pressure (P_3), the primary flow remains attached (eg., Fig. B-1a) and primary nozzle exit Mach number (M_2) is well represented by the Mach number determined from Eq. (B-1). However, at higher values of P_3 where primary nozzle flow separation may occur (Fig. B-1b), the isentropic relationship no longer applies, and the basic EPES performance analysis must be modified to exclude this assumption.

The amount which the back pressure-to-nozzle exit static pressure ratio ($\sim P_3/P_2$, Fig. B-1a) can exceed unity without separating the nozzle exit flow is the subject of much conjecture because of significant uncertainties in available experimental data and limitations of existing analytical models. However, a simple, empirically derived correlation (Ref. 19), which describes (Fig. B-2) the general trend of available nozzle separation data, is represented by

$$(P_3/P_{T_2})_{sep} = \frac{M_{sep}}{\left(1 + \frac{\gamma - 1}{2} M_{sep}^2\right)^{\frac{\gamma}{\gamma-1}}} \tag{B-2}$$

Theoretical results for EPES configurations which may have had primary nozzle flow separation were recomputed using the basic performance analysis (Section 2.2.1) (Eq. (B-2)), a modified primary nozzle geometry, and the following procedure. $(P_3/P_{T_2})_{theo}$ was determined from the performance analysis results for the specified EPES geometry (A_2/A_2^*, A_{2b}/A_2^*, A_B/A_{ex}^*, A_B/A_2^*, L/D_B, L_B/D_B) and the selected secondary-to-primary mass flow ratio (k_E). $(P_3/P_{T_2})_{sep}$ was then determined from Eq. (B-2) for a Mach number equal to the nozzle exit Mach number that would exist if no separation occurred (i.e., the supersonic branch solution of Eq. (B-1) for A_2/A_2^*). If

$$(P_3/P_{T2})_{theo} > (P_3/P_{T2})_{sep}$$

the flow was assumed to be separated in the primary nozzle at the point where the Mach number (M_{sep}) corresponds to the solution of Eq. (B-2) for $(P_3/P_{T2})_{theo}$. The nozzle area ratio at the separation point ($(A/A^*)_{sep}$) corresponding to M_{sep} was then established from Eq. (B-1) and an "effective" base area defined by

$$(A_{2b}/A_2^*)_{eff} = A_{2b}/A_2^* + A_2/A_2^* - (A/A^*)_{sep} \tag{B-3}$$

An "effective" EPES geometry was then established with A_B/A_2^*, A_B/A_{ex}^*, L/D_B, and L_B/D_B as before but with A_2/A_2^* and A_{2b}/A_2^* replaced by $(A/A^*)_{sep}$ and $(A_{2b}/A_2^*)_{eff}$, respectively.

A theoretical solution was then obtained with the performance analysis for the "effective" EPES geometry at the same value of k_E as before. The ratio $(P_3/P_{T2})_{theo}$ established from the new solution was compared with the initial value of $(P_3/P_{T2})_{theo}$. If the difference was greater than 10 percent, the process was repeated. Generally, no more than three iterations were required to obtain an acceptable solution. Theoretical EPES performance results from the final iteration (e.g., dashed lines in Fig. 14) are in much better agreement with the experimental data than the results from the basic performance analysis (solid lines in Fig. 14).
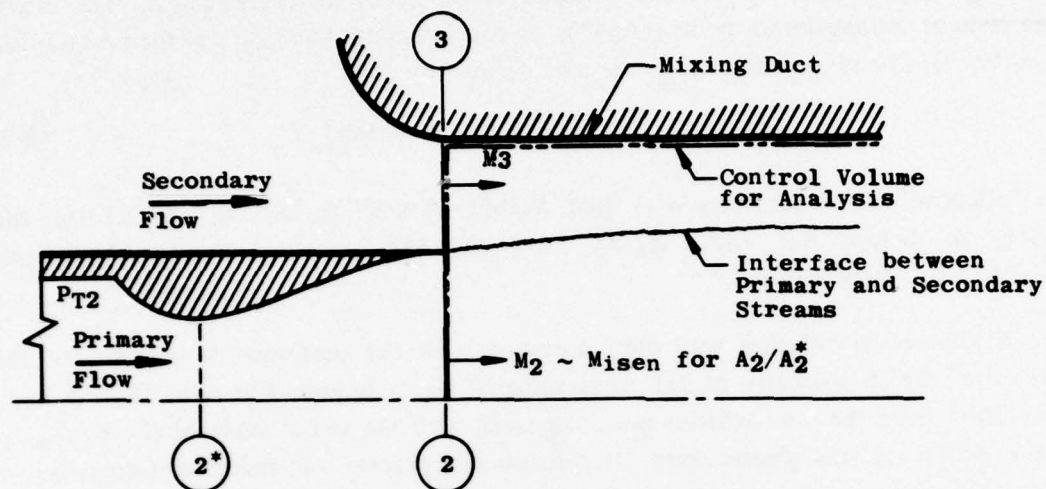
a. (P_3/P_{T_2}) less than $(P_3/P_{T_2})_{sep}$
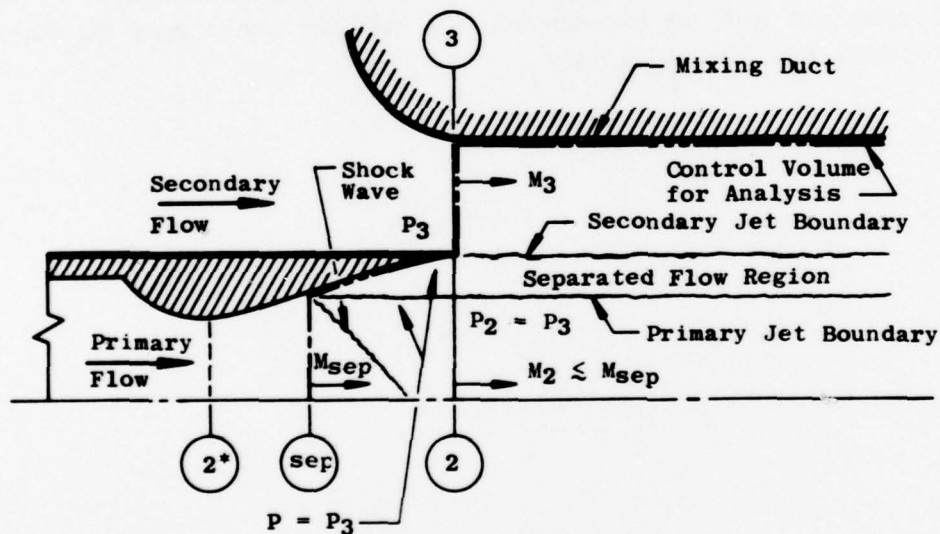
b. (P_3/P_{T_2}) greater than $(P_3/P_{T_2})_{sep}$

Figure B-1. General effect of mixing duct inlet static pressure
level on primary nozzle flow.

$$\left(\frac{P_3}{P_{T_2}}\right)_{sep} = \frac{M_{sep}}{\left(1 + \frac{\gamma-1}{2} M_{sep}^2\right)^{\gamma/(\gamma-1)}}$$

$\gamma = 1.4$

(From Correlation
Used in Ref. 19)

Flow Separated

Flow Attached
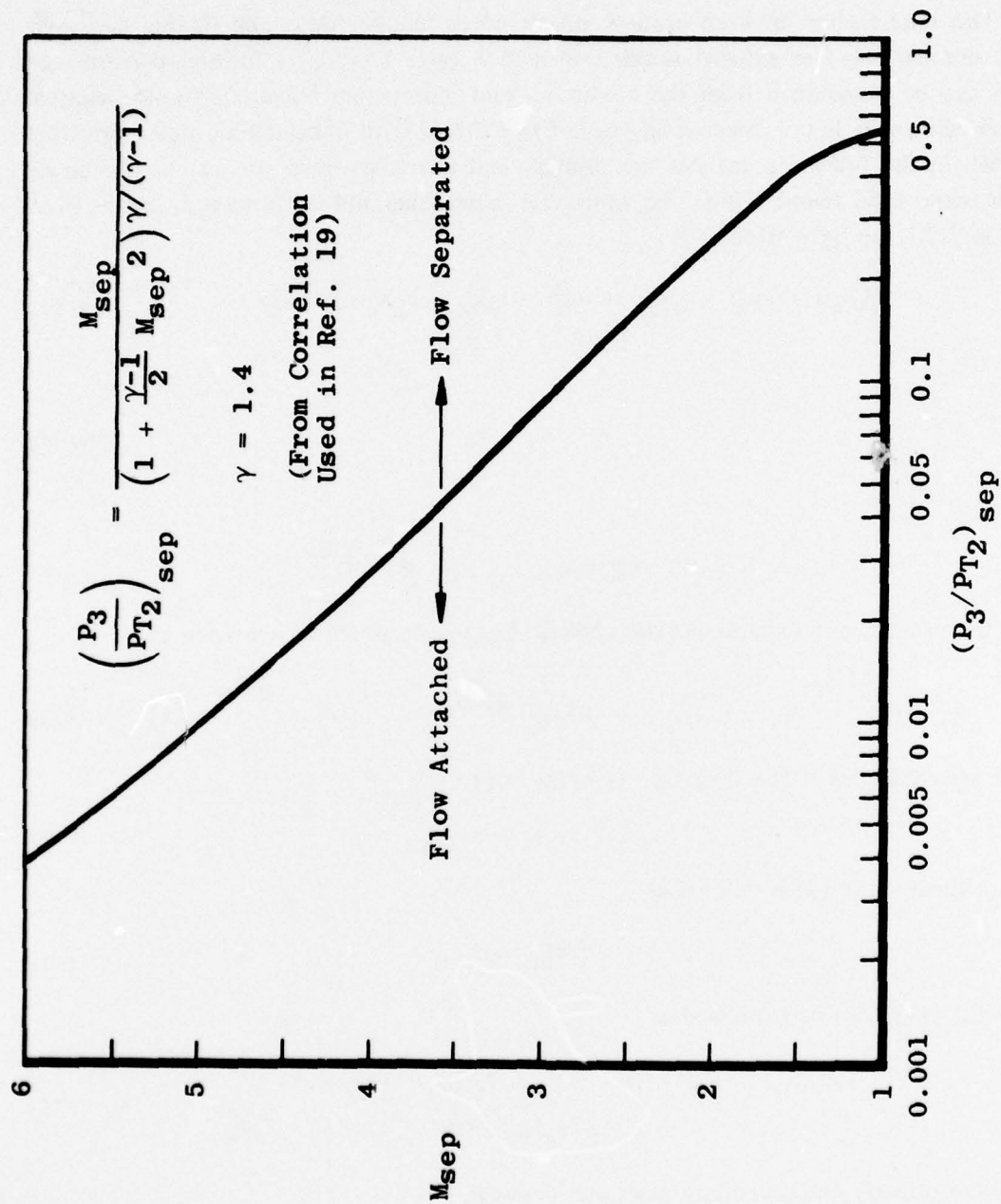
M_{sep}

$\left(P_3/P_{T_2}\right)_{sep}$

Figure B-2. Variation of separation Mach number with nozzle pressure ratio.

79

APPENDIX C
EVALUATION OF EPES PERFORMANCE CRITERION

The relationship between primary nozzle Mach number (M_2) and mixing duct exit Mach number (M_B) or exhaust nozzle contraction ratio (A_B/A_{ex}^*) for high-performance EPES can be determined from the continuity and momentum equations for the control volume shown in Fig. 4. Since single-stage EPES driven with unheated air are of principal interest, in the following analysis the primary and secondary gases are assumed to be air at the same total temperature. The applicable momentum and continuity equations from Section 2.2.1 can be written as

$$P_2 A_2 (1 + \gamma M_2^2) + P_3 A_3 (1 + \gamma M_3^2) + P_3 A_{b2} = P_B A_B (1 + \gamma M_B^2) + F_s \tag{C-1}$$

and

$$W_2 + W_3 = W_B \tag{C-2}$$

Since

$$W = P_T A / \sqrt{T_T} \sqrt{\gamma g_c / R} \, M [1 + (\gamma - 1)/2 M^2]^{-\frac{\gamma + 1}{2(\gamma - 1)}}$$

With the primary and exhaust nozzles choked, Eq. (C-2) can then be written as

$$\left(\frac{2}{\gamma + 1}\right)^{\frac{\gamma + 1}{2(\gamma - 1)}} P_{T_2} A_2^* + M_3 \left[1 + \frac{\gamma - 1}{2} M_3^2\right]^{-\frac{\gamma + 1}{2(\gamma - 1)}} P_{T_3} A_3 = \left(\frac{2}{\gamma + 1}\right)^{\frac{\gamma + 1}{2(\gamma - 1)}} P_{T_B} A_B^* \tag{C-3}$$

If the secondary inlet flow is choked (i.e., $M_3 = 1$),

$$P_{T_2} A_2^* + P_{T_3} A_3 = P_{T_B} A_B^* \tag{C-4}$$

Stream thrust ratio (ϕ) is defined as

$$\phi = \frac{PA(1 + \gamma M^2)}{P^* A^* (1 + \gamma)} \tag{C-5}$$

Then Eq. (C-1) can be expressed as

$$\phi_2 P_{T_2} A_2^* P_2^* / P_{T_2} (1 + \gamma) + \phi_3 P_{T_3} A_3 P_3^* / P_{T_3} (1 + \gamma) =$$
$$\phi_B P_{T_B} A_B^* P_B^* / P_{T_B} (1 + \gamma) + F_s - P_3 A_{2b} \tag{C-6}$$

Since the primary and secondary gases are identical,

$$P_2^* / P_{T_2} = P_3^* / P_{T_3} = P_B^* / P_{T_B} = (2/(\gamma + 1))^{\frac{\gamma}{\gamma - 1}}$$

80

Then Eq. (C-6) becomes

$$\phi_2 P_{T_2} A_2^* + \phi_3 P_{T_3} A_3 = \phi_B P_{T_B} A_B^* + \frac{F_s - P_3 A_{2b}}{(1 + \gamma)\left(\frac{2}{\gamma + 1}\right)^{\frac{\gamma}{\gamma - 1}}} \tag{C-7}$$

substituting Eq. (C-4) into Eq. (C-7) along with $\phi_3 = 1$ (which corresponds to $M_3 = 1$)

$$\phi_2 \frac{P_{T_2} A_2^*}{P_{T_B} A_B^*} - \phi_B = \frac{F_s - P_3 A_{2b}}{(1 + \gamma)(2/(\gamma + 1))^{\frac{\gamma}{\gamma - 1}} P_{T_B} A_B^*} - \frac{P_{T_B} A_B^* - P_{T_2} A_2^*}{P_{T_B} A_B^*}$$

or

$$\phi_2 \frac{P_{T_2} A_2^*}{P_{T_B} A_B^*} - \phi_E = \frac{F_s - P_3 A_{2b}}{(1 + \gamma)(\gamma/(\gamma + 1))^{\frac{\gamma}{\gamma - 1}} P_{T_B} A_B^*} - 1 + \frac{P_{T_2} A_2^*}{P_{T_B} A_B^*}$$

Rearranging,

$$\frac{P_{T_2} A_2^*}{P_{T_B} A_B^*} (\phi_2 - 1) = \phi_B - 1 + \frac{F_s - P_3 A_{2b}}{(1 + \gamma)(2/(\gamma + 1))^{\frac{\gamma}{\gamma - 1}} P_{T_B} A_B^*}$$

or

$$\frac{\phi_B - 1 + \dfrac{F_s - P_3 A_{2b}}{(1 + \gamma)(2/(\gamma + 1))^{\frac{\gamma}{\gamma - 1}} P_{T_B} A_B^*}}{\phi_2 - 1} = \frac{P_{T_2} A_2^*}{P_{T_B} A_B^*} \tag{C-8}$$

But

$$\frac{P_{T_2} A_2^*}{P_{T_B} A_B^*} = \frac{W_2}{W_2 + W_3}$$

and

$$k_E = \frac{W_2}{W_3}$$

so

$$\frac{P_{T_2} A_2^*}{P_{T_B} A_B^*} = \frac{1}{1 + k_E} \tag{C-9}$$

Combining Eq. (C-8) and Eq. (C-9) and noting that $A_B^* = A_{ex}^*$ give

$$\frac{\phi_B - 1 + \dfrac{F_s - P_3 A_{2b}}{(1 + \gamma)(2/(\gamma + 1))^{\frac{\gamma}{\gamma - 1}} P_{T_B} A_{ex}^*}}{\phi_2 - 1} = \frac{1}{k_E + 1} \tag{C-10}$$

In the EPES application only $k_E > 0$ is of interest so the right side of Eq. (C-10) is less than one. For Eq. (C-10) to be valid, then

$$\phi_B + \frac{F_s - P_3 A_{2b}}{(1 + \gamma)(2/(\gamma + 1))^{\frac{\gamma}{\gamma - 1}} P_{T_B} A_{ex}^*} < \phi_2 \tag{C-11}$$

For configurations having negligible primary nozzle base area (A_{2b}) and mixing duct wall drag (F_s), Eq. (C-11) reduces to

$$\phi_B < \phi_2 \tag{C-12}$$

which is only a function of exhaust nozzle contraction ratio (or M_B) and primary nozzle Mach number (M_2). The locus of subsonic and supersonic conditions corresponding to a given stream thrust ratio (i.e., from Fig. C-1, $\phi = 1.342$ corresponds to a subsonic Mach number of 0.415 and a supersonic Mach number of 5.0) then defines (Fig. C-2) the subsonic mixing duct exit Mach number (or exhaust nozzle contraction ratio (A_B/A_{ex}^*)) required for high-performance EPES operation with a particular supersonic primary nozzle geometry.

$$\phi = \frac{PA\ (1 + \gamma M^2)}{P^*A^*\ (1 + \gamma)}$$

$$\gamma = 1.4$$

$\phi = 1.429$ at $M = \infty$

Mach Number, M
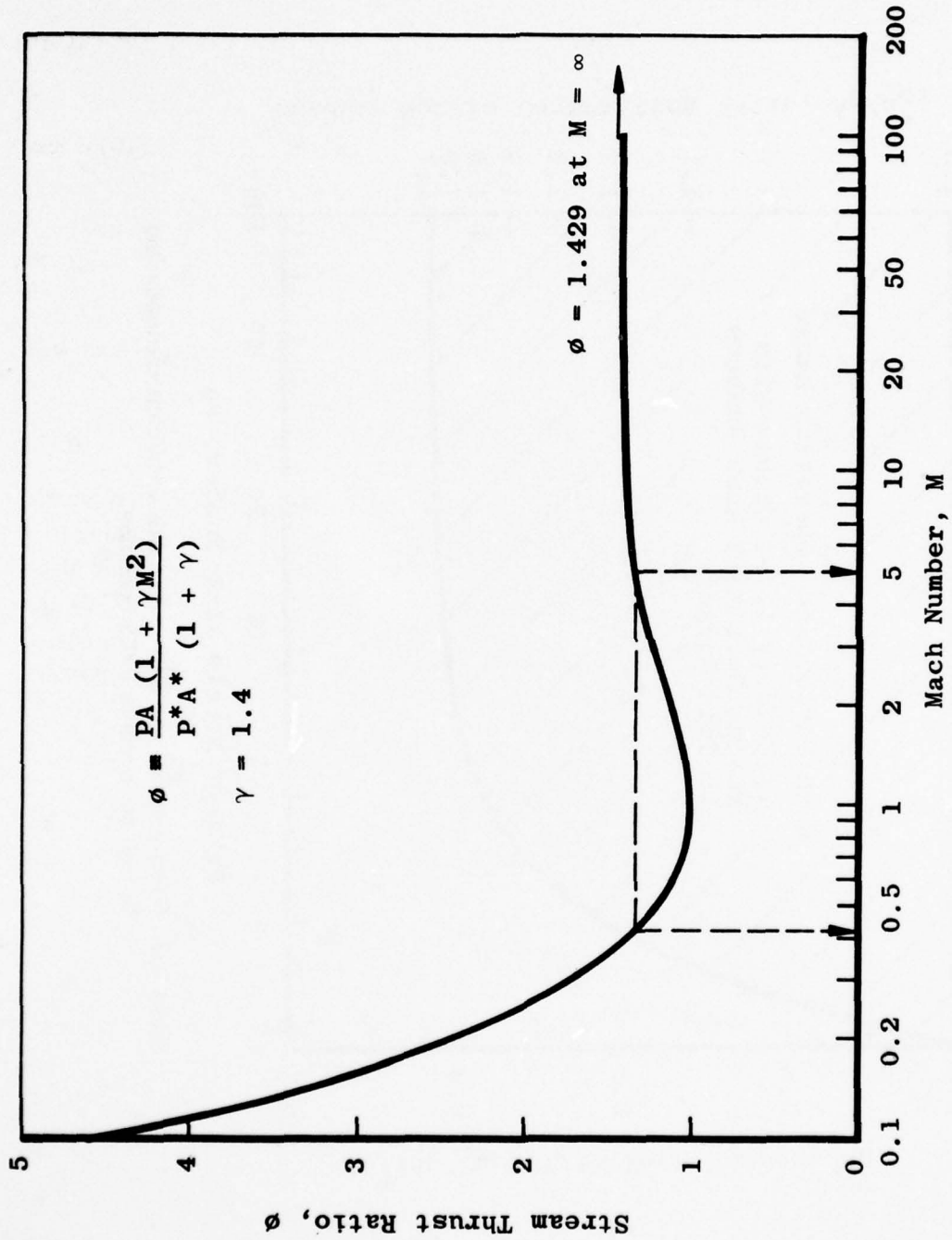
Stream Thrust Ratio, ϕ
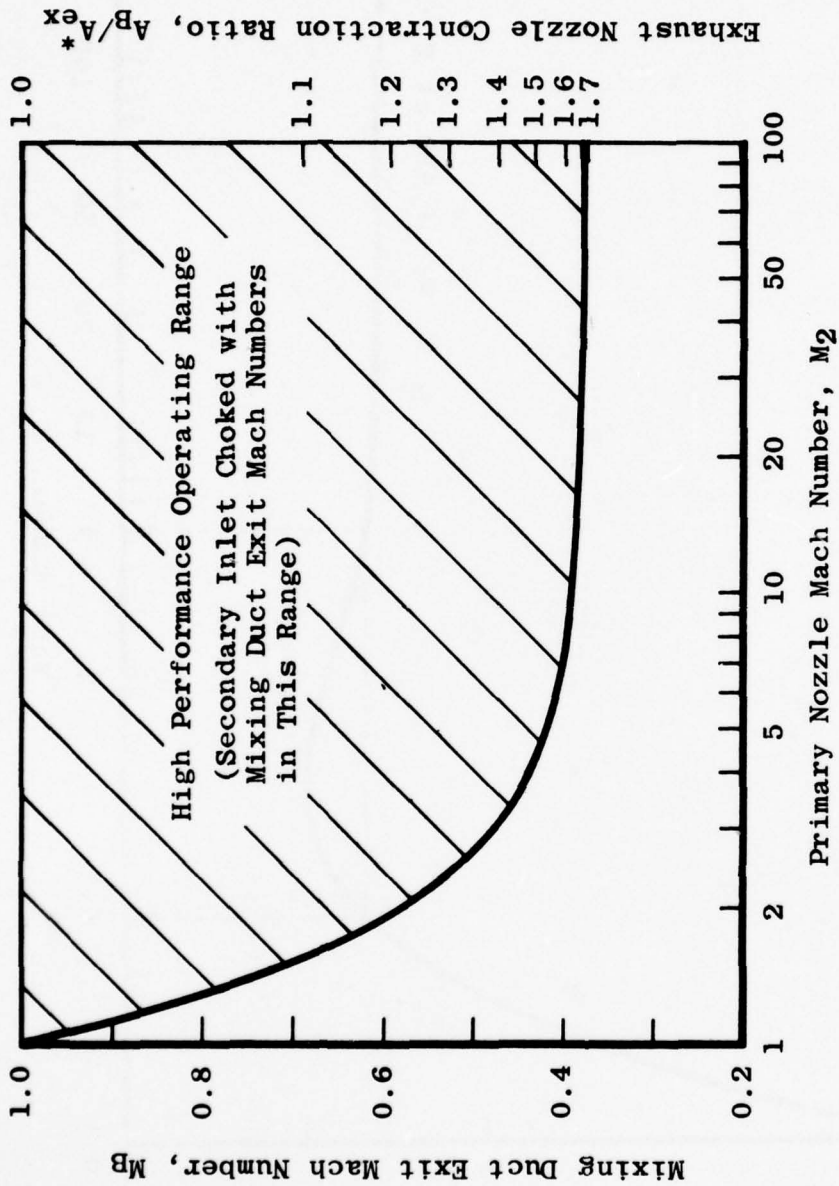
Figure C-1. Variation of stream thrust ratio with Mach number.

83

Figure C-2. Primary nozzle and mixing duct exit conditions corresponding to high performance EPES operation.

84

NOMENCLATURE

A	Area, ft^2, in.^{2}
A_s, A_{s1}	Mixing duct surface area, ft^2
A_{strut}	Frontal area, second-stage injector support strut, ft^2
C_{DS}, C_{DS1}	Wall drag coefficient
C_d	Discharge coefficient
C_p	Specific heat at constant pressure
C_R	Mass flow correction factor for real gas effects
D	Diameter, ft, in.
EPR	Engine exhaust-to-inlet total pressure ratio
F	Force, lbf
F_s, F_{s1}	Skin friction drag force on mixing duct, lbf
g_c	Dimensional constant, 32.174 lbm-ft/lbf-sec^2
k_E	Ratio of EPES inlet mass flow-to-primary nozzle mass flow, W_3/W_2
L	Gap between primary nozzle exit and mixing duct inlet, ft, in.
L_B	Mixing duct length, ft, in.
M	Mach number
$\dot{m}$	Mass flow function, $\dot{m} = W\sqrt{T_T}/PA$
P	Static pressure, psfa
P_T	Total pressure, psfa

85

q	Dynamic pressure, psfa
$\bar{q}_s$	Mean dynamic pressure along mixing duct wall, psfa
R	Radial position
R_{ex}	Exhaust nozzle exit radius, in.
$\bar{R}$	Gas constant
SPR	Simulator exhaust-to-inlet total pressure ratio, $P_{T_{ex}}/P_{T_3}$
T_T	Total temperature, °R
U	Velocity, ft/sec
W	Flow rate, lbm/sec
W_{EC}	Ratio of engine inlet corrected airflow to exhaust nozzle throat area, lbm/sec-ft^2
W_{SC}	Ratio of simulator inlet corrected airflow to exhaust nozzle throat area, lbm/sec-ft^2
X	Axial position
γ	Ratio of specific heats
ϕ	Stream thrust ratio, $\phi = \dfrac{PA(1 + \gamma M^2)}{P^*A^*(1 + \gamma)}$

SUBSCRIPTS

2,3,4,etc.	Stations in experimental and analytical models
2I	Measurement station in Fig. 6
B, B1	Mixing duct, mixing duct exit
b	Base region

$\mathfrak{C}$ Centerline

ex   Exhaust nozzle, exhaust nozzle exit

in   Inlet

ref   Reference condition

sep   Flow separation condition

T   Total or stagnation condition

theo   Theoretical

w   Mixing duct wall

∞ Flight conditions

SUPERCRIPTS

*   Throat region, sonic condition